KTH Industrial Engineering
and Management

Thermodynamic Cycles using Carbon Dioxide as Working Fluid

CO_2 transcritical power cycle study

Doctoral Thesis
by
Yang Chen

Stockholm, October, 2011

School of Industrial Engineering and Management
Department of Energy Technology
Division of Applied Thermodynamics and Refrigeration

Thermodynamic Cycles using Carbon Dioxide as Working Fluid
CO_2 transcritical power cycle study
Yang Chen

Trita REFR Report 11/03
ISSN 1102-0245
ISRN KTH/REFR/11/03-SE
ISBN 978-91-7501-187-5

Doctoral Thesis by Yang Chen
School of Industrial Engineering and Management
Department of Energy Technology
Division of Applied Thermodynamics and Refrigeration

Printed by Universitetsservice US AB
Stockholm, 2011

Abstract

The interest in utilizing the energy in low-grade heat sources and waste heat is increasing. There is an abundance of such heat sources, but their utilization today is insufficient, mainly due to the limitations of the conventional power cycles in such applications, such as low efficiency, bulky size or moisture at the expansion outlet (e.g. problems for turbine blades).

Carbon dioxide (CO_2) has been widely investigated for use as a working fluid in refrigeration cycles, because it has no ozone-depleting potential (ODP) and low global warming potential (GWP). It is also inexpensive, non-explosive, non-flammable and abundant in nature. At the same time, CO_2 has advantages in use as a working fluid in low-grade heat resource recovery and energy conversion from waste heat, mainly because it can create a better matching to the heat source temperature profile in the supercritical region to reduce the irreversibility during the heating process. Nevertheless, the research in such applications is very limited.

This study investigates the potential of using carbon dioxide as a working fluid in power cycles for low-grade heat source/waste heat recovery.

At the beginning of this study, basic CO_2 power cycles, namely carbon dioxide transcritical power cycle, carbon dioxide Brayton cycle and carbon dioxide cooling and power combined cycle were simulated and studied to see their potential in different applications (e.g. low-grade heat source applications, automobile applications and heat and power cogeneration applications). For the applications in automobile industries, low pressure drop on the engine's exhaust gas side is crucial to not

reducing the engine's performance. Therefore, a heat exchanger with low-pressure drop on the secondary side (i.e. the gas side) was also designed, simulated and tested with water and engine exhaust gases at the early stage of the study (Appendix 2).

The study subsequently focused mainly on carbon dioxide transcritical power cycle, which has a wide range of applications. The performance of the carbon dioxide transcritical power cycle has been simulated and compared with the other most commonly employed power cycles in low-grade heat source utilizations, i.e. the Organic Rankin Cycle (ORC). Furthermore, the annual performance of the carbon dioxide transcritical power cycle in utilizing the low-grade heat source (i.e. solar) has also been simulated and analyzed with dynamic simulation in this work.

Last but not least, the matching of the temperature profiles in the heat exchangers for CO_2 and its influence on the cycle performance have also been discussed. Second law thermodynamic analyses of the carbon dioxide transcritical power systems have been completed.

The simulation models have been mainly developed in the software known as Engineering Equation Solver (EES)[1] for both cycle analyses and computer-aided heat exchanger designs. The model has also been connected to TRNSYS for dynamic system annual performance simulations. In addition, Refprop 7.0[2] is used for calculating the working fluid properties, and the CFD tool (COMSOL) [3] has been employed to investigate the particular phenomena influencing the heat exchanger performance.

[1] Engineering Equation Solver: http://www.fchart.com/ees/ees.shtml

[2] Refprop 7.0: http://www.nist.gov/srd/nist23.htm

[3] http://www.comsol.se/

Publications

This thesis is based on the following papers, which are enclosed at the end. A short summary of each paper can also be found in Appendix 3.

I. **Y. Chen, P. Lundqvist, P. Platell**
"Theoretical Research of Carbon Dioxide Power Cycle Application in Automobile Industry to Reduce Vehicle's Fuel Consumption"
Paper published in Applied Thermal Engineering 25 (2005), pp 2041–2053

II. **Y. Chen, P. Lundqvist, A. Johansson, P. Platell**
"A comparative study of the Carbon Dioxide Transcritical Power Cycle compared with an Organic Rankine Cycle with R123 as working fluid in Waste Heat Recovery"
Paper published in Applied Thermal Engineering 26 (2006), pp 2142–2147

III. **Y. Chen, W. Pridasawas, P. Lundqvist**
"Dynamic Simulation of a Solar-Driven Carbon Dioxide Transcritical Power System for Small Scale Combined Heat and Power Production"
Paper published in Solar Energy 84 (2010), pp 1103–1110

IV. **Y. Chen , A. B. Workie , P. Lundqvist**
"Second Law Analysis of a Carbon Dioxide Transcritical Power System in Low-grade Heat Source Recovery"
Paper submitted to Applied Thermal Engineering

V. **Y. Chen, P. Lundqvist**
"Carbon dioxide cooling and power combined cycle for mobile applications".
Paper published and presented at 7th IIR Gustav Lorentzen Conference on Natural Working Fluids, Trondheim, Norway, May 28-31, 2006

VI. **Y. Chen, P. Lundqvist**
"Analysis of supercritical carbon dioxide heat exchangers in cooling process"
Paper published and presented at International Refrigeration and Air Conditioning Conference at Purdue, USA, July 17-20, 2006.

VII. **Y. Chen, P. Lundqvist**
"Low-grade Heat Source Utilization by Carbon Dioxide Transcritical Power Cycle"
Paper published and presented at ASME-JSME Thermal Engineering Summer Heat Transfer Conference, Vancouver, British Columbia, Canada, July 9-13, 2007

VIII. **Y. Chen, P. Lundqvist**
"Theoretical study of carbon dioxide double loop system"
Paper published and presented at IIR internal refrigeration congress, Beijing, China, August 21-26, 2007.
This paper has been selected as a keynote speech in one parallel section in the conference

IX. **Y. Chen, P. Lundqvist, B. Palm**
"A novel gas-water heat exchanger with minichannels"
Paper published and presented at ASME Summer Heat Transfer Conference, Jacksonville, Florida USA, August 10-14, 2008

X. **Y. Chen, P. Lundqvist**
"The CO_2 transcritical power cycle for low grade heat recovery- discussion on temperature profiles in system heat exchangers"
Paper published and presented at ASME Power and ICOPE Conference, Denver, USA, July 12-14, 2011

Other reviewed reports

I. **Y. Chen**
"Carbon Dioxide Transcritical Power Cycle Discussion"
Trita REFR Report 2005, No. 05/49, ISSN 1102-0245, ISRN KTH/REFR/R-05/49-SE.

II. **Y. Chen**
"Novel cycles using carbon dioxide as working fluid"
Licentiate Thesis in Energy Technology, Royal Institute of Technology, ISSN: 1102-0245, ISRN: KTH/REFR/R-06/50-SE, ISBN: 91-7178-410- 1, 2006

XI. **Y. Chen, P. Lundqvist, A. Alves, L. Brachert**
"CO_2 heat pumps for the Swedish market ---Test and analysis of the SANYO ECO-CUTE heat pump modified for Swedish conditions"
Effsys2 - project report 2009 (http://www.effsys2.se/P3.htm)

XII. **Y. Chen , A. B. Workie , P. Lundqvist**
"Investigation on high pressure pumps for CO_2 transcritical power cycle in low grade heat source utilization"
CREATIV- project report 2010

Acknowledgements

There are so many people that I should like to thank. Without all your assistance, support and encouragement, I would not have achieved this much.

First of all, I would like to express my sincere gratitude to my supervisor, Professor Per Lundqvist. You opened the door for me to this scientific world and guided me all the way through with your wise ideas, enormous patience, good humor and constant encouragement.

Thanks are also due to:

Peter Platell and his father Ove Platell, for initiating the interesting idea, which was the original motivation of this thesis.

Prof. Björn Palm, for your support and help whenever I have had questions. You never said "no" to me when I needed help and your hard work has always inspired me.

My "CO_2 colleague", Dr. Samer Sawalha, for all the nice and interesting discussions, no matter if they were CO_2 related or just wild.

Mr. Henrik Öhman for being my "pie-throwing" seminar opponent and giving me so many constructive suggestions.

Dr. Getachew Bekele, for being such a good officemate and sharing all those talks. Dr. Wimolsiri Pridasawas, for the help with TRNSYS models and all the other support. Dr. Primal Fernando, for your humor and friendship. Inga Du Rietz, for

having kept everything at the division in order during my study time.

Special thanks and deep sorrow also go to Benny Andersson, who had helped a lot with my test rig and passed away before I finished this study. It feels as if those late night discussions with you for the test rig construction just happened yesterday.

I would like to thank the entire faculty at the Department of Energy Technology and all the PhD students at the Division of Applied Thermodynamics and Refrigeration (especially, Professor Emeritus Eric Granryd, Guest Prof. Timothy Ameel, Dr. Claudi Martin, Dr. Raul Anton, Dr. Rashid Ali, Dr. Marino Grozdek, Dr. Rahmatollah Khodabandeh, Peter Hill, José Acuña, Dr. Anders Johansson, Dr. Nabil Kassem , Dr. Hans Jonsson, Dr. Åke Melinder, Dr. Jaime Arias, Dr. Joachim Claesson, Jan Erik Nowacki, Benny Sjöberg, Susy Mathew, Dr. Wahib Owhaib, Hatef Madani, Maqbool Muhammad Mamayun, Jörgen Wallin, Aleh Kliatsko, Stina Gustafsson, Monika Ignatowicz, Sad Jarall, Oxana Samoteeva, Richard Furberg, Cecilia Hägg, Shota Nozadze, Branko Simanic, Dr. Paulina Bohdanowicz), for being such good colleagues. Our division was more like a big family.

I also want to specially thank Björn Qvist, Stefan Cartling, Göran Dalaryd, Mikael Welander and Jörgen Persson for your constant support and encouragement, Jörgen Carlsson, for being a nice gym mate and all the other colleagues, for you are great!

Moreover, I want to thank all my relatives, friends and especially my parents, Xiaoming Tian and Jiabao Chen, and my grandparents, Surun Yan and Zairen Tian for your love, support and constant care.

To my beloved wife Sha Liu for your love, patience, understanding and the sacrifice in order for me to finalize this thesis.

Preface

I have been thinking of this moment for long until today, when I am really sitting here and finalizing the last part of my thesis. At this moment, I am starting to realize how much the time flies.

Almost every kid has been asked the same question: "What do you want to be when you grown up?" The answers were always very similar in China when I was a child:" I want to be a scientist!" and I was no exception.

However, during the time when I grew up, my real answer has changed many times, since I learned more and more about the world and so many things have caught my interest.

Apart from those minor wishes, my first dream was to become a pilot. After I passed the first selection exam after graduating from high school, the dream almost came true, until my parents thought I should still continue to the engineering college, so that I could follow my father's career path and become a hotel manager.

Although I followed their advice and entered engineering college, I changed my mind about following my father's career path and instead chose to study abroad. I had been working hard in college on my English and took all the required exams such as GRE, TOEFL, etc. in order to apply for a graduate school in the U.S. After I finished all these tests, I was facing two options: either to wait for about 8 months for the start of the application period for US graduate schools or to apply, as recommended by a schoolmate, to the Royal Institute of Technology in Sweden directly, since the application deadline

was in April. I tried option 2 and that brought me to the Energy Department of the Royal Institute of Technology in Sweden. Here, I spent one and half years finishing my Masters degree.

I was then planning to use the still valid scores from the GRE test to apply for a school in the U.S. again in the last part of my study in Sweden, until I met Prof. Lundqvist and Peter Platell for this interesting topic of using CO_2 to recover energy from low-grade heat sources and waste heat. I feel very lucky that I decided to pursue this topic and they opened the door for me to this really interesting scientific research world!

After so many years staying in Sweden, I indeed love this beautiful country from the bottom of my heart and I am very proud that I have been studying at the Royal Institute of Technology. During these years, I have matured and made so many friends here. I always feel life is amazing and I am so lucky that I even got married to my beautiful and beloved wife in the last year of my Ph.D. study!

Now, after this long, my thesis is finally submitted for a Ph.D. degree.

Yang Chen, 2011-10-30
Late night in Stockholm

Table of Contents

List of Tables

List of Figures

1 Introduction

1.1 Motivation

Energy security, economic development and environment protection are not well balanced today and the energy demand is still closely connected to the economic growth. At the same time, fossil fuels still play the dominant role in energy resources worldwide, accounting for 77% of the increasing energy demand 2007-2030 (IEA, 2009). Therefore, the global economic growth has led to dramatic environmental problems, such as air pollution and climate change.

Improving the energy efficiency by utilizing the energy in low-grade heat source / waste heat offers a great opportunity for a sustainable energy future and fewer environmental problems. Figure 1-1 shows some examples of the most typical low-grade and waste heat sources.

Figure 1-1 Typical temperature range of different heat sources for heat recovery[4]

[4] Pictures are taken from the Internet and only to symbolize different heat sources

The most commonly investigated cycles in low-grade heat source and waste heat utilizations today are Organic Rankine Cycles (ORCs) and Kalina cycle (binary fluids and fluid mixtures).

The ORC uses an organic working fluid (such as R113 and R123) to generate power (electricity). The working fluid is heated to saturated vapor and the expanding vapor is used to drive an expansion machine. The main advantage of ORC is that for many organic compounds, it is not necessary to superheat the working fluid to avoid moisture erosion at the turbine outlet, which may result in higher cycle efficiency. For the Kalina cycle, the advantage is that the zeotropic fluid mixtures can match the heat source temperature profile better, so that better efficiency can be expected. However, the drawbacks of these cycles are also numerous: for ORC, the working fluids such as R113 and R123 are expensive, strong climate gases themselves, and also ozone-depleting. In addition, the change of phase for organic compounds during the heating process (evaporation) may introduce so-called "pinching" [5] in the heat exchanger, which produces irreversibility and counteracts the effort to improve the cycle efficiency from a thermodynamic viewpoint. For Kalina cycles, using fluid mixtures will yield a poorer heat transfer performance than using pure working fluid. Moreover, ammonia water, which is the most commonly used working fluid in the Kalina cycle, is highly toxic and corrosive (Yan, 1991, Thorin, 2000).

Compared to the working fluids that have been mentioned, carbon dioxide is a natural working fluid and has many advantages: it is inexpensive, non-explosive and non-flammable. It also has low Global Warming Potential (GWP=1) and no Ozone Depleting Potential (ODP). For many years, CO_2 has been proposed by many scientists as a replacement for

[5] Pinching is the smallest temperature difference in the heat exchanger

synthetic refrigerants in refrigeration fields (Gustav, 1992, Peter, 1998, Armin, 2000, Man-Hoe *et al.*, 2004, Tomoichiro, 2005, Samer, 2008, Silvia, 2011).

Theoretically, all the refrigeration cycles can be reversed as power cycles, as illustrated below:

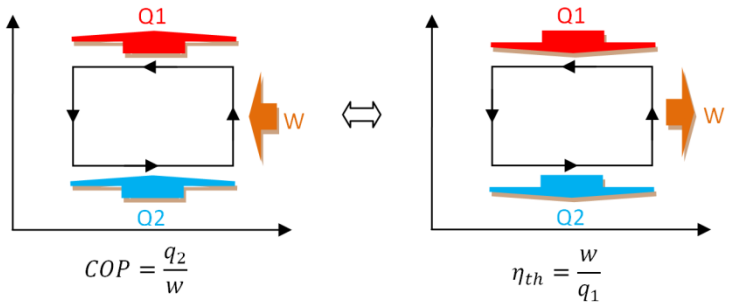

Figure 1-2 Illustration of cycle reversibility

Due to the low critical temperature of CO_2 (31.1 °C), the CO_2 heating process in a reversed carbon dioxide refrigeration cycle is likely be located in the supercritical region and the cycle will then be called a carbon dioxide transcritical power cycle or a supercritical power cycle respectively, depending upon where the cooling process of CO_2 is located.

One of the main advantages revealed when a CO_2 refrigeration cycle is run reversely as a power cycle is the temperature profile in the heating process of supercritical CO_2. Figure 1-3 illustrates the temperature profiles of the low-grade heat source and different working fluids in the heat exchanger for the working fluid heating process. As shown in the figure, the carbon dioxide temperature profile in the supercritical region can provide a better match to the heat source temperature glide than working fluids used in ORCs and Kalina cycles. Thus, the so-called "pinching", which commonly occurs for other working fluids, can be avoided inside the CO_2 counter flow heat exchanger. This is crucial to reducing the irreversibility of the

cycle and achieving good thermal efficiency, especially when utilizing the energy in low-grade heat sources is utilized[6].

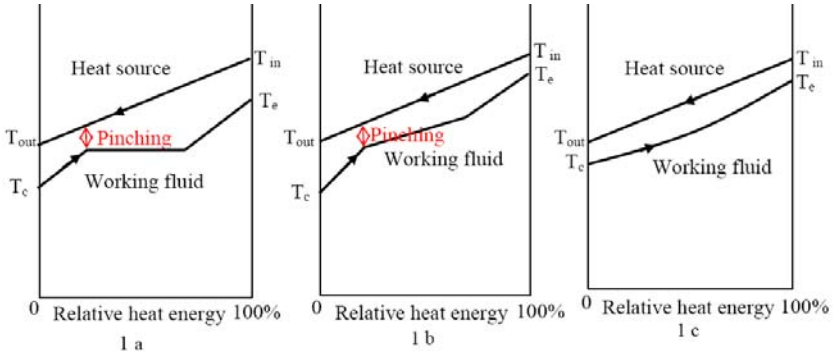

Figure 1-3 Schematic representation chart of the heat transfer between the low-grade heat source and working fluid in the main heat exchanger: (1a) pure fluid; (1b) zeotropic fluid mixtures; (1c) carbon dioxide

For the reasons mentioned above, CO_2 seems to have great potential for use as a working fluid in power cycles in utilizing the energy in low-grade heat sources and waste heat. This thesis work was therefore proposed.

1.2 Objectives and Approach

The main objective of this project is to investigate the potential of the proposed CO_2 cycles and systems in utilizing the energy from low-grade heat sources and waste heat. The research work is performed mainly by computer-aided simulations.

To achieve the goal of the study, this work covers mainly the following aspects:

[6] The reason for the temperature profile matching being important will be explained in more detail in chapter 4 in this book.

- General computer-aided investigation on the possibility and potential of the proposed cycles in exploiting the energy from low-grade heat sources and waste heat.

- Detailed computer-aided studies of selected cycles on their characteristics, such as the influences of different working parameters on the cycle performance.

- Computer-aided dynamic performance simulations of the selected cycles in certain applications.

- Thermodynamic analyses of the proposed cycles and comparisons between the selected cycles and other commonly adopted cycles in the same application fields (i.e. comparison between CO_2 transcritical power cycle and a typical ORC cycle).

During the study, the work also involved studies in other parallel and related topics such as component design for certain applications (i.e. low air side pressure drop heat exchanger for recovering the waste heat from engines).

Cycle and system models and computer simulations are mainly performed with Engineer Equation Solver (EES). TRNSYS is adopted to provide the boundary conditions for dynamic simulations. The properties of the working fluid under different conditions are calculated by Refprop 7.0. Commercial CFD software (COMSOL) has also been used to simulate relevant heat transfer problems and to analyze the air flows in heat exchanger designs.

2 Background

2.1 Working Fluid Comparison

There are many thermophysical properties that should be considered when selecting a proper working fluid for utilizing the energy in low-grade heat sources and waste heat. For instance, the critical temperature and critical pressure will indicate whether the cycle will be run as a transcritical cycle or a subcritical cycle, the possibility for condensing and the system working pressure respectively; the Cp value will influence the shape of the temperature profiles in the system heat exchangers; the specific volume and specific power density will predict the sizes of the system components for certain applications; the value of dS/dT will indicate the possibility of moisture content at the turbine outlet (i.e. the need for superheating), etc.

Meanwhile, there are also other issues that need to be considered, such as environmental aspects (i.e. GWP and ODP), safety, availability, and cost.

More than 50 working fluids have been proposed in the literature, among which there is, however, no best fluid that can meet all the criteria. Therefore, certain compromises may be needed to find the most suitable working fluid for a certain application.

Table 2-1 gives the properties of some typical working fluids that represent different categories of working fluids proposed in the literature (water is used as a reference).

Table 2-1Properties of different fluids

Fluid name	ASHRAE No.	Critical temp. (°C)	Critical press. (Bar)	ASHRAE Level for safety[7]	ODP	GWP 100yr[8]	dS/dT[9]
Trifluoromethane	R23	26.29	48.3	A1	0	11700	-6.49
Difluoromethane	R32	78.26	57.8	A2	0	580	-4.33
2.2-Dichloro-1.1.1-trifluoroethane	R123	183.83	36.6	B1	0.02	93	0.26
Pentafluoroethane	R125	66.17	36.2	A1	0	2800	-1.08
Hydroflorocarbon	R134a	101.1	40.7	A1	0	1300	-0.39
1.1.1-Trifluoroethane	R143a	72.86	37.6	A2	0	3900	-1.49
1.1-Difluoroethane	R152a	113.41	45.2	A2	0	140	-1.14
Octafluoropropane	R218	72.02	26.4	A1	0	7000	0.45
Propane	R290	369.8	42.47	A3	0	<10	-0.79
Zeotropic mixture	R407C	87.3	48.2	A1	0	1525	?
Azeotropic mixture	R500	102.1	41.7	A1	0,74	6 310	?

[7] In ANSI/ASHRAE Standard 15, refrigerants are classified according to the hazard involved in their use. Group A1 refrigerants are the least hazardous, Group B3 the most hazardous. Details can be found in Appendix 1

[8] GWP 100 yr is a measure of how much a given mass of a gas contributes to global warming over 100 years. GWP is a relative scale which compares the greenhouse gas to carbon dioxide where GWP by definition is 1.

[9] Chen H.j., Goswami D. Y., Stefanakos E. K., A review of thermodynamic cycles and working fluids for the conversion of low-grade heat, renewable and sustainable energy reviews 14 (2919) 3059-3067.

Butane	R600	152	37.9	A3	0	<10	1.03
Isobutane	R600a	134.7	36.4	A3	0	<10	1.03
Ammonia	R717	132.89	112.8	B2	0	0	-10.48
Water	R718	373.89	22.1	A1	0	0	-17.78
Carbon dioxide	R744	30.98	73.8	A1	0	1	-8.27
Propylene	R1270	92.57	46.6	A3	0	0	-1.77

If one considers toxicity and flammability, working fluid of ASHRAE level A1 should be the safest one to use. Therefore, working fluids like ammonia and isobutene are not preferred. If one considers the environmental impacts, working fluid with the lowest ozone depleting potential (ODP) and global warming potential (GWP) should be selected. Consequently, working fluids like Trifluoromethane (R23), Octafluoropropane (R218) and Azeotropic mixture (R500) can then be neglected. If one considers moistures at the expansion outlet, working fluids that have negative values of dS/dT (e.g. Difluoromethane, R32 and Pentafluoroethane, R125) may lead to moisture creation at the turbine outlet without a proper superheating and therefore they are not desired. Moreover, although it is reported that the Kalina cycle can achieve better performance than conventional ORCs (fluids such as 2.2-Dichloro-1.1.1-trifluoroethane, R123), fluid mixtures often show poorer heat transfer performance than pure working fluids. Because of this, fluid mixtures are less desirable, if a transcritical power cycle can be realized. Meanwhile, working fluids that have high critical temperatures will have difficulty being utilized in transcritical power cycles if low-grade heat sources are to be utilized. After taking all these aspects into account, carbon dioxide proved to be a promising working fluid for utilizing the energy in low-grade heat sources and waste heat in transcritical power cycles with good temperature matching.

Carbon dioxide has thus many advantages as a working fluid for utilizing the energy in low–grade heat sources and waste heat. It is an environmentally benign natural working fluid and safe to use. Furthermore, it is abundant in nature and it is available at low cost. Moreover, the chemical and thermodynamic properties of carbon dioxide have been thoroughly studied and there is therefore sufficient knowledge about them.

Compared to other working fluids listed in Table 2-1, carbon dioxide has a low critical temperature and relative high critical

pressure (31.1 °C / 87.98 °F and 7.38 MPa / 1070.38 psi). Thanks to the low critical temperature, even a low-grade heat source can give a transcritical cycle whose "gliding" temperature profile can provide a better match to the heat source temperature glide than other working fluids (as mentioned above). Moreover, since the heating process takes place in the supercritical region, some complexity involved in a phase-changing process (e.g. flow maldistribution) can be avoided. Although the high pressure may have created some challenges in system component design in the past, this field has fast developed in recent years with faster and faster technical improvements. Furthermore, due to its high specific power, the CO_2 system is more compact than systems using other working fluids. Moreover, the energy in the expansion outlet carbon dioxide can be recovered within the cycle through a regenerative heat exchanger (i.e. a regenerator); thus, the high working pressure is helpful in reducing the regenerator size and the excellent heat transfer characteristics of CO_2 help to minimize the influence of pressure drop on the cycle efficiency.

2.2 History of CO_2 Power Cycle

Research on the CO_2 power cycle was first proposed by Sulzer Bros in 1948 and later several countries, such as the Soviet Union, Italy and the United States, became involved in the research on such a cycle (Feher, 1962 and 1967, Dekhtiarev, 1962; Angelino, 1966). However, after the great interest during the 60-ties, research on such cycles dwindled for many years until the 1990s, mainly due to the limited amount of suitable heat sources e.g. nuclear) and limited knowledge of suitable compact heat exchangers and expansion machines (Dostal, 2004). After the 1990s and the development of compact heat exchangers and materials, renewed interest was shown in carbon dioxide power cycles and much research has been carried out (Dostal, 2004; Chang, 2002). Nevertheless, most investigations have focused on a carbon dioxide power cycle with a nuclear reactor as a heat source, thus a cycle working

with a high-grade heat source (up to 800 °C) and high pressures in both the gas heater and gas cooler (CO_2 Brayton cycle). Research on employing such a cycle for low-grade heat source recovery has been relatively limited.

In recent years, more and more interest has been shown in CO_2 transcritical power cycles for utilizing the energy in low–grade heat sources. For instance, Zhang and his colleagues investigated the potential of CO_2 power cycle in utilizing solar energy both theoretically and experimentally (Zhang *et al.*, 2006 and 2007). The author and his colleagues investigated the performance of the carbon dioxide power cycle in utilizing low-grade heat sources and compared its performance with ORCs (Chen *et al.*, 2005, 2006 and 2010). Moreover, Cayer and his colleagues studied CO_2 power system under fixed system working conditions and discussed system optimizations (Cayer *et al.*, 2009). Wang *et al.* tried to optimize the working parameters of supercritical CO_2 power cycle under a fixed heat source condition by using a genetic algorithm and artificial neural network with an assumption that the system heat exchangers will provide sufficient heating /cooling to the desired cycle working conditions (Wang *et al.*, 2010). Furthermore, Baik *et al*. compared the power based performance between CO_2 and R124 transcritical power cycle (Baik *et al*.2011)

2.3 System Illustration and Corresponding Cycle Description

There are two systems proposed in this study: the carbon dioxide bottoming system and the carbon dioxide cooling and power combined system.

2.3.1 The CO_2 bottoming system and corresponding cycles

The CO_2 bottoming system consists of four main parts, namely: a gas heater, a turbine, a condenser (gas cooler), and a pump

(Figure 2-1). In this system, the carbon dioxide is first pumped to a supercritical pressure, and then heated in the gas heater. The heated supercritical carbon dioxide will expand in an expansion machine (e.g. a turbine). The vapor discharged from the expansion machine outlet will then be cooled and condensed in a condenser (gas cooler). An Internal Heat Exchanger (IHX, regenerator) can be added to the basic system to optimize the system performance. The importance of utilizing a regenerator in a carbon dioxide transcritical power cycle will be shown in the latter part of this thesis.

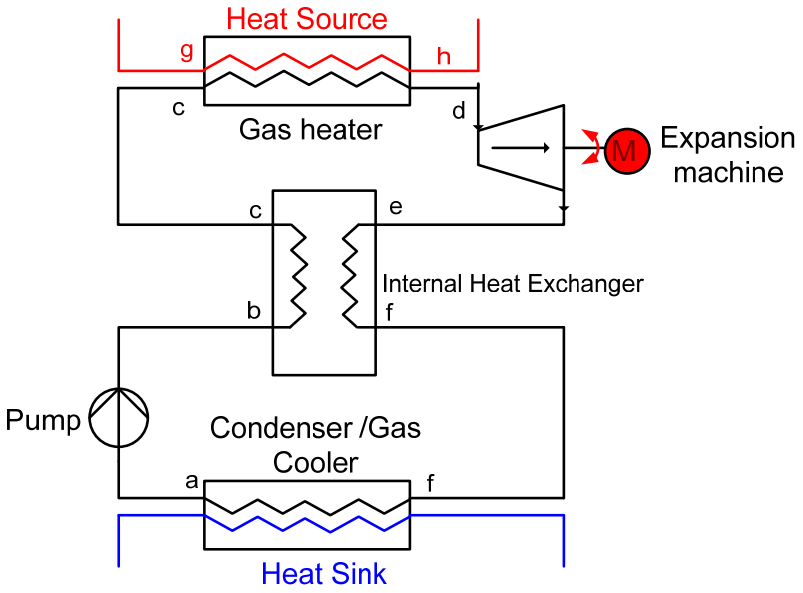

Figure 2-1 Schematic of the carbon dioxide power system (for both Brayton cycle and transcritical cycle)

The corresponding cycles of this system are carbon dioxide transcritical power cycle and carbon dioxide Brayton cycle respectively. Both cycles consist of four processes, namely: compression (a-b), isobaric heat supply (b-d), expansion (d-e), isobaric heat rejection (e-a). The only difference between these two cycles is whether part of the cycle is located in the sub-critical region or not. Therefore, both cycles are sometimes

related to supercritical cycles in the literature. Both cycles are illustrated in the T-S charts as follows (Figure 2-2 & Figure 2-3).

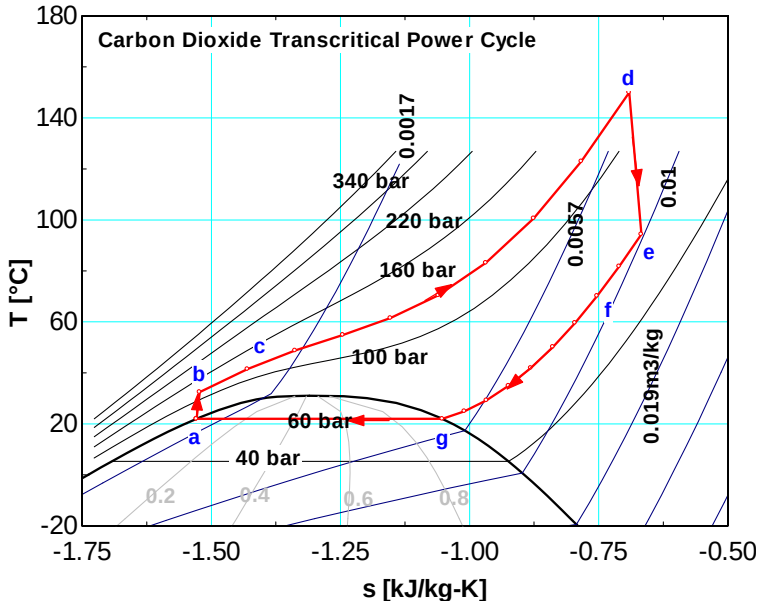

Figure 2-2 Carbon dioxide transcritical cycle T-S chart

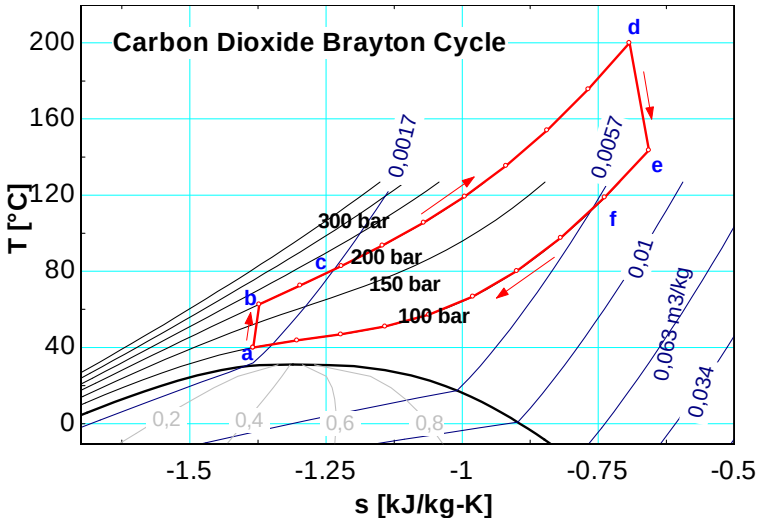

Figure 2-3 Carbon dioxide Brayton cycle T-S chart

It is worth noticing from the figures that carbon dioxide at the expansion outlet still holds a very high energy content (i.e. high temperature). At the same time, the cycle heat rejection process has an obvious temperature glide, which enables the carbon dioxide power system to produce heat (e.g. hot water) and power (e.g. electrical energy) at the same time. For the cases where power is most sought, the regenerator will be very beneficial for the cycle efficiency.

2.3.2 The CO_2 cooling and power combined system and the corresponding cycle

The carbon dioxide cooling and power combined system is mainly composed of six parts, namely: an evaporator, a compressor, a gas heater, an expander, a gas cooler, and a throttling valve. The system schematic layout and the T-S chart of the corresponding cycle are shown respectively in Figure 2-4 and Figure 2-5.

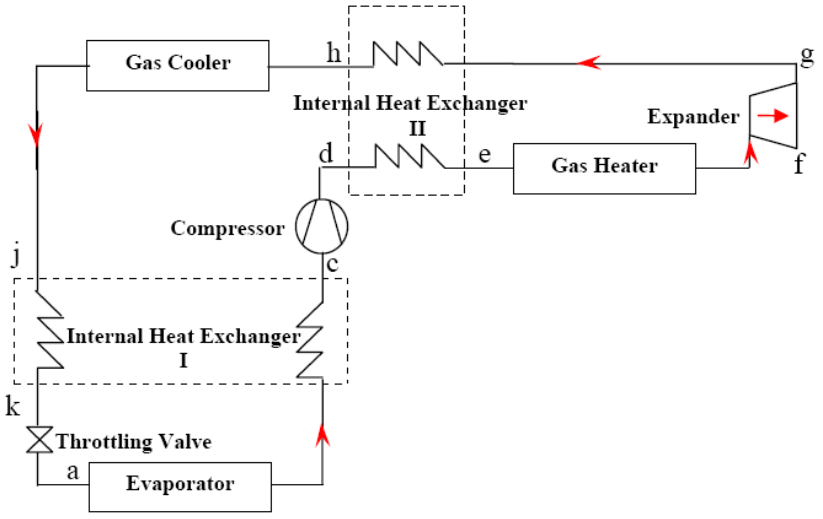

Figure 2-4 Carbon dioxide cooling and power combined system schematic layout

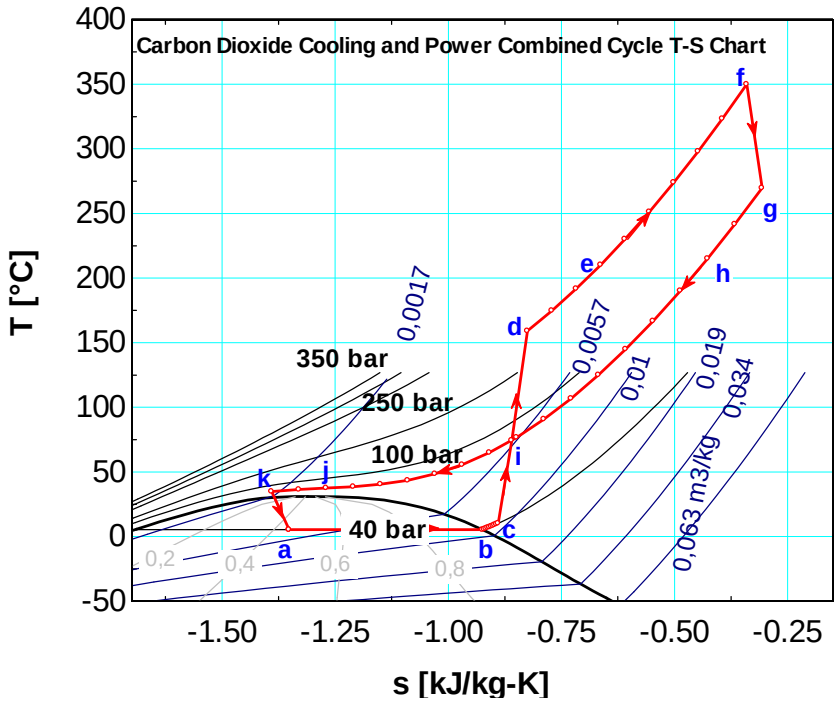

Figure 2-5 Carbon dioxide cooling and power combined cycle T-S chart

The corresponding cycle consists of six processes, namely: compression (c-d), isobaric heat supply (d-f), expansion (f-g), isobaric heat rejection (g-k), throttling (k-a) and isobaric heat apply (a-c).

After absorbing heat in the evaporator (a-b), the carbon dioxide will be further heated in the IHX I until it becomes slightly superheated (b-c). The superheated carbon dioxide vapor will then be compressed by a compressor to a supercritical pressure (c-d), where supercritical carbon dioxide absorbs the heat firstly from the expansion outlet carbon dioxide in IHX II (d-e) and then from the heat source in a gas heater (e-f). After that, the supercritical carbon dioxide will be expanded in an expander (f-g) and then cooled by IHX II (g-h), a gas cooler (h-j) and IHX I (j-k) in turn. Finally, it flows though a throttling valve and enters the evaporator (k-a). In the power part of the combined cycle (d-f-g-i), carbon dioxide will absorb the heat from the low-

grade heat sources or waste heat and convert it into useful mechanical work.

The combined cycle is designed to be employed in automobile applications (i.e. trucks), for which the power part of the combined cycle will utilize the energy in the engine exhaust gases to produce power for the compressor of the cooling part.

3 CO_2 Transcritical Cycle Applications and Performance Simulations

3.1 Basic Cycles and the Parameters that Influence the Cycle Performances

As mentioned in the previous chapter, there are three cycles, namely carbon dioxide transcritical power cycle, carbon dioxide Brayton cycle, and carbon dioxide cooling and power combined cycle, which have been proposed in the current study for utilizing the energy in low-grade heat sources and waste heat.

Thermodynamically, the larger the temperature difference between the cycle's heat absorbing temperature and its heat rejecting temperature, the higher the cycle efficiency. From this viewpoint, for the same heat absorbing temperature, the CO_2 transcritical power cycle will achieve a higher efficiency than the CO_2 Brayton cycle if a low temperature heat sink is available. To achieve a satisfactory efficiency from a carbon dioxide Brayton cycle, a significantly higher heat source temperature is needed. The current study mainly focuses on the systems that work with carbon dioxide transcritical power cycles in low-grade heat source utilization. However, the Brayton cycle and carbon dioxide cooling and power combined cycle have also been analyzed for their potential in waste heat utilization (i.e. the engine's waste heat) by basic cycle analyses.

Several definitions are needed to analyze the performance of the proposed carbon dioxide systems in low-grade heat source

and waste heat utilization. The cycle thermal efficiency of carbon dioxide power cycles can be defined by Equation 3-1:

$$\eta_{th} = \frac{W_{net}}{Q_{input}} = \frac{W_{\exp.} - W_{pump}}{Q_{input}} = \frac{(h_d - h_e) - (h_b - h_a)}{(h_d - h_c)} \quad \textit{Equation 3-1}$$

where Q_{input} is the heat input to the system and W_{net} is the power production by the system.

The Coefficient of Performance (COP) of the carbon dioxide refrigeration cycle and the COP of the cooling part of the carbon dioxide cooling and power combined cycle can be defined as Equation 3-2:

$$COP = \frac{Q_{cooling}}{W_{basic}} \quad \textit{Equation 3-2}$$

where $Q_{cooling}$ is the cooling capacity of the cooling system and W_{basic} is the required compression work of the compressor.

One of the original motivations of the current study was to reduce the energy usage of refrigeration / air conditioning systems by utilizing the energy in low-grade heat source or waste heat by carbon dioxide power systems. In other words, the aim was to employ a carbon dioxide power system or the power part of the carbon dioxide cooling and power combined system to utilize the energy in low-grade heat source or waste heat to produce power. The produced power will be then used to partly, or totally, cover the compressor power demand in a refrigeration system or in the cooling part of the carbon dioxide combined system. In such applications, the COP of the cooling system can be redefined as Equation 3-3 , since the power produced by the CO_2 power system or the power part of the combined system is gained "free of charge" from the low-grade heat source or waste heat.

$$COP_{new} = \frac{Q_{cooling}}{W_{basic} - W_{output}} = \frac{Q_{cooling}}{W_{new}}$$ [10] *Equation 3-3*

where $Q_{cooling}$ is the required cooling capacity, W_{basic} is the original compression work of the cooling cycle, and W_{output} is the work output from the CO_2 power system or the power part of the combined system, i.e. the "free" energy gained from the low-grade heat source or waste heat. W_{new} is the work needed by the compressor after taking away the energy gained from low-grade heat source or waste heat.

Although the applications will determine the possible temperature levels and the capacity as well as the obtainable efficiencies for the various components, several assumptions are made in this chapter based on the published literatures to be able to specify the cycle working conditions and gain a general picture of basic cycle performance.

3.1.1 Carbon dioxide transcritical power cycle

For carbon dioxide transcritical power cycles, the gas heater pressure can be selected arbitrarily. An optimum pressure can be found as a function of other cycle parameters, such as the condensing pressure and the heat source temperature. If an Internal Heat Exchanger (IHX) is part of the system, an optimal gas heater pressure around 120 bar appears likely for an expansion inlet temperature of 100 °C, for instance (Figure 3-3). At the same time, the selection of the gas heater pressure needs to consider the practical issues, such as the material durability durance and safety. Most of the calculations for transcritical power cycles in the current study have chosen 120 bar for the initial calculation and the influence of the gas heater pressure is analyzed afterwards. The expansion inlet temperature is, of course, related to the heat source temperature. Furthermore,

[10]The definition may be questionable from a strictly thermodynamic perspective since the COP may go to infinity if W basic – W output =0.

considering the availability of the low temperature water in reality and the limitation of the cycle's critical temperature (31.1 °C), the condenser pressure is set to 60 bar, which corresponds to approximately 22 °C condensing temperature. The pump efficiency is assumed to be 0.8, based on Tadano *et al.'s* research on CO_2 hermetic compressors (Tadano *et al.,* 2000), due to the fact that research on CO_2 pumps is relatively limited compared to the research on CO_2 compressors. At the same time, it is well known that a pump's efficiency is normally higher than a compressor's, mainly due to the smaller volume change during the pumping process than during the compressing process, and, moreover, Tadano *et al.*'s research was done under similar working conditions. Different expansion efficiencies ranging from 70% (conservative valve used in the earlier studies) to 85% (in the latest studies) have been used in this study. Since there is very limited research on CO_2 expanders in the low-grade heat source utilization field, the efficiency values are chosen based on the research on carbon dioxide expansion machines in transcritical refrigeration cycles, where they are used to replace the throttling valve in order to increase the cycle COP (Nickl *et al.*, 2003; Zha *et al.,* 2003; Huff *et al.,* 2003). In addition, the IHX's effectiveness is assumed to be 90% according to Boewe *et al.* (Boewe *et al.*2001).

3.1.2 The influences of the cycle working parameters on the CO_2 transcritical power cycle performance

There are many factors that may influence the performance of CO_2 transcritical power cycles, such as the effectiveness of the IHX, the heat source temperature, as well as the compressor and expander's specifications.

By plotting the expansion inlet temperature *vs.* cycle efficiency for a given pump efficiency with various expansion efficiencies, and by plotting the expansion inlet temperature *vs.* cycle efficiency for a given expansion efficiency with various pump efficiencies (Figure 3-1 & Figure 3-2), it is found that the cycle

efficiency will be improved by increasing the expansion inlet temperature. However, after a sharp increase at the beginning, the efficiency slope becomes flat if one further increases the expansion inlet temperature to the high temperature region[11]. These figures also illustrate that the efficiencies of expansion units will have more crucial impact on the cycle efficiency than the efficiencies of compression units.

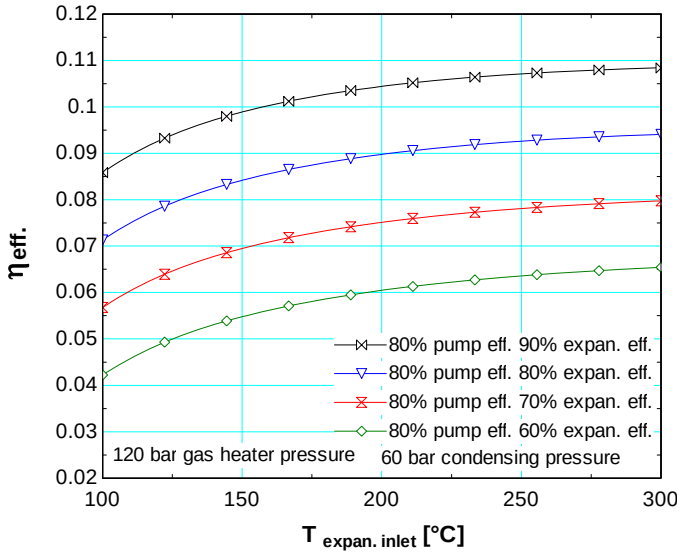

Figure 3-1 Carbon dioxide transcritical cycle efficiency vs. expansion inlet temperature against various expansion efficiencies (from EES, basic cycle without IHX)

[11] This result is based on the given gas heater pressure, which is in the lower pressure region compared with the carbon dioxide Brayton cycle. In the current research in utilizing the low-grade heat source by transcritical power cycle, only relatively lower gas pressure is considered, for the consideration of system safety, etc.

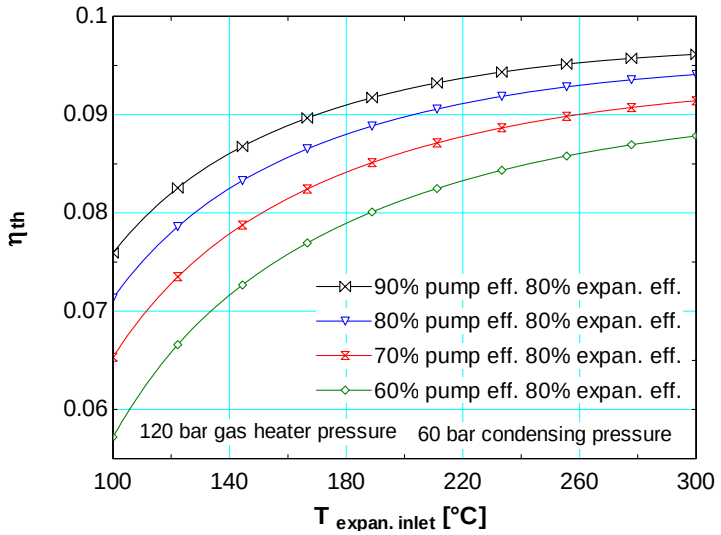

Figure 3-2 Carbon dioxide transcritical cycle efficiency vs. expansion inlet temperature against various pump efficiencies (from EES, basic cycle without IHX)

Furthermore, the influence of the cycle gas heater pressure on the cycle efficiency of a carbon dioxide transcritical power cycle without IHX and with a 90% effectiveness[12] IHX are plotted respectively for different expansion inlet temperatures (Figure 3-3). It is shown that there is an optimum gas heater pressure for a certain expansion inlet temperature and condensing temperature. At a certain condensing pressure, the lower the expansion inlet temperature, the lower the optimum gas heater pressure. Moreover, the cycle with an IHX has a lower optimum gas heater pressure than a cycle without IHX under the same working conditions.

[12] $Effectiveness(\varepsilon) = \dfrac{T_{c,o} - T_{c,i}}{T_{h.i} - T_{c.i}}$

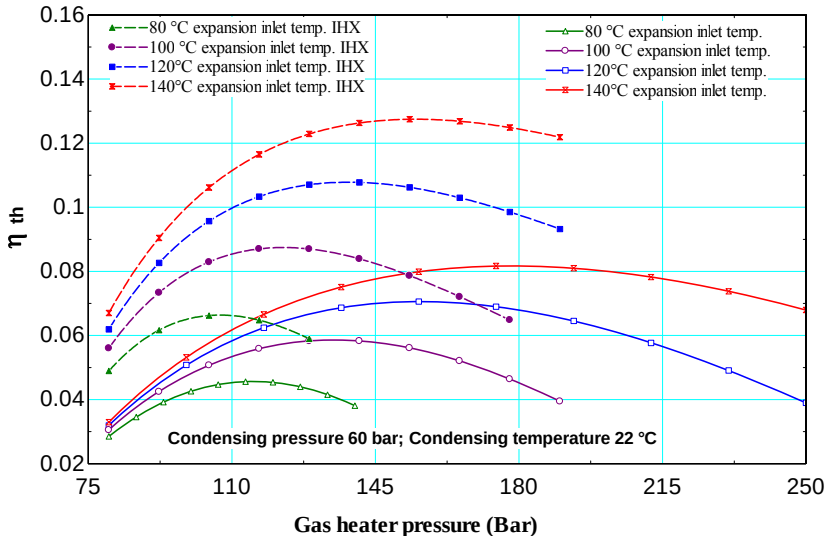

Figure 3-3 Optimum gas heater pressure of a carbon dioxide transcritical cycle (from EES, without IHX and with a 90% effectiveness IHX)

As mentioned in the previous section, the carbon dioxide transcritical power benefits strongly from internal heat regeneration. Therefore, the IHX (regenerator) will have a crucial influence on the cycle performance. The influence of IHX on the cycle efficiency has been plotted in Figure 3-4.

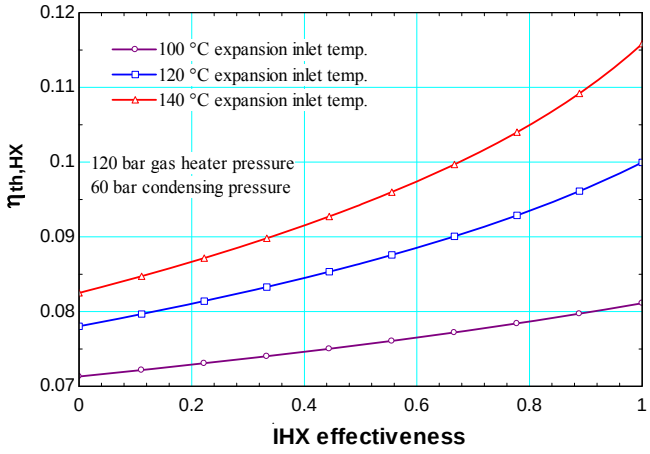

Figure 3-4 The IHX effectiveness' influence on carbon dioxide transcritical cycle efficiency (from EES)

3.1.3 Carbon dioxide Brayton cycle

When the cycle works as a Brayton cycle, the heat rejection process will take place in the supercritical region and the condenser will, therefore, be called a gas cooler. The same efficiencies as those chosen for the pump and the expansion machine for carbon dioxide transcritical power cycles are adopted for the compressor and the expansion machine for carbon dioxide Brayton cycles as initial analysis conditions (i.e. 75% for the compressor and 75-85% for the expansion machine). The gas heater pressure and gas cooler pressure are assumed to be 200 bar and 100 bar respectively for the initial cycle analysis and the influences of different gas cooler and gas heater pressures are also analyzed separately.

3.1.4 The influence of the cycle working parameters on the CO_2 Brayton cycle performance

Unlike the carbon dioxide transcritical power cycle, the carbon dioxide Brayton cycle lies completely in the supercritical region. For this reason, both the gas heater pressure and the gas cooler pressure will influence the cycle performance besides the influence by the effectiveness of the IHX, the heat source temperature and the compressor and expander's specifications, etc.

By plotting the expansion inlet temperature *vs.* cycle efficiency for a given pump efficiency with various expansion efficiencies, and by plotting the expansion inlet temperature *vs.* cycle efficiency for a given expansion efficiency with various pump efficiencies (Figure 3-5 & Figure 3-6), it is found that the cycle efficiency will be improved by increasing the expansion inlet temperature. Moreover, the improvements of the cycle thermal efficiency are less obvious in the higher temperature regions. In general, the Brayton cycle achieves lower thermal efficiency than the transcritical power cycle at the same expansion inlet temperature. Furthermore, it can be noticed that the efficiencies

of expansion units will have more crucial impact on the cycle efficiency than the efficiencies of compression units.

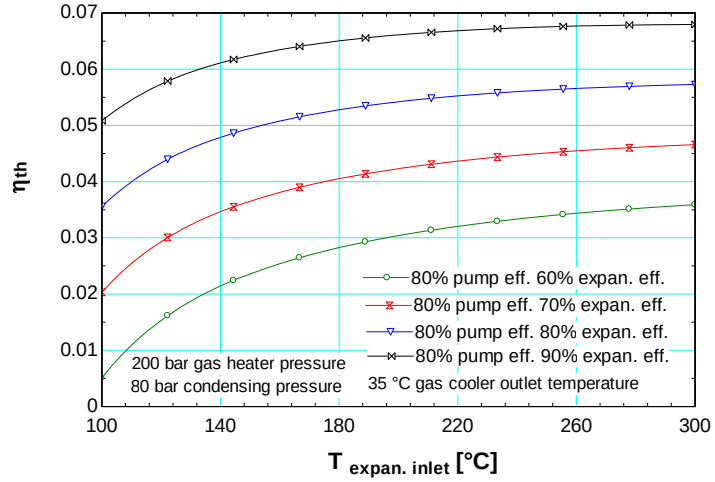

Figure 3-5 Carbon dioxide Brayton cycle efficiency vs. expansion inlet temperature against various expansion efficiencies (from EES, basic cycle without IHX)

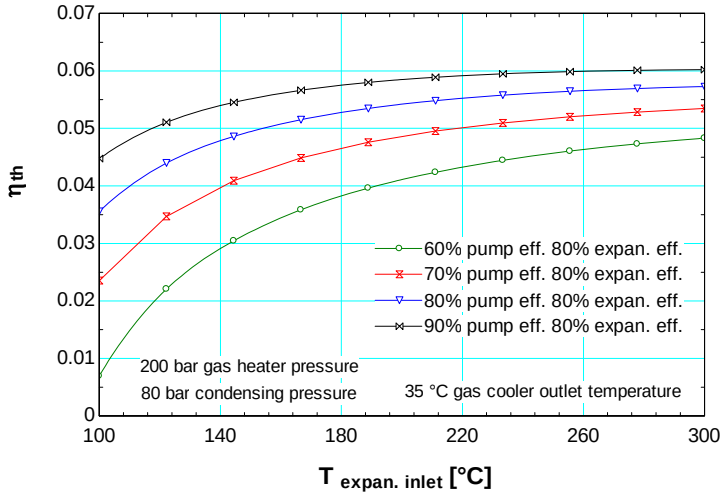

Figure 3-6 Carbon dioxide Brayton cycle efficiency vs. expansion inlet temperature against various pump efficiencies (from EES, basic cycle without IHX)

Furthermore, the influence of the cycle gas heater pressure on the cycle efficiency of a carbon dioxide Brayton cycle without IHX and with a 90% effectiveness IHX respectively are plotted for different expansion inlet temperatures (Figure 3-7). It is shown that there is an optimum gas heater pressure for a certain cycle working condition. Moreover, the cycle with an IHX has a lower optimum gas heater pressure than a cycle without IHX under the same working conditions.

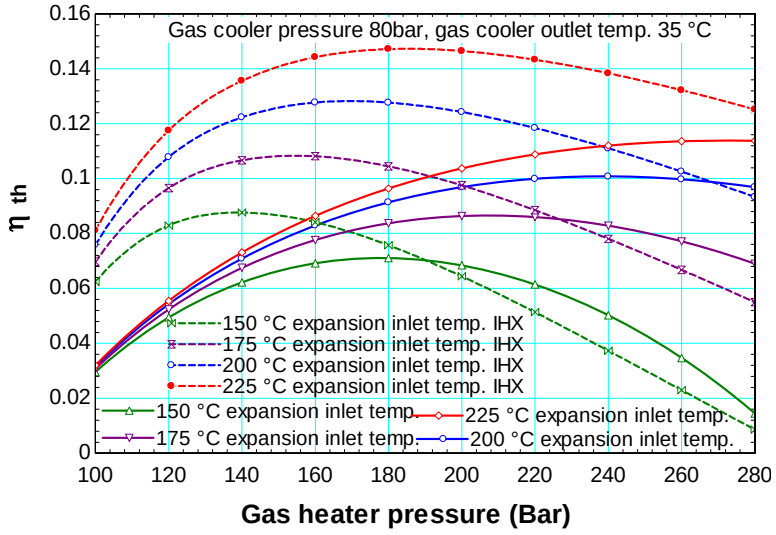

Figure 3-7 Optimum gas heater pressure of a carbon dioxide Brayton cycle (from EES, without IHX and with a 90% effectiveness IHX)

Besides the optimum gas heater pressure, the Brayton cycle also has an optimum gas cooler pressure for a certain cycle working condition which is shown in Figure 3-8.

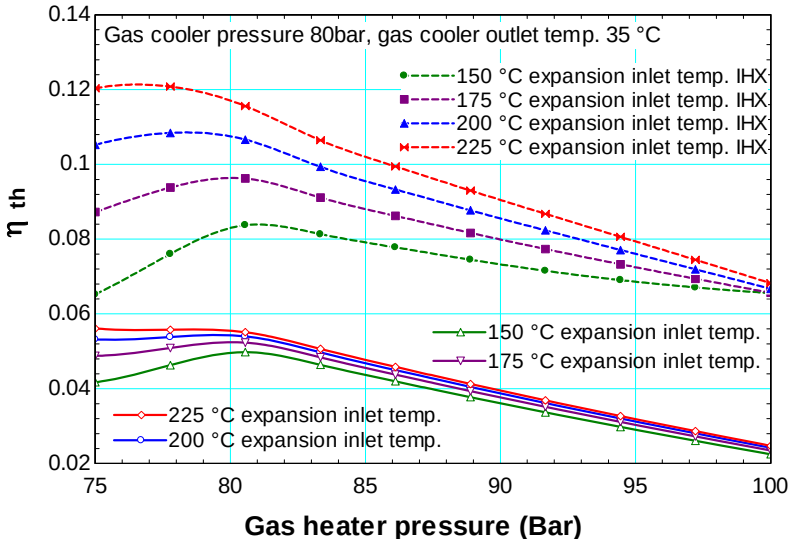

Figure 3-8 Optimum gas cooler pressure of a carbon dioxide Brayton cycle (from EES, without IHX and with a 90% effectiveness IHX)

Furthermore, the influence of the IHX (regenerator) on the cycle thermal efficiency has also been plotted in Figure 3-9. As shown in the figure, the effectiveness of the IHX has critical influence on the cycle thermal efficiency as well.

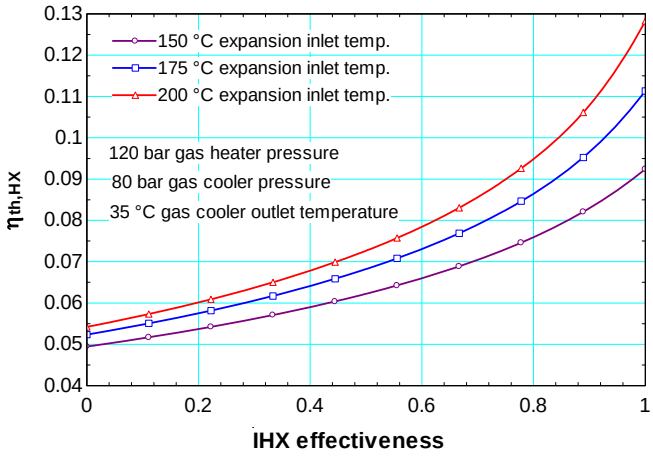

Figure 3-9 The influence of IHX effectiveness on carbon dioxide transcritical cycle efficiency (from EES)

3.1.5 Carbon dioxide cooling and power combined cycle

The author is not aware of any similar cycle suggested in the literature. Therefore, there is no reference cycle operating condition available for carbon dioxide cooling and power combined cycle.

For the cooling part of the combined cycle, the working conditions are selected according to the most commonly used working conditions in other research and in CO_2 automobile A/C prototype testing (Kim *et al.*, 2004). The evaporation pressure is set to 40 bar and the evaporation temperature will be 5.3 °C accordingly. As it is mentioned frequently in other research, there is an optimum gas cooler pressure for the carbon dioxide transcritical refrigeration cycle (Petterssen and Aarlien, 1998, Kauf 1999).

For the heat rejection pressure, Liao and his colleagues (Liao *et al.*,2000) proposed a correlation to predict the optimum heat rejection pressure in terms of evaporation temperature and the gas cooler's outlet temperature, which is expressed by Equation 3-4

$$p_{opt} = (2.778 - 0.0157 t_e) t_c + (0.381 t_e - 9.34) \quad \textit{Equation 3-4}$$

The gas cooler pressure is then set to 85 bar, which is the optimum gas cooler pressure calculated by this equation, based on the assumed evaporation temperature and the 35°C gas cooler outlet temperature.

Moreover, an IHX is included in the system to secure a 5 K superheat at the evaporator outlet as a fixed value to ensure there is no moisture at the compressor inlet. Furthermore, the compressor's isentropic efficiency is assumed to be 75% according to the research done by Rozhentsev and Wang (Rozhentsev and Wang, 2001).

For the power part, the gas heater pressure is selected to 200 bar. The gas cooler pressure (85 bars) and the gas cooler outlet temperature (35 °C) are the same as for the cooling part. Furthermore, the compression and expansion efficiencies are assumed according to the cycle operating conditions listed above. Moreover, the combined cycle is designed mainly for automobile (i.e. truck) applications, and thus the expansion inlet temperature is assumed to be 350 °C, based on the fact that engine exhaust gas can have a temperature of 500°C at the exhaust gas manifold.

3.1.6 The influence of cycle working parameters on the CO_2 cooling and power combined cycle performance

The cooling part COP of the combined cycle is plotted against different gas cooler pressures, while keeping other cycle working conditions constant (Figure 3-10).

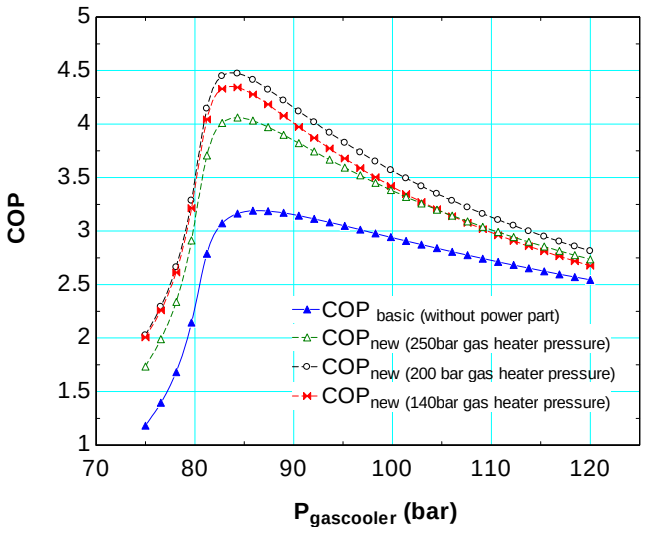

Figure 3-10 The COP of cooling part of the combined cycle vs. different gas cooler pressure

From the figure, one can see that at the optimum gas cooler pressure, the improvement of the cooling cycle's COP is

tremendous (e.g. around 40% as mentioned above in the basic cycle analysis) and the enhancement of COP is different for different gas heater pressures.

Keeping the optimum gas cooler pressure constant, the COP of the combined cycle's cooling part is plotted against different gas heater pressures for different expansion inlet temperatures

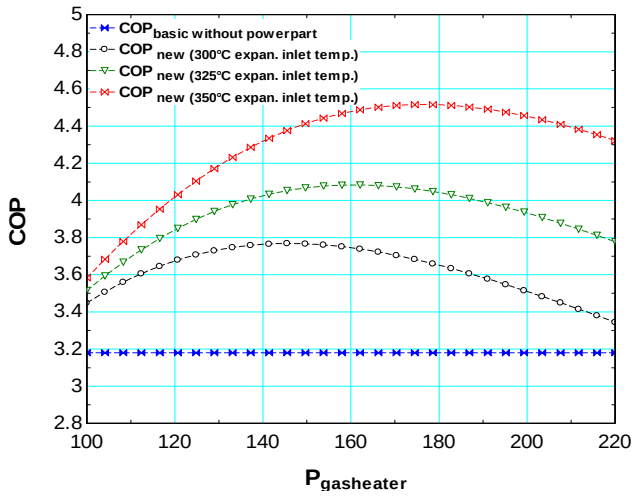

Figure 3-11 The COP of cooling part of the combined cycle vs. different gas heater pressure

The results show that there is an optimum gas heater pressure for the combined cycle's new COP for certain expansion inlet temperatures (i.e. the gas heater pressure for combined cycle power part to achieve the highest W_{output} for a certain expansion inlet temp.). Furthermore, the optimum gas heater pressure increases with increasing expansion inlet temperature.

3.2 CO_2 Power Cycle Applications and Performance Simulations

3.2.1 CO_2 double loop system

One of the CO_2 power cycle applications being studied in the current work is what the author calls the CO_2 double loop system. The schematic system layout and the corresponding T-S chart are shown as follows (Figure 3-12 and Figure 3-13).

As shown in Figure 3-12, a CO_2 double system contains two parts: the power part (upper part) and the refrigeration part (lower part). The power part is composed of five main parts: a pump, a gas heater, an expansion machine, a gas cooler, and an internal heat exchanger. The refrigeration part consists of four main parts: a compressor, a gas cooler, an expansion valve, and an evaporator. Furthermore, an internal heat exchanger is also included in the system to ensure the refrigerant vapor is slightly superheated (i.e. 5°C superheat) before it enters the compressor. In the current analyses, the system employs CO_2 as a working media for both parts and adopts the advantages of both the CO_2 power subsystem and CO_2 refrigeration subsystem.

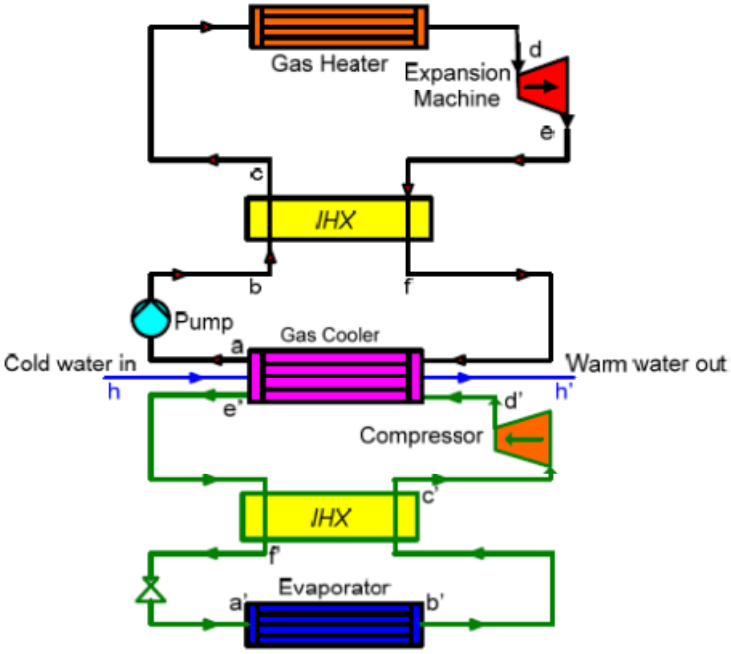

Figure 3-12 Double loop system schematic system layout

The corresponding CO_2 power cycle can be a transcritical power cycle or a CO_2 Brayton power cycle, depending upon the condensing media temperature. For the system proposed in Figure 3-12, one gas cooler for both systems is adopted for system simplicity. Thus, the corresponding power cycle is a CO_2 Brayton cycle and the cooling part is a CO_2 transcritical refrigeration cycle (Figure 3-13).

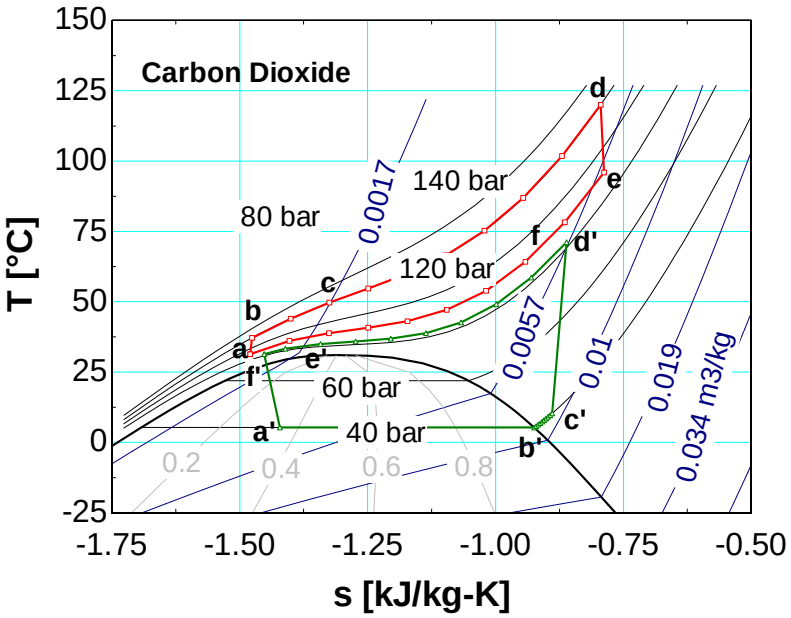

Figure 3-13 Double loop system T-S chart (EES)

Based on the assumptions of system working conditions listed in Table 3-1, the CO_2 double loop system performance is calculated and the results (Table 3-2) show that if a low-grade heat source such as solar thermal or waste heat is used, the proposed double loop system can improve the COP of the parallel running CO_2 refrigeration system by 34 %.

Table 3-1 Carbon dioxide double loop system basic operating conditions

Simulation Parameters	Value	Unit
Evaporator pressure	40	bar
Evaporation temperature	5.3	°C
Refrigerant mass flow	0.08	Kg/s
Superheat after evaporator	5 (fixed value)	K
Gas cooler pressure	83	bar
Gas cooler outlet temperature	35[13]	°C

[13] This temperature is the temperature before the IHX. The real gas cooler outlet temperature is the temperature after providing 5°C superheat at evaporator outlet (I.e. 33°C in the current case).

Gas heater pressure	120	bar
Expansion inlet temperature	120	°C
Compression efficiency	75%	-
Expansion efficiency	85%	-
Pump efficiency	80%	-
Power part IHX effectiveness	0.9	-
Cooling water inlet temperature	15	°C
Cooling water mass flow rate	0.15	Kg/s

Table 3-2 Carbon dioxide double loop system's performance under the basic operating conditions

Performance Parameters	Value	Unit
Double loop power part thermal efficiency (without IHX)	4.8%	-
Double loop power part thermal efficiency (with IHX)	7.5%	-
Basic refrigeration system COP	3.1	-
Double loop system COP^{14} $_{double}$	4.1	-
Water outlet temperature	60.8	°C
System cooling capacity	9.8	kW
Power of hot water production	25.1	kW

The influence of the gas cooler pressure in the power part of the double loop system on the COP of the double loop system has also been investigated and the simulation results are shown in Figure 3-14.

[14] $COP_{double} = COP_{new}$ and is defined as Equation 3-3

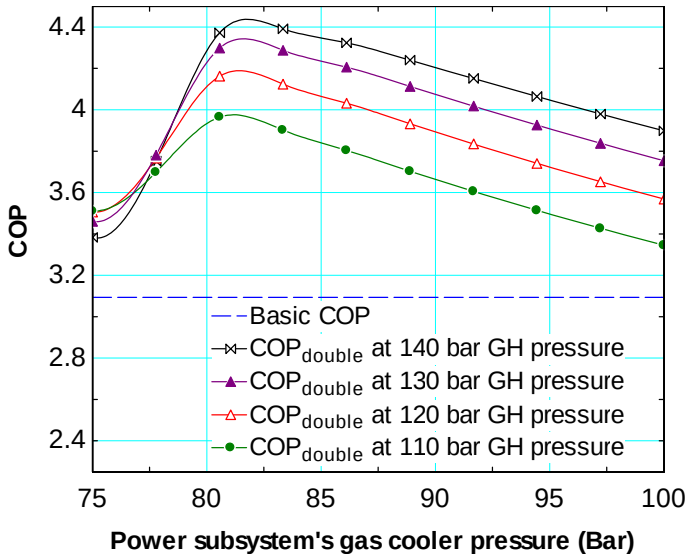

Figure 3-14 Basic refrigeration system's COP and double loop system's COP vs. different gas cooler pressures at different gas heater pressures

It may be noticed that with the contribution from the system's power part, the proposed double loop system can achieve a much higher COP than the basic carbon dioxide refrigeration system. For a certain system working condition, there is an optimum power subsystem gas cooler pressure, which enables a maximum COP for the double loop system.

Furthermore, the influence of the power sub-system's gas heater pressure and the expansion inlet temperature (heat source temperature) were also studied and the results are shown in Figure 3-15.

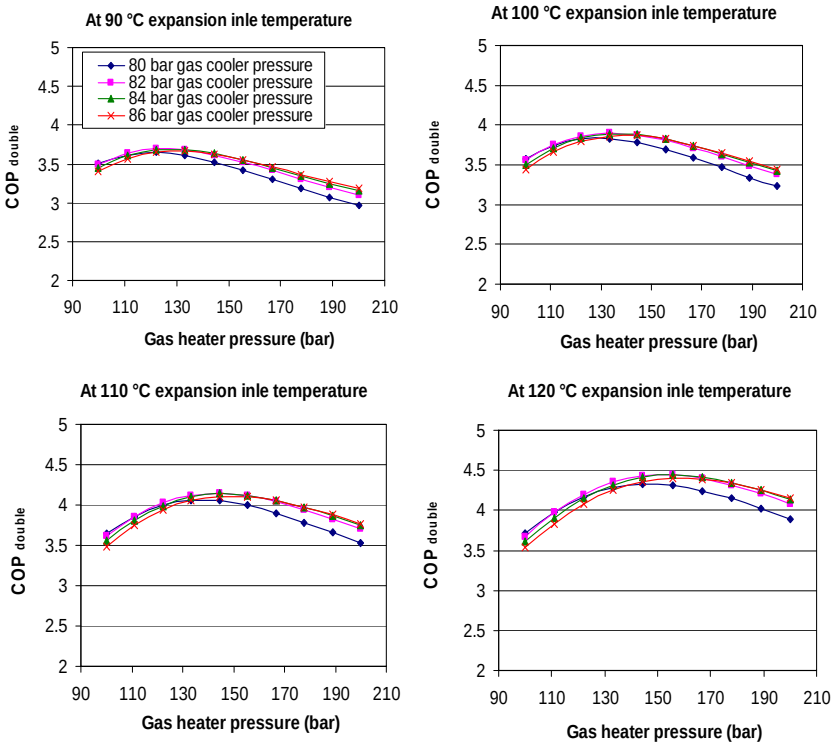

Figure 3-15 Double loop system's COP against different gas heater pressures at different gas cooler pressures and different expansion inlet temperatures

It can be seen from the figure that for a certain expansion inlet temperature and a certain gas cooler pressure, there is an optimum gas heater pressure, which enables the maximum COP.

The influences of the compressor, expansion machine and pump's isentropic efficiencies on the double loop system performance are shown in Figure 3-16. The results indicate that the compressor has a more critical influence on the system's COP than the pump and the expansion machine.

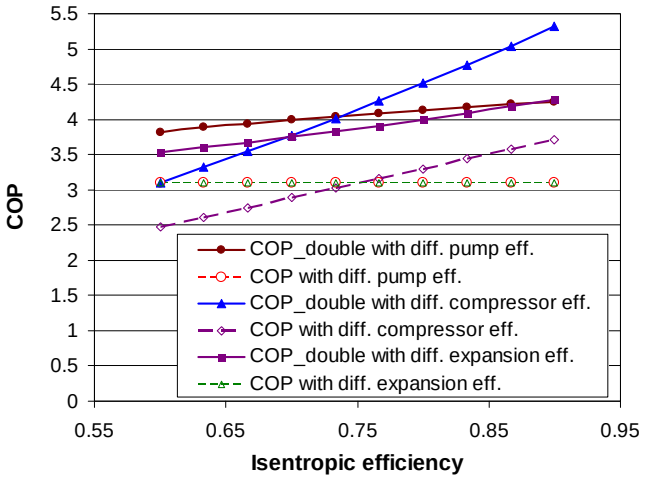

Figure 3-16 Double loop system's COP against different components' efficiencies

3.2.2 Solar driven CO_2 transcritical power system

Another interesting application of CO_2 power cycle is to utilize solar energy for heat and power co-production (i.e. a so called solar-driven CO_2 Rankine cycle).

The basic solar-driven carbon dioxide transcritical power system consists of four main components, namely: a solar collector, an expansion machine, a condenser, and a pump (Figure 3-17).

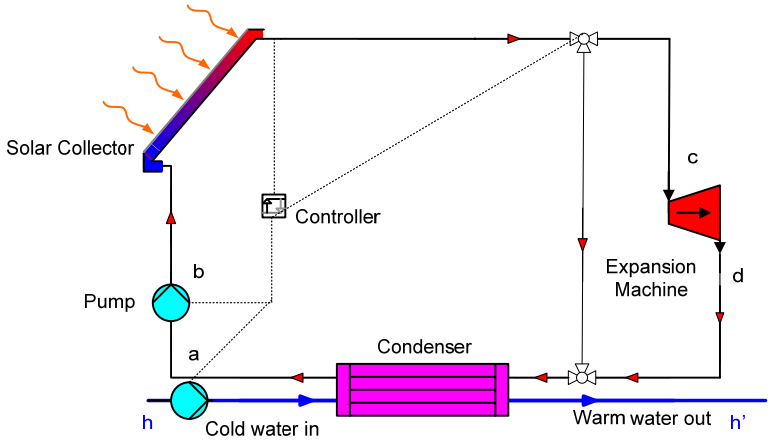

Figure 3-17 Solar-powered transcritical carbon dioxide power system

The dynamic performance of a small scale solar-driven carbon dioxide power system has been analyzed by the dynamic simulation tool TRNSYS 16 (Klein, 2004) and the Engineering Equation Solver (EES) (Klein, 2004) using co-solving technique. The thermodynamic model of the transcritical carbon dioxide power subsystem is developed in EES, while the solar collector and the system boundary conditions are simulated in TRNSYS 16.

A controller that senses the temperature of the CO_2 at the solar collector outlet is also added to the system to control the system work under three modes, depending upon the temperature of CO_2 at the solar collector outlet:

- When the temperature of the CO_2 at the solar collector outlet is higher than 80°C, the system will work under the power mode. The controller will then direct the CO_2 from the solar collector to the expansion machine to produce power and the condenser in the power system will produce heat (hot water) at the same time. The flow rate of the cooling water to the condenser is assumed to be 360kg/h (0.1 kg/s).

- When the temperature of the CO_2 at the solar collector outlet is between 35°C and 70°C, the controller will control the three-way valve at the solar collector outlet to bypass the expansion machine. CO_2 will then be led to the condenser directly to produce heat (hot water) and the water flow rate to the condenser will be reduced to 180 kg/h (0.05kg/s).

- When the temperature of the CO_2 at the solar collector outlet is lower than 35°C, the controller will switch off the pump and the entire system will be stopped until the temperature of the CO_2 is higher than 35°C again.

Based on the simulation parameters listed in Table 3-3, the annual dynamic system performance has been simulated with Swedish climate. METEONORM v5.0 (2006) was adopted for generating the hourly weather data.

Table 3-3 Simulation Parameters

Simulation Parameters	**Descriptions**
Climatic Data	Weather data is generated by METEONORM v5.0. TRNSYS TYPE109 reads the weather data from weather data files and recalculates the solar radiation at different wall orientations. Location: Stockholm, Sweden
Solar Collector Subsystem	
Collector	TRNSYS model type 71 is used for modeling the evacuated tube solar collector. Collector angle: 30° Collector direction: South Collector type: Evacuated Tube (ETC) η_{sc} =0.8-1.5((T_i-T_a)/G)
Power Cycle Subsystem	
	TRNSYS model TYPE66 calls the

	external model which is built in EES. Working Medium: Carbon dioxide CO_2 mass flow:180 kg/h Cooling water mass flow: 360kg/h (under power mode). 180kg/h (under heating mode). Inlet temperature: 15 °C
Pump	Pump efficiency: 0.8
Turbine	Turbine efficiency: 0.85
Gas heater	The basic system gas heater pressure (solar collector pressure) is selected as 120 bar
Condenser	Condenser pressure is 60 bar, corresponding to the temperature of 22 °C, and with 80% efficiency

The system performance for power and hot water production respectively on a typical Swedish summer day (July 15th) are shown in Figure 3-18 and Figure 3-19. Due to the controller, which ensures the system operates only when the supercritical carbon dioxide temperature at the solar collector outlet is higher than 80 °C , the system operates from 8 to 17 during this day.

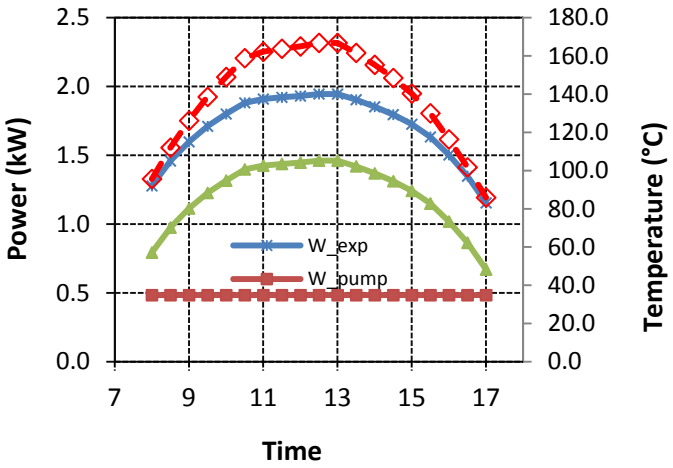

Figure 3-18 Daily performance of solar-driven carbon dioxide power system during a summer day in Stockholm (at 120 bar gas heating pressure)

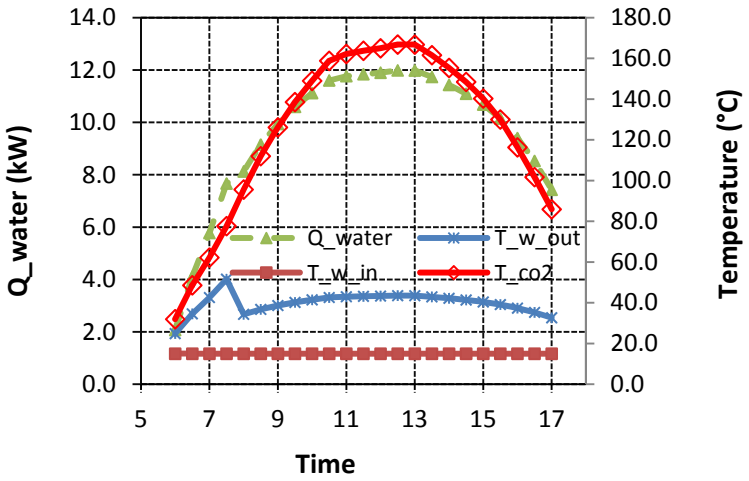

Figure 3-19 Daily performance of the solar- driven carbon dioxide power system during a summer day in Stockholm (at 120 bar gas heater pressure)

As shown in the figures, the temperature of the supercritical carbon dioxide varies with time and has a peak value (about 170 °C) around 13:00, when the system net power production also reaches its maximum (about 1.5 kW). The average system thermal efficiency during the system working period is about 9% and the average power production is consequently about 1.2 kW. Besides the period when the system is working under power mode, the system also works under the heating mode in the early morning (6:00 to 8:00). The sudden change of water temperature (around 8:00) is due to the shift between different working modes and the difference in cooling water flow rates in different working modes. This can be further adjusted by optimizing the cooling water flow rates in different working modes. During the system working period, the system reaches its peak capacity around 13:00 and its peak capacity is around 12 kW.

Figure 3-20 to Figure 3-23 show the daily and monthly performance of the solar driven carbon dioxide power system for power and hot water productions for an entire year.

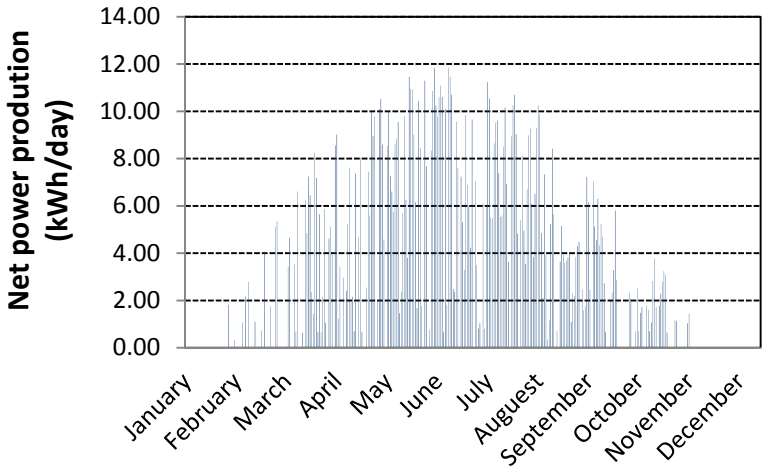

Figure 3-20 Daily net power production (kWh/day) of a solar driven carbon dioxide power system in one year (at 120 bar gas heating pressure)

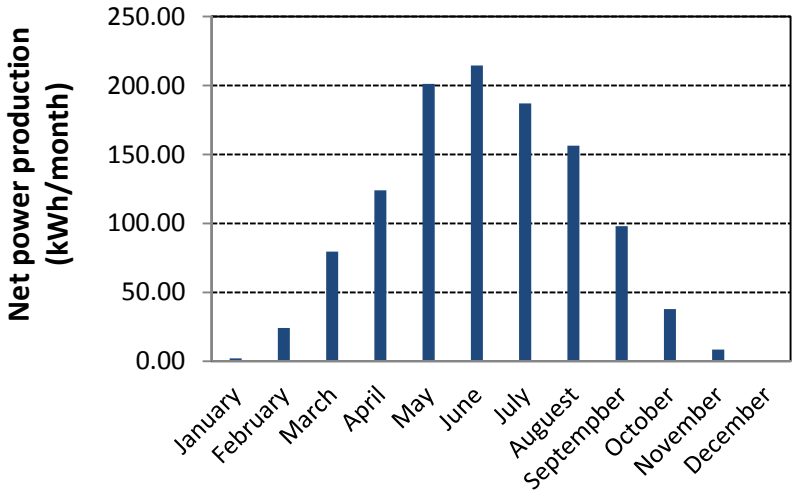

Figure 3-21 Monthly net power production (kWh´s) of the solar-driven carbon dioxide power system in one year (at 120 bar gas heating pressure)

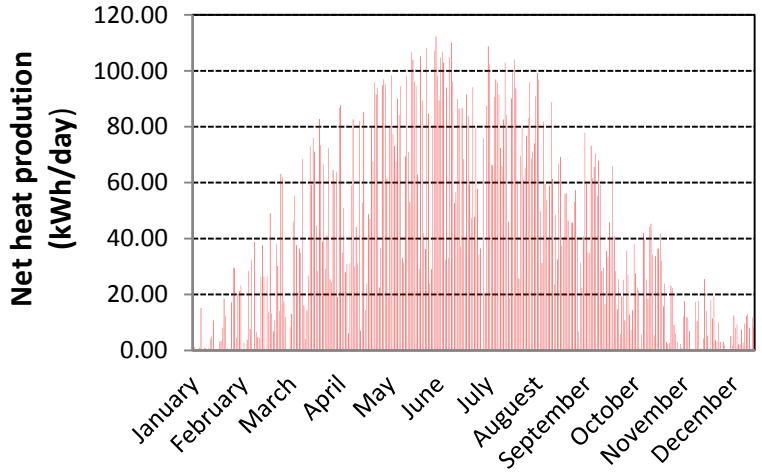

Figure 3-22 Daily heat production (kWh´s) of the solar-driven carbon dioxide power system in one year (at 120 bar gas heating pressure)

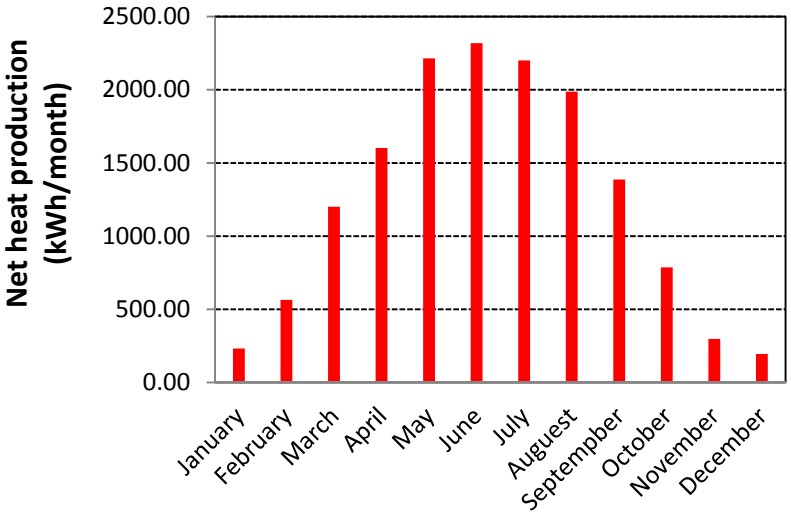

Figure 3-23 Monthly heat (kWh´s) of the solar-driven carbon dioxide power system in one year (at 120 bar gas heating pressure)

One can see that for Swedish climate conditions, the proposed system can work from March to September and reaches both the maximum power and maximum hot water production in June. Over the whole year, the maximum daily power production is about 12 kWh and the maximum monthly power

production is about 215 kWh. Furthermore, the annual average thermal efficiency for power production is 8%. For the hot water production, the maximum daily thermal energy production is about 112 kWh and the maximum monthly thermal energy production is about 2320 kWh.

Figure 3-24 and Figure 3-25 show the influences of the expansion machine's isentropic efficiency and gas heating pressure on the power production system performance. It can be seen from the figures that the efficiency of the expansion machine will have a great influence on the power production system performance. Furthermore, for a certain expansion inlet temperature, there is an optimum gas heating pressure. However, the selection of the gas heating pressure should also consider the material of the solar collector and the annual temperature change of supercritical CO_2 at the expansion inlet.

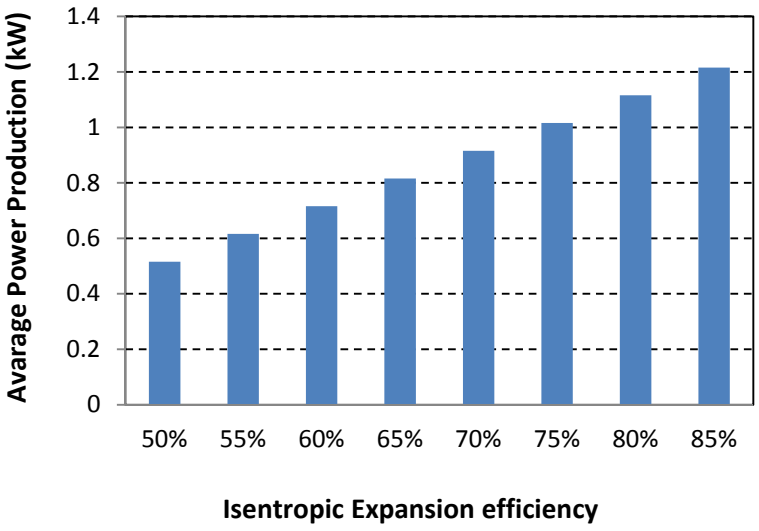

Figure 3-24 Daily average power production of solar-driven carbon dioxide power system at different expansion isentropic efficiencies

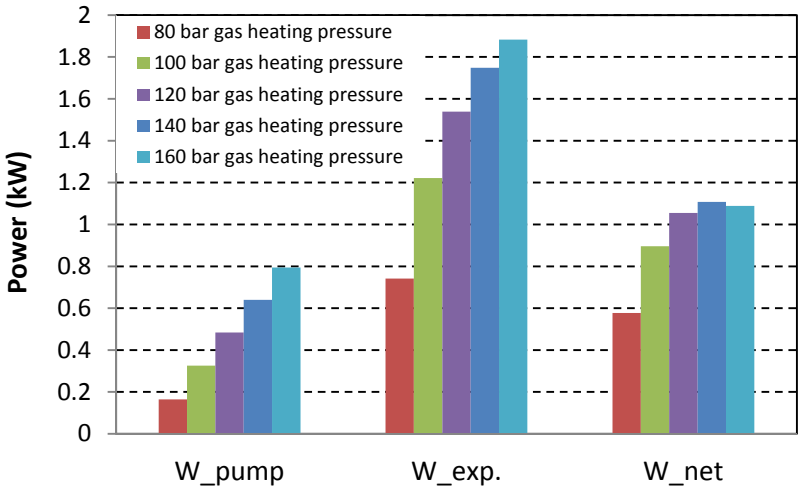

Figure 3-25 Daily average power production of solar-driven carbon dioxide power system at different gas heating pressures

By defining the relative thermal efficiency improvement for the system by Equation 3-5, the influence of IHX's effectiveness on system power output and the relative thermal efficiency improvements can be plotted (Figure 3-26). The results indicate that the system thermal efficiency can be increased by inserting an IHX, and the maximum increase of thermal efficiency with a thermodynamically ideal IHX can reach about 50%.

$$\text{Thermal efficiency improvement} = \frac{\eta_{IHX} - \eta_{withoutIHX}}{\eta_{withoutIHX}} \quad \textit{Equation 3-5}$$

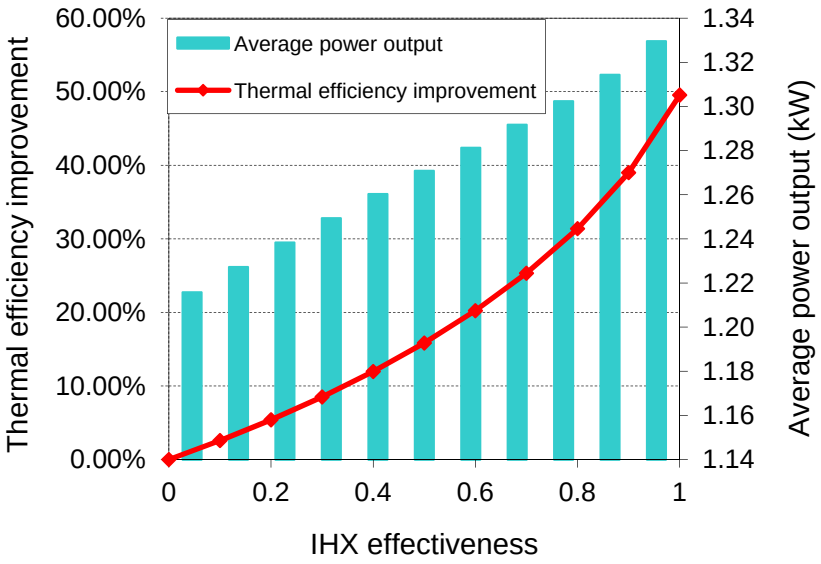

Figure 3-26 Solar-driven carbon dioxide power system power output and thermal efficiency improvement vs. IHX effectiveness (results calculated for the same day that chosen for Figure 3-18)

A simple economic analysis was also conducted to show the economic aspects of the solar-driven CO_2 power system. The simulation results show that the simulated system will have a payback time around 12 years, which can be further shortened if the system is under mass production or being used in a hot climate region, where much higher solar energy is available.

3.3 Summary

In this chapter, the basic working conditions of the three proposed carbon dioxide power cycles, namely carbon dioxide transcritical power cycle, carbon dioxide Brayton cycle and carbon dioxide cooling and power combined cycle, are specified.

To utilize the energy in low-grade heat sources (i.e. heat source with low available temperatures), a carbon dioxide transcritical power cycle will be more preferable due to its higher thermal

efficiency than the carbon dioxide Brayton cycle with the same heat sink condition. When utilizing the energy in waste heat (e.g. engine exhaust gasses), a carbon dioxide Brayton cycle and carbon dioxide cooling and power combined cycle will be of interest.

The simulation results of basic cycle performances show that the carbon dioxide transcritical power cycle has an optimum gas heater pressure for a certain cycle working condition. The efficiency of expansion units will have more crucial impact on the cycle efficiency than the efficiencies of compression units. Due to the character of the cycle, an Internal Heat Exchanger (regenerator) is very crucial to improving the cycle performance, if power is sought.

For the carbon dioxide Brayton cycle and the power part of carbon dioxide cooling and power combined cycle, there is both an optimum gas heater pressure and an optimum gas cooler pressure for a certain cycle working condition.

For the applications of carbon dioxide power systems:

A carbon dioxide double loop system is proposed and its performance has been simulated. The results show that by utilizing the energy in a low-grade heat source, the proposed carbon dioxide double loop system can improve the cooling COP of a carbon dioxide cooling system by 34 %.

For the proposed carbon dioxide cooling and power combined systems, the COP of the basic carbon dioxide cooling system can be improved by 40% by utilizing the energy in the exhaust gas of truck engines.

The performance of a solar driven carbon dioxide power system in the Swedish climate has been simulated in detail by dynamic simulations.

The daily simulation results for a typical Swedish summer day (15th of July) show that the system can achieve 8% average thermal efficiency and 1.2 kW average power productions during the system working period. At the same time, the system can produce heat (hot water) with an average capacity of about 10 kW. The average temperature of the produced hot water is about 40 °C, which can be further increased by decreasing the water flow rate or by system modification. Annually, the system achieves both maximum power production and maximum thermal energy production in June. The maximum daily power production is about 12 kWh and maximum monthly power production is about 215 kWh. The maximum daily thermal energy production is about 110 kWh and the maximum monthly thermal energy production is about 2300 kWh.

A simple economic analysis is also conducted to show the economic aspects of the solar-driven CO_2 power system. The simulation results show that the simulated system will have a payback time around 12 years, which can be further shortened if the system is under mass production or being used in the hot climate region, where much higher solar energy is available.

4 Temperature Profiles in CO_2 Power System Heat Exchangers

4.1 Cp Variation and Its Influence on the CO_2 Power Cycle Temperature Profiles in the Heat Exchangers

As mentioned in previous chapters, carbon dioxide has a low critical temperature (31.1 °C), which allows the carbon dioxide power cycle to work either as a transcritical power cycle or a Brayton cycle depending upon the heat sink temperature. This means that at least part of the cycle will be located in the supercritical region.

The thermophysical properties of supercritical CO_2 will have sharp variations in the region close to its critical point, which is also the region where the heat receiving process of supercritical CO_2 takes place for a transcritical carbon dioxide power cycle. Therefore, the thermophysical properties of supercritical CO_2 need to be carefully examined, when analyzing the CO_2 transcritical power cycles, due to their significant influence on the performance of both the gas heater and the Internal Heat Exchanger (IHX) in the heat transfer processes. The specific heat (Cp), which is the main factor that influences the supercritical CO_2 temperature profile in the heat exchangers, is plotted as a function of temperature at different pressures in the following figure (Figure 4-8).

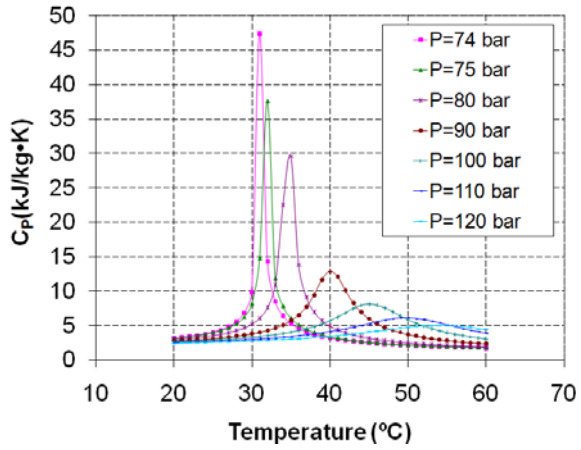

Figure 4-1 Specific heat of supercritical CO_2 vs. temperature at different pressures

It can be seen from the figure that the specific heat of supercritical CO_2 changes more obviously when the pressure approaches its critical level. Furthermore, it may also be noted that the temperature corresponding to the peak value of specific heat increases with increasing pressure.

Compared to the sharp variation in the Cp value of supercritical CO_2, the Cp variations of the low-grade heat source and the expansion outlet CO_2 are more modest.

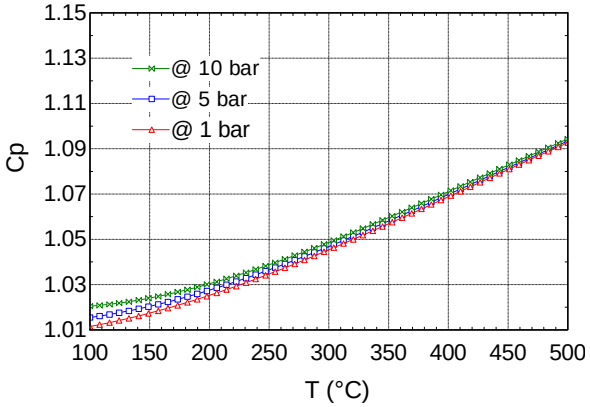

Figure 4-2 Specific heat of air vs. temperature at different pressures (note the scale difference from Figure 4-1)

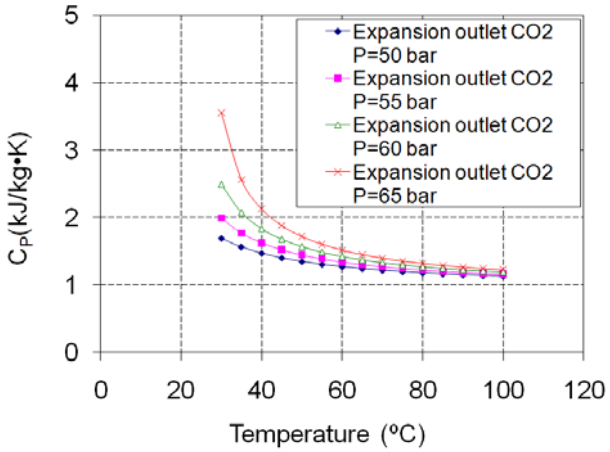

Figure 4-3 Specific heat of exhaust gas and expansion outlet carbon dioxide (note the scale difference from Figure 4-1)

A basic carbon dioxide transcritical power system is employed to show the influence of the Cp variation of supercritical CO_2 on the temperature profiles of CO_2 system heat exchangers. The schematic layout of the basic carbon dioxide power system is shown in Figure 4-4 and the assumptions of system working conditions and heat source conditions are listed in Table 4-1 and Table 4-2 respectively.

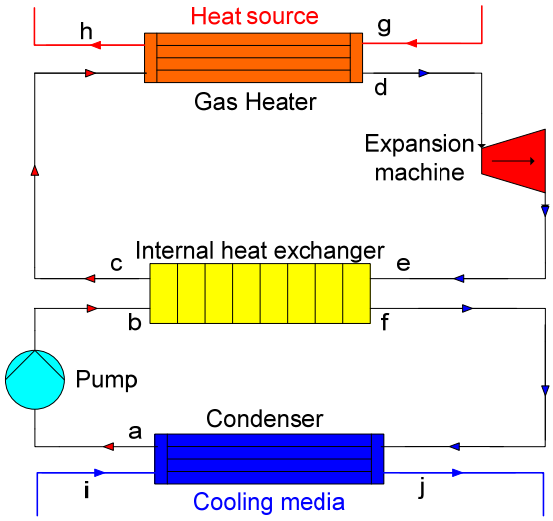

Figure 4-4 Schematic layout of a basic carbon dioxide CO_2 power system

Table 4-1Carbon dioxide transcritical power cycle operating conditions

Items	Value	Unit
Gas heater pressure	100	bar
Condenser pressure	60	bar
Expansion inlet temperature	Related to the heat source temp.	°C
Condensing temperature	22	°C
Pump efficiency	0.8	—
Expansion efficiency	0.7	—
Gas heater effectiveness	0,9	—
IHX effectiveness	0,9	—

Table 4-2 Heat source (exhaust gas) data

Items	Value	Unit
Exhaust gas mass flow	0,4	kg/s
Exhaust gas inlet temperature	150	°C

A Cp-Δh chart is plotted for the integrated total heat exchanger[15] length, which includes both IHX and the gas heater[16] to show the specific heat variations of all the working fluids (i.e. supercritical CO_2, expansion outlet carbon dioxide and the exhaust gas) along the heat exchangers for a certain cycle working condition (Figure 4-5). It can be seen from the figure that for the IHX part, the Cp of the incoming supercritical CO_2 (point b) is higher than the Cp of the outgoing expansion outlet carbon dioxide (point f) at one end of the IHX, and this difference increases rapidly along the IHX until it reaches a high value at the other end, where the supercritical CO_2 flows out (point c) and the expansion outlet carbon dioxide comes in (point e).

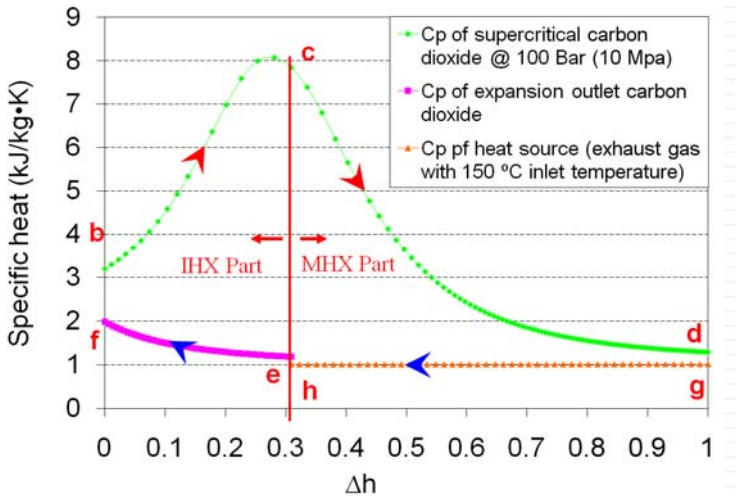

Figure 4-5 Cp —Δh chart for supercritical CO_2, expansion outlet carbon dioxide and heat source for the integrated total heat exchanger length

For the gas heater part, a reverse trend is shown. After being preheated in the IHX, supercritical CO_2 enters the gas heater (point c) with a much higher Cp than the outgoing heat source

[15] All the heat exchangers analyzed in this chapter refer to counter flow heat exchangers.

[16] Labeled as Main Heat Exchanger (MHX) in the diagrams

(exhaust gas, point h), then the difference decreases rapidly along the gas heater until it reaches a very small value on the other end of the gas heater, where the inlet of the heat source (exhaust gas, point g) and the outlet of the supercritical CO_2 (point d) are located.

Due to the difference in Cp variations, the temperate profiles in both MHX and IHX will be influenced. T-Δh charts for the integrated total heat exchanger length (MHX and IHX) with different CO_2 mass flow rates are plotted in the following figures to show this influence (Figure 4-6 a and b)[17]. From the figures, one can see that except for a short increase when supercritical CO_2 first enters the IHX (point b), the temperature profile of supercritical CO_2 in the IHX is fairly flat due to the sharp increase of its Cp (point b-point c). When it flows further through the gas heater (point c – point d), the temperature of supercritical CO_2 will increase rapidly due to the sharp decrease of its Cp value (see Figure 4-5).

This characteristic provides the carbon dioxide transcritical power cycle with more advantages in low-grade heat source recovery than power cycles using other working fluids. Due to the sharp increase of its Cp value in the IHX, the supercritical CO_2 can recover a substantial amount of energy from the expansion outlet (point e to point f in Figure 4-6) without an obvious increase in its temperature (point c). Therefore, after recovering a significant amount of energy from the expansion outlet, the supercritical CO_2 still has a huge potential to further recover the energy in low-grade heat source when it enters the gas heater. Consequently, the specific energy content of supercritical CO_2 will be higher, and thus a lower mass flow can be achieved compared to the working fluids that do not have this characteristic of Cp variation.

[17] The state points correspond to points in figure 2

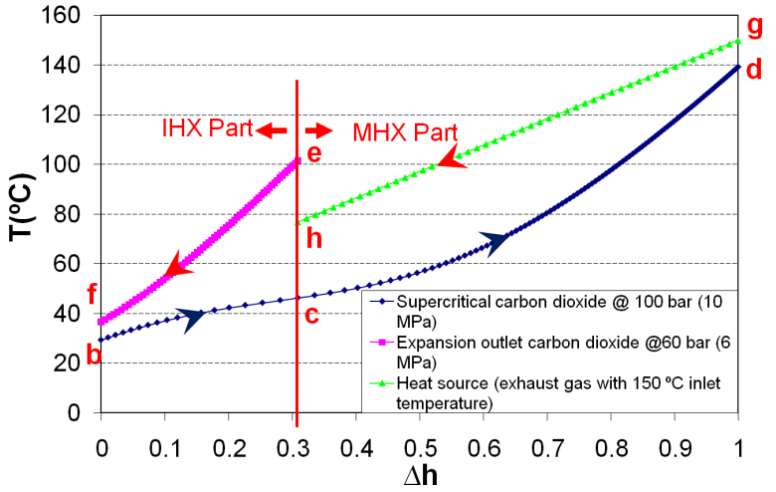

(a)

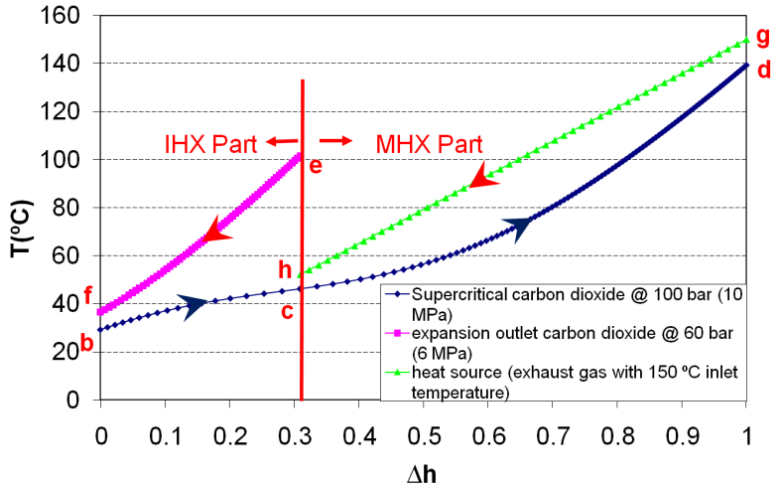

(b)

Figure 4-6 Integrated heat exchanger's T--ΔH chart of carbon dioxide transcritical power cycle with different mass flow rates of supercritical CO_2 (a): m_{CO2}=0.1 kg/s, $m_{exhaust\ gas}$=0.4 kg/s, IHX effectiveness=0.9, MHX effectiveness =0.9 (b): m_{CO2}=0.2 kg/s, $m_{exhaust\ gas}$=0.4 kg/s, IHX effectiveness=0.9, MHX effectiveness =0.9

4.2 Comparison between a Typical CO_2 Power and a Typical ORC Cycle

The benefit of Cp variation in supercritical CO_2 for the carbon dioxide transcritical power cycle in low-grade heat source recovery (i.e. better temperature matching) can be showed more obviously, if a comparison is made with other working fluids. A T-Δh chart of the integrated total heat exchanger length for an ORC (without superheating) using R123 as a working fluid is plotted for the same heat source condition as that used for the CO_2 power cycle analysis (Figure 4-7). For the R123 ORC, part of the working fluid heating process takes place in the subcritical region as boiling (i.e. constant temperature) and does not have Cp variation during the heating process as supercritical CO_2 does. It can be seen from the figure that R123 will have more temperature lift in the IHX than supercritical CO_2, due to its relatively linear Cp change. Furthermore, due to its boiling process, pinching will also appear in the MHX, which leads to the consequence that only a very limited amount of energy in the heat source can be utilized.

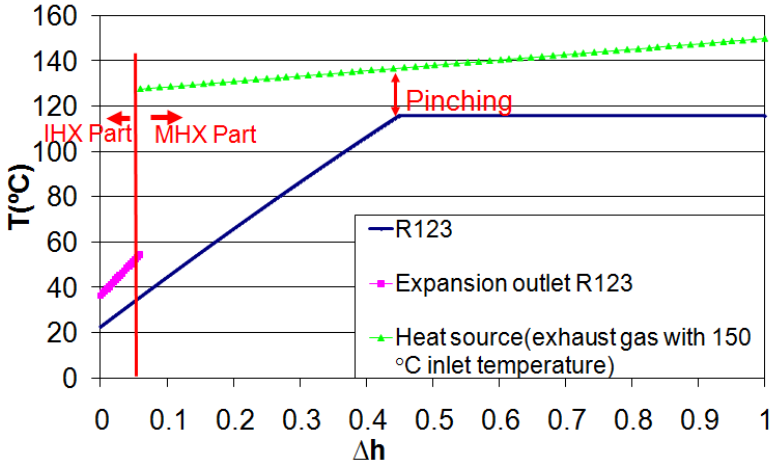

Figure 4-7 Integrated heat exchanger T-Δh chart of R123 ORC. m_{R123}=0.15 kg/s, $m_{exhaust\ gas}$=0.4 kg/s, IHX effectiveness =0.9, MHX effectiveness =0.9 (the process in the figure does not include the superheating of vapor)

4.3 The Importance of the Temperature Profile Matching

The reason that the matching between the heat source temperature profile and the working fluid temperature profile is so important when utilizing the energy in low-grade heat source or waste heat can be further explained by a simple example. A "typical" cycle (Carnot cycle) with a varying heat source temperature and a constant heat sink temperature of 293 K is employed for this example, which is schematically shown in Figure 4-8

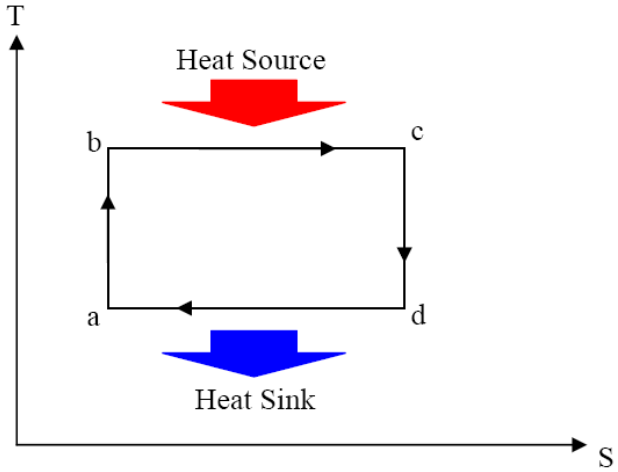

Figure 4-8 Schematic illustration of a typical cycle— Carnot cycle

As show in Figure 4-8, the "typical" cycle consists of the following processes:

- a to b: Isentropic compression
- b to c: Isothermal heat supply
- c to d: Isentropic expansion
- d to a: Isothermal heat rejection

The thermal efficiency of the cycle will then be:

$$\eta = \frac{W_{output}}{Q_{input}} = 1 - \frac{T_{da}}{T_{bc}} \qquad \textit{Equation 4-1}$$

but since $T_{bc} = T_{source} - \Delta T$ and $T_{da} = T_{sink} + \Delta T$ we get:

$$\eta = 1 - \frac{T_{\text{sink}} + \Delta T}{T_{source} - \Delta T} \qquad \textit{Equation 4-2}$$

The calculated cycle efficiency is illustrated in Figure 4-9, from which one can see that the cycle with the smaller temperature differences, ΔT, in the heat exchangers will achieve a higher efficiency. Furthermore, the temperature difference plays a more important role at low heat source temperatures than at high heat source temperatures. For example, at a heat source temperature of 360 K, the cycle with ΔT = 10 K in both heat exchangers achieves almost two times higher efficiency than the cycle with ΔT = 20 K. By contrast, at 440 K heat source temperature, the cycle with ΔT = 10 K in both heat exchangers only achieves an efficiency of 1.2 times that of the cycle with ΔT = 20 K. Therefore, the better heat source matching characteristics of CO_2 make this cycle more interesting for the utilization of energy in low-grade heat sources.

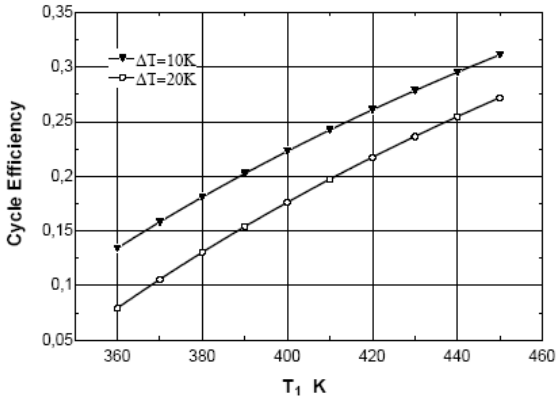

Figure 4-9 Cycle efficiency with varying heat source temperatures and a constant heat sink temperature (293 K) for different temperature differences in the two heat exchangers (gas heater and condenser)

The discussions above show that the temperature profile matching between the working fluid temperature profile and the heat source temperature profile is crucial for the cycle to achieve a good performance when utilizing the low-grade heat source and waste heat.

4.4 Summary

In this chapter, the Cp variation of supercritical CO_2 and its influence on the temperature profiles in CO_2 power system heat exchangers have been analyzed.

The simulation results show that the Cp of supercritical CO_2 will have dramatic variations in the region close to its critical point. The differences in the trends of Cp variations of supercritical CO_2, expansion outlet CO_2 and the heat source will influence the temperature profiles in the system heat exchangers. This influence will create a concave-shaped temperature profile in the system heat exchanger, which enables CO_2 transcritical power cycle to achieve a better temperature profile matching than conventional power cycles used in low-grade heat source recovery with other working fluids (e.g. R123 in ORC).

Due to the shape of its temperature profile, the CO_2 gas heater can achieve its minimum temperature difference at the end of the heat exchanger to avoid pinching. At the same time, the "driving force" for heat transfer to take place (i.e. the temperature difference) can still be maintained inside the heat exchanger. For the CO_2 system with internal heat exchangers, the temperature profile also enables supercritical CO_2 to recover energy in the expansion outlet CO_2 substantially without an obvious temperature increase, before it enters the gas heater to further recover the energy in low-grade heat source effectively.

5 Second Law Thermodynamic Analysis

Second law thermodynamic analysis has become more and more popular in energy system analysis, since it gives a clearer picture of the system performance and its losses.

A second law analysis has also been performed for the proposed carbon dioxide transcritical power system in this study to show the possible system losses and the potential for improving the system performance. The basic carbon dioxide power system that is described in previous chapters can be employed for this analysis (Figure 5-1).

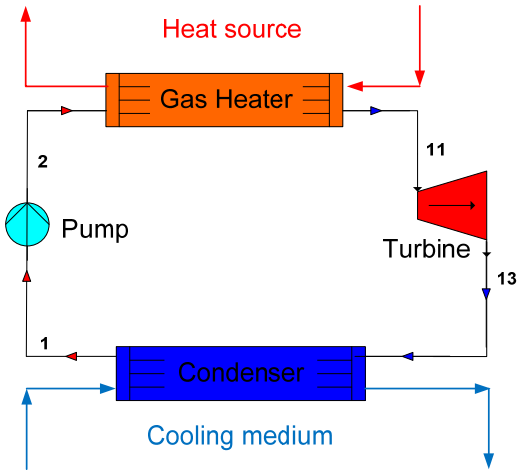

Figure 5-1 schematic layout of the basic carbon dioxide power system

5.1 Exergy and Entropy Calculations

The exergy concept as one of the main interests in second law system analysis can help to locate the system non-idealities by showing the significance of system components in system exergy destruction. The exergy destruction of each system component can be calculated by the following equation generally:

$$\Delta\emptyset = \varphi_{supplied} - \varphi_{recovered} \qquad \textit{Equation 5-1}$$

where

$$\varphi = (h - h_0) - T_0(s - s_0) \qquad \textit{Equation 5-2}$$

In the equation above, h_0 and S_0 are the enthalpy and entropy respectively at the reference temperature (environmental temperature). Based on Equation *5-1* and Equation 5-2, the exergy destruction in different CO_2 power system components can then be calculated as follows(
Equation 5-3 — Equation 5-6):

$$\Delta\emptyset_{gh} = \dot{m}_{gas}(\varphi_{gasin} - \varphi_{gasout}) - \dot{m}_{co_2}(\varphi_{11} - \varphi_2) \qquad \textit{Equation 5-3}$$

$$\Delta\emptyset_{gc} = \dot{m}_{co_2}(\varphi_{13} - \varphi_{22}) - \dot{m}_{wgc}(\varphi_{wgco} - \varphi_{wco}) + \dot{m}_{co_2}(\varphi_{22} - \varphi_1) - \dot{m}_{wc}(\varphi_{wco} - \varphi_{wci}) \qquad \textit{Equation 5-4}$$

$$\Delta\emptyset_p = \dot{m}_{co_2}(h_2 - h_1 - (\varphi_2 - \varphi_1)) \qquad \textit{Equation 5-5}$$

$$\Delta\emptyset_{exp} = \dot{m}_{co_2}(\varphi_{11} - \varphi_{13} - (h_{11} - h_{13})) \qquad \textit{Equation 5-6}$$

The exergy efficiency of the cycle can then be defined as Equation 5-7:

$$\eta_{exg} = 1 - \frac{\sum \Delta\emptyset}{\dot{m}_{gas} \cdot \varphi_{in}} \qquad \textit{Equation 5-7}$$

Furthermore, as an alternative calculation of exergy in second law thermodynamic analysis, the entropy generation for each component can also depict a clear picture of the distribution of

the irreversibility generated by each component that influences the system performance.

The entropy generation by each system component can be expressed by the following equations:

$$\delta_{s,gh} = \frac{Q_{gas}}{T_{evh}} - \frac{Q_{gas}}{T_{a,gas}} \qquad \textit{Equation 5-8}$$

in which

$$T_{a,gas} = \frac{h_{gas\ in} - h_{gas\ out}}{s_{gas\ in} - s_{gas\ out}} \qquad \textit{Equation 5-9}$$

$$\delta_{s,c} = \frac{Q_{gc}}{T_{a,w,gc}} - \frac{Q_{gc}}{T_{a,gc}} + \frac{Q_c}{T_{a,w,c}} - \frac{Q_c}{T_{a,c}} \qquad \textit{Equation 5-10}$$

in which

$$T_{evh} = \frac{h_{11} - h_2}{s_{11} - s_2} \qquad \textit{Equation 5-11}$$

$$T_{a,w,gc} = \frac{T_{w,o} + T_{w,s}}{2} + 273 \qquad \textit{Equation 5-12}$$

$$T_{a,w,c} = \frac{T_{w,i} + T_{w,s}}{2} + 273 \qquad \textit{Equation 5-13}$$

$$T_{a,gc} = \frac{h_{13} - h_{22}}{s_{13} - s_{22}} \qquad \textit{Equation 5-14}$$

$$T_{a,c} = \frac{h_{22} - h_1}{s_{22} - s_1} \qquad \textit{Equation 5-15}$$

$$\delta_{s,p} = s_2 - s_1 \qquad \textit{Equation 5-16}$$

$$\delta_{s,exp} = s_{13} - s_{11} \qquad \textit{Equation 5-17}$$

$$\delta_{s,total} = \delta_{s,gh} + \delta_{s,c} + \delta_{s,p} + \delta_{s,exp} \qquad \textit{Equation 5-18}$$

Based on the equations above, the contribution from each component to the total system entropy generation can be expressed as below:

$$C_{gh} = \frac{\delta_{s,gh}}{\delta_{s,total}} \qquad \textit{Equation 5-19}$$

$$C_c = \frac{\delta_{s,c}}{\delta_{s,total}}$$ *Equation 5-20*

$$C_p = \frac{\delta_{s,p}}{\delta_{s,total}}$$ *Equation 5-21*

$$C_{exp} = \frac{\delta_{s,exp}}{\delta_{s,total}}$$ *Equation 5-22*

5.2 Simulation Assumptions

The following general assumptions are made for the thermodynamic analysis of the carbon dioxide transcritical power system:

- The heat source is assumed to have an available temperature of 160 °C and a mass flow rate of 10kg/s
- The cycle is considered to work at steady state
- Pressure drops in the heat exchangers are neglected
- Isentropic efficiencies of the pump and the expansion machine are assumed to be 0.85 and 0.8 respectively and the mechanical efficiency is assumed to be 0.95 for both
- The pinching in the condenser is assumed to be 5 °C
- The condensing pressure and gas heater pressure are assumed to be 60 bar and 120 bar respectively
- The cooling water inlet temperature is assumed to be 15°C
- The set value for the water outlet temperature from the gas cooler is 50 °C

5.3 Simulation Results and Discussion

Maintaining other simulation assumptions constant, while changing heat source mass flow rate, the exergy destruction, entropy generation as well as the mean temperature difference and pinch temperature in the gas heater and gas cooler respectively are plotted against CO_2 mass flow rate (Figure 5-1 and Figure 5-2).

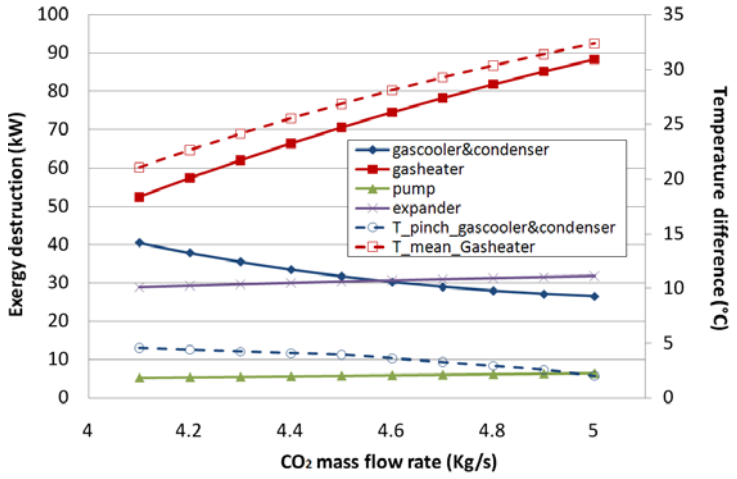

Figure 5-2 Exergy destruction vs. CO_2 mass flow rate

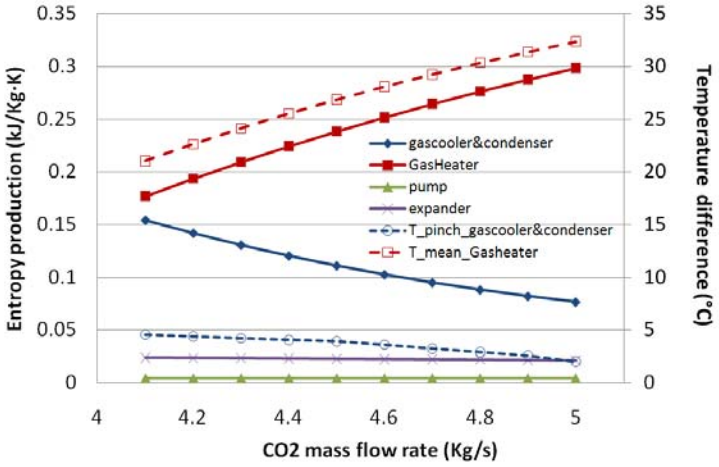

Figure 5-3 Entropy generation vs. CO_2 mass flow rate

It can be seen from the figures that the exergy destructions and entropy generations are almost constant in the pump and the expander. At the same time, they increase in the gas heater, but decrease in the gas cooler & condenser with an increasing CO_2 mass flow rate. Meanwhile, it can also be seen from the figures that the changes in exergy and entropy in the heat exchangers have close relations with the temperature matching as well. With an increasing mean temperature difference in the gas heater and a decreasing pinch temperature in the gas cooler & condenser, the exergy destruction and entropy generation increase in the gas heater, while decreasing in the gas cooler & condenser respectively.

Figure 5-4 shows the change in the distribution of entropy generations in the system with increasing CO_2 mass flow rate. It can be seen from the figure that distribution of entropy generation increases in the gas heater, while decreasing in the gas cooler & condenser and almost constant in the pump and the expander.

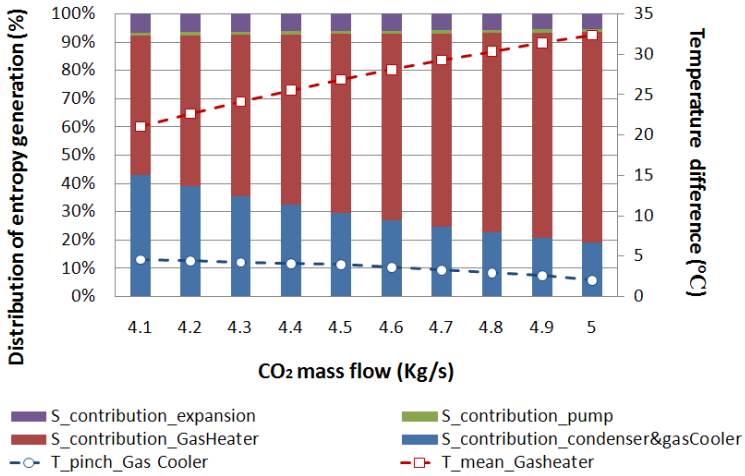

Figure 5-4 Distribution of entropy generation vs. CO_2 mass flow rate

Figure 5-5 and Figure 5-6 show the exergy destruction and entropy generation in different system components against an

increasing system high pressure side pressure, while maintaining other simulation assumptions constant. It can be seen from the figures that the exergy destructions and entropy generations increase in both the pump and the expander. As mentioned previously, the matching of the temperature profiles in the system heat exchangers has a crucial influence on their performance. With decreasing mean temperature difference in the gas heater and decreasing pinch temperature in the gas cooler & condenser, the exergy destructions and entropy generations also decrease in the system heat exchangers.

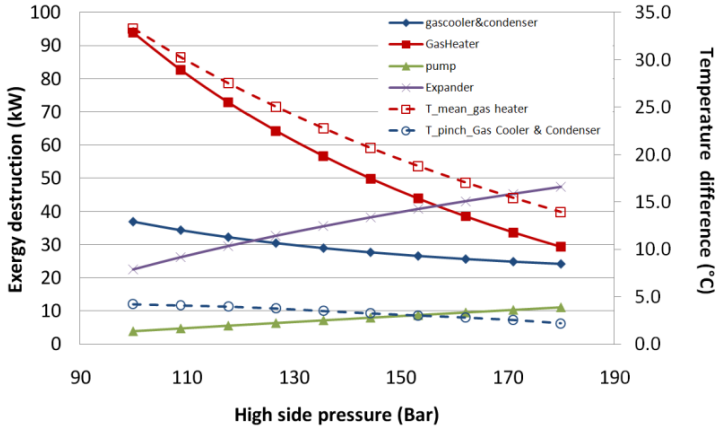

Figure 5-5 Exergy destruction vs. system high pressure side pressure

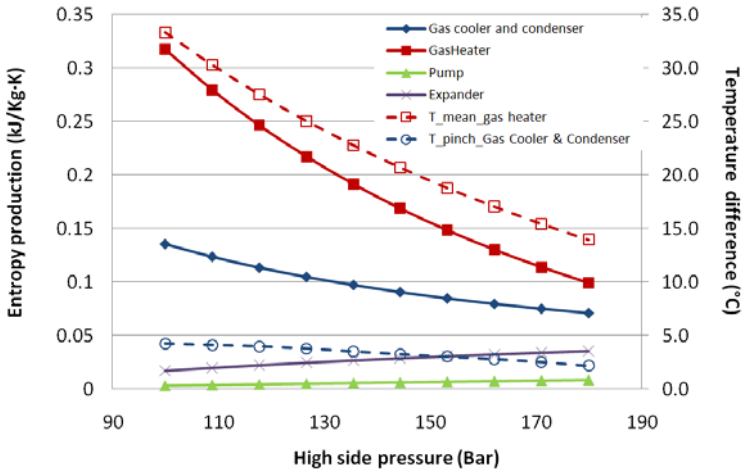

Figure 5-6 Entropy generation vs. system high pressure side pressure

Figure 5-7 shows the change in the distribution of entropy generation with an increasing system high pressure side pressure. Due to the dramatic decrease in entropy generation in the gas heater, the distribution of entropy generation in the gas heater decreases, while it increases in other system components.

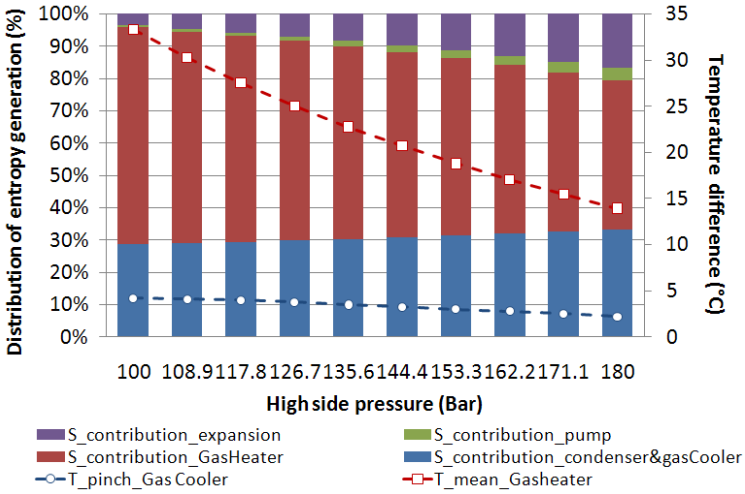

Figure 5-7 Distribution of entropy generation vs. system high pressure side pressure

Figure 5-8 and Figure 5-9 show the exergy destruction and the entropy generation in different system components against an increasing heat source temperature, while keeping other simulation assumptions constant. It can be seen from the figures that the exergy destruction and the entropy generation are almost constant in the pump and the expander, while increasing in the gas heater as well as in the gas cooler & condenser with the increasing heat source temperature at the gas cooler inlet. Furthermore, it can be noted from the figure that both the mean temperature difference in the gas heater and the pinch temperature in the gas cooler & condenser increase, while the increment is more obvious in the gas cooler & condenser. As a consequence, although the exergy destruction and the entropy generation increase in both gas heater and the gas cooler & condenser, the increments are more obvious in the gas cooler & condenser than in the gas heater.

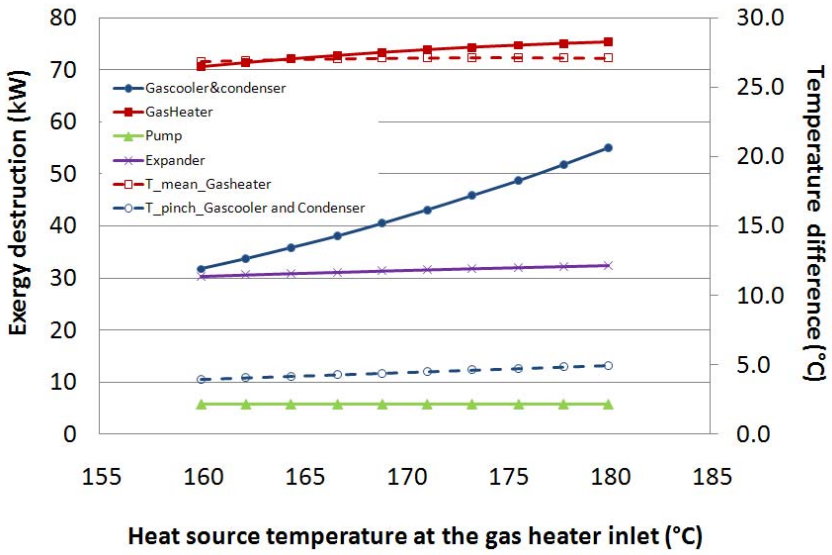

Figure 5-8 Exergy destruction vs. heat source temperature at the gas heater inlet

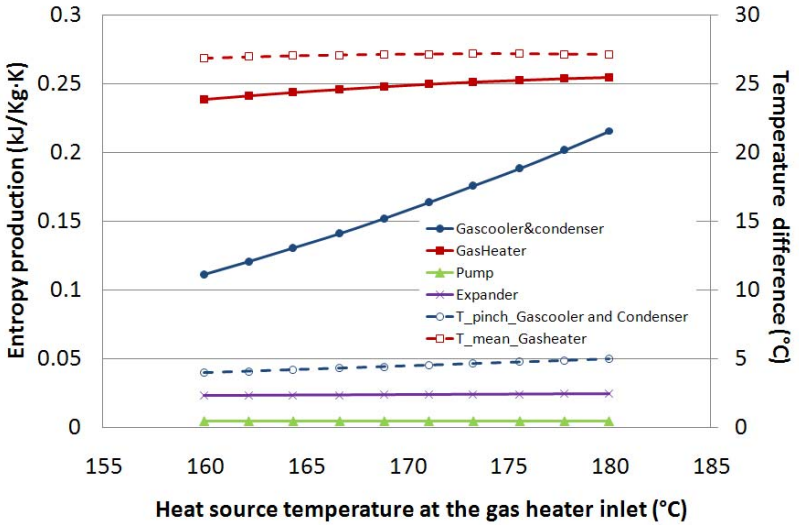

Figure 5-9 Entropy generation vs. heat source temperature at the gas heater inlet

Figure 5-10 shows the change in the distribution of entropy generation with an increasing heat source temperature at the

gas heater inlet. As shown in the figure, with the increasing heat source temperature at the gas heater inlet, the distribution of entropy generation increases in the gas cooler & condenser, while decreasing in the gas heater and almost constant in the pump and the expander.

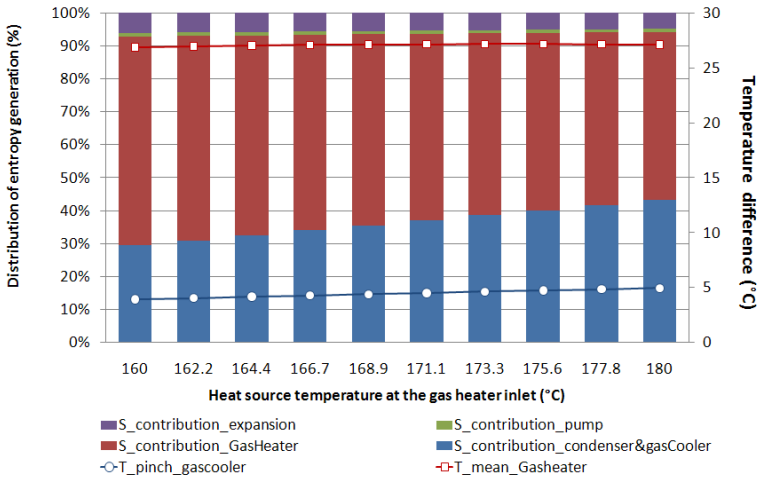

Figure 5-10 Distribution of entropy generation vs. heat source temperature at the gas heater inlet

Figure 5-11 to Figure 5-13 show the CO_2 power system exergy efficiencies and the mean temperature differences in the system heat exchangers against different system operating parameters and the results show that the system exergy efficiency will decrease with an increasing CO_2 mass flow rate, while it increases with an increasing system high pressure side pressure or an increasing heat source temperature at the gas heater inlet. Furthermore, the simulation results also indicate that the matching of the temperature profiles in the system gas heater may have a crucial influence on the system exergy efficiency.

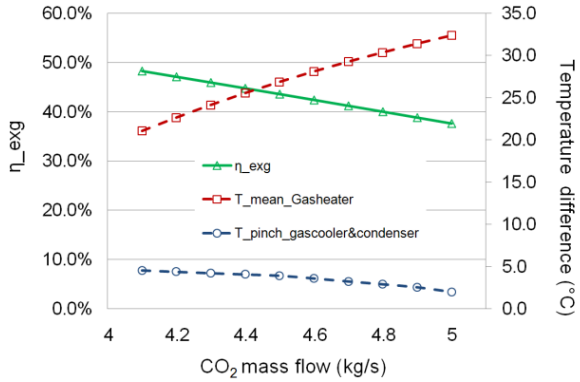

Figure 5-11 CO_2 power cycle exergy efficiency and the heat exchangers' min temperature differences vs. CO_2 mass flow rate

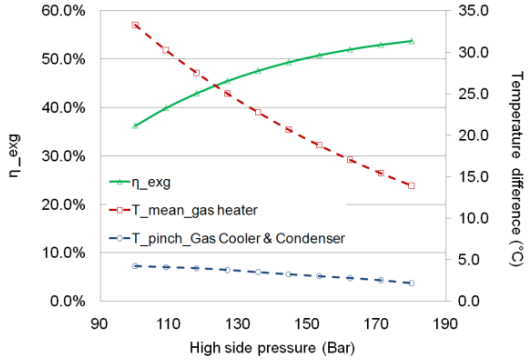

Figure 5-12 CO_2 power cycle exergy efficiency and the heat exchangers' min temperature differences vs. system high pressure side pressure

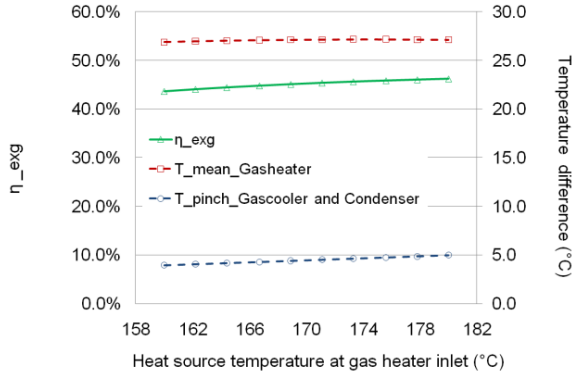

Figure 5-13 CO_2 power cycle exergy efficiency and the heat exchangers' min temperature differences vs. heat source temperature at gas heater inlet

5.4 Summary

In this chapter, second law analyses have been performed for the carbon dioxide transcritical power system to show the possible system losses and the potential for improvement. The exergy destruction and the entropy generation are calculated by varying one system operating factor at a time, while keeping other assumed system operating conditions constant.

Generally, the results show that the matching of the temperature profiles in the system heat exchangers will have crucial influence on the performance of the heat exchangers. The pressure ratio will be one of the main factors influencing the performance of the pump and the expander.

By plotting the distribution of entropy generations against different system operating parameters, it can be noted that the main system losses are from the system heat exchangers under the assumed system working conditions.

With an increasing CO_2 mass flow rate, the exergy destruction and entropy generation are almost constant in the pump and the expander. At the same time, they increase in the gas heater, but decrease in the gas cooler & condenser, due to the changes of the temperature profile matching in the heat exchangers. Meanwhile, the distribution of entropy generation increases in the gas heater, while decreasing in the gas cooler & condenser and almost constant in the pump and the expander.

If other system operating parameters are kept constant, but the system high pressure side pressure is increased, the exergy destruction and entropy generation will increase in the pump and the expander. Furthermore, due to the better matching of the temperature profiles in the system heat exchangers at higher system high pressure side pressures, their exergy destruction and entropy generation decrease. For the whole

system, the distribution of entropy generation decreases in the gas heater, while increasing in other components.
The simulation results with increasing heat source temperatures show that the increasing heat source temperature will have a minor influence on the exergy destruction and the entropy generation in the pump and the expander. However, the exergy destruction and entropy generation in the gas heater as well as in the gas cooler & condenser will increase with the increasing heat source temperature. At the same time, the increment will be less obvious in the gas heater, but more obvious in the gas cooler & condenser due to the influence of their temperature profile matching. For the distribution of entropy generation in the system, it will increase in the gas cooler & condenser, while decreasing in the gas heater and remaining almost constant in the pump and the expander.

Furthermore, by plotting the CO_2 power system exergy efficiencies and the minimum temperature differences in the system heat exchangers against different system operating parameters, it is found out that the system exergy efficiency will decrease with an increasing CO_2 mass flow rate, while it increases with an increasing system high pressure side pressure or an increasing heat source temperature. The simulation results also indicate that the matching of the temperature profiles in the system gas heater may have a crucial influence on the system exergy efficiency.

6 Conclusion and Suggestions for Further Work

6.1 Conclusion

In the current study, the potential of utilizing carbon dioxide power cycles in recovering energy in low-grade heat sources and waste heat has been investigated.

Two basic systems as carbon dioxide power system and carbon dioxide cooling and power combined system are proposed. The performance of the corresponding cycles as carbon dioxide transcritical power cycle, carbon dioxide Brayton cycle and carbon dioxide cooling and power combined cycle are studied. The influence of different cycle working parameters on the cycle performance is simulated by computer simulations. The simulation results show that there will be an optimum gas heater pressure for carbon dioxide power cycles at certain cycle working conditions. The optimum gas heater pressure will increase with increasing heat source temperature. Furthermore, the efficiency of the expansion machine will have more crucial influence on the cycle thermal efficiency than the pump efficiency does. For carbon dioxide Brayton cycles, there is also an optimum gas cooler pressure besides the optimum gas heater pressure for a certain cycle working condition. Moreover, the simulation results show that the carbon dioxide power cycle is highly regenerative, which makes the internal heat exchanger (regenerator) very important for the cycle if power production is sought.

For the applications of the carbon dioxide power system, a carbon dioxide double loop system and a solar-driven carbon dioxide power system are studied and discussed as examples.

For the carbon dioxide double loop system, the simulation results indicate that the proposed double loop system can improve the cooling COP of a carbon dioxide cooling system by 34 % by utilizing the energy in low-grade heat sources.

For the solar-driven carbon dioxide system, the system performance is simulated with Swedish climate data by dynamic simulation technique. The simulation results indicate that the solar-driven carbon dioxide power system has the potential for heat and power combined productions. The daily simulation results for a typical Swedish summer day (15th of July) show that the system can achieve about 9% average thermal efficiency and 1.2 kW average power productions during the system working period. At the same time, the system can produce heat (hot water) with an average capacity of about 10 kW. The average temperature of the produced hot water is about 40 °C, which can be further increased by decreasing the water flow rate or by system modification. Annually, the system achieves both maximum power production and maximum thermal energy production in June. The maximum daily power production is about 12 kWh and maximum monthly power production is about 215 kWh. The maximum daily thermal energy production is about 112 kWh and the maximum monthly thermal energy production is about 2320 kWh. Furthermore, a simple economic analysis of the system shows the payback time for the simulated system is about 12 years, which can be further shortened if the system is under mass production or being used in the hot climate region, where much higher solar energy is available.

The Cp variation of supercritical CO_2 and its influence on the temperature profiles in the heat exchangers of CO_2 power systems are also studied and compared with a typical Organic

Rankine Cycle with R123 as a working fluid. The simulation results show that the Cp variation of supercritical CO_2 will provide it with more advantages to be used as a working fluid in utilizing the energy in low-grade heat sources than conventional working fluids. This is mainly due to the concave-shaped temperature profile created in its system heat exchangers, which enables CO_2 transcritical power cycle to achieve a better temperature profile matching than power cycles with other commonly used working fluids (e.g. R123 in ORC) in low-grade heat source recovery. Consequently, pinching, which will normally be encountered in the heat exchangers of conventional power systems in low-grade heat source recovery, can be avoided. Furthermore, the Cp variation of supercritical CO_2 also enables it to recover the energy in both expansion outlet CO_2 and the low grade heat source efficiently.

Second law thermodynamic analyses have also been conducted for the carbon dioxide transcritical power system in the study. The influences of different system working parameters on the system irreversibilities and the system exergy efficiencies have been studied. The simulation results with an increasing CO_2 mass flow rate show that the exergy destruction and the entropy generation are almost constant in the pump and the expander. At the same time, they increase in the gas heater, but decrease in the gas cooler & condenser, due to the change of temperature profile matching in the system heat exchangers. Meanwhile, the distribution of entropy generation increases in the gas heater, while decreasing in the gas cooler & condenser and remaining almost constant in the pump and the expander. Furthermore, if one keeps other system working parameters constant, but increases the system high pressure side pressure, the exergy destruction and entropy generation will increase in the pump and expander, but decrease in the system heat exchangers, due to their better temperature profile matching at higher system high pressure side pressures. For the distribution of entropy generation, it decreases in the gas heater, while increasing in other system components. Moreover, the

simulation results with an increasing heat source temperature at the gas heater inlet show that the increasing heat source temperature will have minor influence on the exergy destruction and the entropy generation in the pump and the expander, but it will increase the exergy destruction and entropy generation in the system heat exchangers. With the increasing heat source temperature at the gas heater inlet, the distribution of entropy generation increases in the gas cooler & condenser, while decreasing in gas heater and remaining almost constant in the pump and the expander.

The simulation results of system exergy efficiency against different system working parameters show that the system exergy efficiency will decrease with an increasing CO_2 mass flow rate, while it increases with an increasing system high pressure side pressure or an increasing heat source temperature at the gas heater inlet. The simulation results also indicate that the matching of the temperature profiles in the system gas heater may have a crucial influence on the system exergy efficiency.

In general, this study shows that the proposed systems and cycles will be a new way to make use of previously unexploited energy sources, which could otherwise be difficult with traditional power cycles.

6.2 Suggestions for Further Work

In the last year of this study, more detailed studies of the system components such as the pump and the expanders have started. A CO_2 test rig has been built in the lab to test the CO_2 heat exchanger performance as well. Preliminary results have been obtained from both of these studies

With regard to further work, the detailed computer models of different system components should be calibrated with the experimental data. Then the models of the calibrated

components can be integrated into the system model and subsequently be connected to the dynamic simulation tools for dynamic system performance simulations. In such a way, the system performance with calibrated component performance can be studied for different applications and the study of the component performance in different system environments can be conducted as well.

Moreover, when the system components are all accessible in the future, the system performance should also be experimentally tested.

7 Nomenclature

Roman

A	Heat transfer area	m^2
A_{sc}	Solar collector area	m^2
b	The mean width of heat exchanger plate	mm
C	Contribution of entropy generation	%
c	The hot air flow length along the heat exchanger	m
CO_2	Carbon dioxide	-
COP	Coefficient of Performance	-
Cp	Specific heat	kJ/kg k
d	Heat exchanger tube diameter	mm
d_h	Hydraulic diameter	mm
Di	Diameter of the gas pipe	cm
EES	Engineer Equation Solver	-
Eff.	Efficiency/Heat exchanger effectiveness	%
ETC	Evacuated tube solar collector	-
F_R	Collector heat removal factor	-
$F_R(\tau\alpha)_e$	Average bliss coefficient	-
F_RU_L	Heat loss coefficient	-
G	Incident solar radiation	W/m^{-2}
GC	Gas Cooler	-
GH	Gas Heater	-
GWP	Global Warming Potential	-
Gz	Graetz number	-
h	heat transfer coefficient	W/m^2 K
h	Enthalpy	kJ/kg
IHX	Internal Heat Exchanger	-
k	Thermal conductivity	W/m K

L	Flow length	m
LMTD	Logarithmic Mean Temperature Difference	K
m	Mass flow rate	kg s^{-1}
MHX	Main Heat Exchanger	
Nu	Nusselt number	-
ODP	Ozone Depleting Potential	-
ORC	Organic Rankine Cycle	-
ORC	Organic Rankine Cycle	-
ORC	Organic Rankine Cycle	-
P	Power	kW
P_{cross}	Wet parameter of the cross section	m
Pr	Prandtl number	-
Q	Energy	kW
$Q_{cooling}$	Cooling capacity	kW
Q_{input}	Heat input	kW
Q_u	Useful energy gained from the solar collector	kW
Re	Reynolds number	-
s	distance between heat exchanger plates	mm
SC CO_2	Supercritical carbon dioxide	
Temp.	Temperature	ºC
U	Overall heat transfer coefficient	W/m^2 K
u	Velocity	m/s
V_{hx}	Heat exchanger volume	m^3
W	Work/power	kW
W_{exp}	Work from the expansion process	kW
W_{net}	Net work from the SC CO_2 cycle	kW
W_p	Work supply to the Pump	kW
$x_{,fd,h}$	Fully developed hydraulic length	m
V	Volume flow rate	m^3/s

Greek

η	Cycle efficiency	%

η_{exg}	Exergy efficiency	%
η_{IHX}	System thermal efficiency with internal heat exchanger	%
η_{sc}	Solar collector efficiency	%
η_{th}	Thermal efficiency	%
$\eta_{withoutIHX}$	System thermal efficiency without internal heat exchanger	%
$(\tau\alpha)_e$	Effective transmittance-absorbance product	-
Δh	Enthalpy difference	kJ/kg·K
φ	Specific exergy	kJ/kg
ϕ	Exergy	kW
ε	Effectiveness	%
β	Pressure ratio	-
δ	Tube thickness	mm
δs	Entropy generation	kJ/kg K
Δt	Temperature difference	K
ν	Kinematic viscosity	m^2/s
μ	Dynamic viscosity	kg/m s
α	Aspect ratio	

Subscript

a	Ambient/average
a-k	Cycle working points
a′-f′	Refrigeration cycle route point
basic	Basic refrigeration system
c	Condenser/Cold
comp	Compression
cooling	Combined cycle cooling part
double	Double loop system
e	Evaporator
evh	Equivalent heating
exp	Expansion /expander
gas	Heat source

gc	Gas cooling
gco	Gas cooler outlet
gh	Gas heater
g-h	Points for air properties
g-j	Points of heat source and heat sink condition
h	Hot
h-h′	Cooling media condition points
hs	Heat source
hx	Heat exchanger
i	Inlet/ In/ inside
in	Heat exchanger inlet
in	Inlet
is	Isentropic
m	Mechanical
net	Net power
new	The new cooling COP of the combined cycle
o	Out
o	Outside
opt	Optimum
out	Outlet
output	The power output the combined cycle power part
p	Pump
power	Combined cycle power part
T	Turbine
th	Thermal
w	Water

8 References

Angelino, G. (2006). Perspectives for the Liquid Phase Compression Gas Turbine. *ASME Paper,* no. 66-GT-111, 13-17.

ASHRAE Handbook .1993. Fundamentals. SI edition.

Baik, Y. J., Kim, M., Chang, K.C., Kim, S.J. (2011). Power-based performance comparison between carbon dioxide and R125 transcritical cycles for a low-grade heat source. *Applied Energy,* 88, 892–898.

Boewe, D.E., Bullard, C.W., Yin, J.M. and Hrnjak, P.S. (2001). Contribution of Internal Heat Exchanger to transcritical R-744 Cycle Performance. *HVAC&R Research*, vol. 7 no. 2.

Cayer, E., Galanis, N., Desilets, M., Nesreddine, H., Roy, P. (2009). Analysis of a carbon dioxide transcritical power cycle using a low temperature source. *Applied Energy* 86, 1055–1063.

Chang, H. (2002). Development of a Supercritical Carbon Dioxide Brayton Cycle: Improving PBR Efficiency and Testing Material Compatibility. *Idaho National Engineering and Environmental Laboratory* (INEEL).

Chen, H.j. , Goswami, D. Y., Stefanakos, E. K. (2010). A review of thermodynamic cycles and working fluids for the conversion of low-grade heat. *Renewable and sustainable energy reviews*, 14, 3059-3067.

Chen, Y., Lundqvist, P., Johansson, A., Platell, P. (2006). A comparative study of the carbon dioxide transcritical power cycle compared with an organic Rankine cycle with R123 as working fluid in waste heat recovery. *Applied Thermal Engineering*, 26, 2142–2147.

Chen, Y., Lundqvist, P., Platell, P. (2005). Theoretical research of carbon dioxide power cycle application in automobile industry to reduce vehicle's fuel consumption, Applied Thermal Engineering, 25, 2041–2053.

Chen, Y, Pridasaws, W., Lundqvist, P. (2010). Dynamic simulation of a solar-driven carbon dioxide transcritical power system for small scale combined heat and power production. *Solar Energy*, 84, 1103–1110.

Dekhtiarev, V. L. (1962). On designing a large, highly economical carbon dioxide power installation. *Elecrtichenskie Stantskii*, 5: 1-6.

DiPippo, R. (2004). Second Law assessment of binary plants generating power from low-temperature geothermal fluids. *Geothermics*, 33, 565–586.

Dostal, V., Driscoll, M. J., Hejzlar, P., Wang, Y. (2004). Supercritical CO_2 cycle for fast gas-cooled reactors. *ASME Turbo Expo*, Power for Land, Sea, and Air.

Energy in Sweden 2004, Report from Swedish Energy Agency.

European Forum for Renewable Energy Sources. (2003). http://www.eufores.org/index.php?id=30#_Toc106430664

Feher E. G. (1962). Supercritical Thermodynamic Cycles for External and Internal Combustion Engines. *Astropower*. Inc. Engineering Report.

Feher, E.G. (1967). The Supercritical thermodynamic power cycle. *Energy Conversion,* vol.8, 85-90

Fukuta, M., Yanagisawa, T., and Radermacher, R. (2003). Performance prediction of vane type expander for CO_2 cycle. *21st IIR Internal congress of refrigeration*. ICR0251.

Hafner, A. (2000). Experimental study on heat pump operation of prototype CO_2 mobile air conditioning system. *The Fourth IIR-Gustav Lorentzen Conference on Natural Working Fluids*, west Lafayette, 183–90.

Hahnemann, V. H., and Ehret, L. (1941). Der druckverlust der laminaren strömung in der anlaufstrecke von geraden, ebenen spalten, *Jahrbuch der deutschen Luftfahrtforschung.*

Huff, H.J., Radermacher, R., Preissner, M. (2003). Experimental Investigation of a Scroll Expander in a Carbon Dioxide Air-Conditioning System. *International Congress of Refrigeration*, ICR0485.

Hung, T.C. (2001). Waste heat recovery of organic Rankine cycle using dry fluids. *Energy Conversion and Management,* 42, 539-553.

Incropera, F.P. and DeWitt, D.P. (2001). *Fundamentals of Heat and Mass Transfer 5th edition*, ISBN 0-471-38650-2.

International Energy Outlook. (2010). http://www.eia.doe.gov/oiaf/ieo/world.html

Kauf, F. (1999). Determination of the optimum high pressure for trasncrtitical CO_2 refrigeration cycles, *International Journal of Thermal Sciences*, 38, 325-330.

Kays, W. M. (1955). Numerical Solutions for Laminar Flow Heat Transfer in Circular Tubes. *Trans. ASME*, 77, 1265–1274.

Kim, M-H., Pettersen, J., Bullard, C.W. (2004). Fundamental process and system design issues in CO_2 vapor compression systems. *Progress in energy and combustion science*, 30,119-174.

Klein, S.A. EES. (2004). Engineering Equation Solver, Klein, S.A. Editor. F-Chart Software: Madison

Klein, S.A., et al. TRNSYS 16. (2004). A TRaNsient SYstem Simulation program. Solar Energy Laboratory. Univ. of Wisconsin-Madison: Wisconsin

Lorentzen, G., Pettersen, J. (1992). New possibilities for non-CFC refrigeration. *IIR International Symposium on Refrigeration, Energy and Environment*, Trondheim, Norway. 147–63.

Liao, S.M., Zhao, T.S., Jakobsen, A. (2000). A correlation of optimum heat rejection pressures in transcritical carbon dioxide cycles. *Applied Thermal Engineering,* 20, 831-841.

Man, H. K., Jostein, P., Clark, W. B. (2004). Fundamental process and system design issues in CO_2 vapor compression systems. *Energy and Combustion Science,* 30, 119–174.

Nekså, P., Rekstad, H., Zakeri, G.R., Schiefloe, P.A. (1998). CO_2 heat pump water heater: characteristics, system design and experimental results. *International Journal of Refrigeration* 21 (3), 171–178.

Nickl, J., Will, G., Kraus, W.E. and Quack, H. (2003). Third generation CO_2 expander. *21st IIR Internal congress of refrigeration*. ICR0571.

Pettersen, J., and Aarlien, R. (1998). Progress in vapor compression systems. *Thermal science and engineering,* vol. 6, no1.

Rozhentsev, A., and Wang, C.C. (2001). Some design features of a CO_2 air conditioner. *Applied Thermal Engineering,* 21, 871-880.

Samer, S. (2008). Theoretical evaluation of trans-critical CO_2 systems in supermarket refrigeration. Part I: Modeling, simulation and optimization of two system solutions. *International Journal of Refrigeration,* 31, 516-524.

Samer, S. (2008). Theoretical evaluation of transcritical CO_2 systems in supermarket refrigeration, Part II: System modifications and comparisons of different solutions, *International Journal of Refrigeration,* 31, 525-534.

Scientific facts on Energy Technologies Scenarios to year 2050, http://www.greenfacts.org/en/energy-technologies/energy-technologies-greenfacts.pdf

Shah, R.K. et.al. (1991). *Heat Exchanger Engineering Volume 2—Compact Heat Exchangers,* In: E.A.Foumeny and P.J.Hegys**,** Ellis Horwood, ISBN 0-13-382391-1,1-27.

Silvia, M. (2011). Theoretical and experimental analysis of a CO_2 heat pump for domestic hot water. *International journal of refrigeration*, 34, 742-751.

Tadano, M., Ebara, T. and Oda, A. (2000). Development of the CO_2 hermetic compressor, *The 4th IIR-Gustav Lorentzen Conference on Natural Working Fluids at Purdue*, 323–330.

Thorin, E. (2000). Power cycles with ammonia-water mixtures as working fluid. *Doctoral Thesis. KTH.* ISRN KTH/KET/R-119-SE.

Tomoichiro, T., Yuuichi, Y., Fumitoshi, N. (2005). Experimental study on automotive cooling and heating air conditioning system using CO_2 as a refrigerant. *International Journal of Refrigeration*, 28 (2005) 1302–1307.

Wang, J.F., Sun, Z.X., Dai, Y.P., Ma, S.L. (2010). Parametric optimization design for supercritical CO_2 power cycle using genetic algorithm and artificial neural network. *Applied Energy*, 87, 1317–1324.

Yamaguchi, H., Zhang, X.R., Fujima, K., Enomoto, M., Sawada, N. (2006). Solar energy powered Rankine cycle using supercritical CO_2. *Applied Thermal Engineering*, 26, 2345–2354.

Yan, J. (1991). On thermodynamic cycles with Non-Azeotropic mixtures as working fluids. *Doctoral Thesis. KTH.* ISBN 91-7179-059-5.

Zha, S.T., Ma, Y.T. and Sun, X. (2003). The development of CO_2 expander in CO_2 transcritical cycles, *21st IIR Internal congress of refrigeration*, ICR0089.

Zhang, X.R., Yamaguchi, H. (2007). Experimental study on the performance of solar Rankine system using supercritical CO_2. Renewable Energy 32, 2617–2628

Zhang, X.R., Yamaguchi, H., Fujima, K., Enomoto, M., Sawada, N. (2007). Theoretical analysis of a thermodynamic cycle for power and heat production using supercritical carbon dioxide. *Energy*, 32, 591–599.

Zhang, X.R., Yamaguchi, H., Uneno, D., Fujima, K., Enomoto, M., Sawada, N. (2006). Analysis of a novel solar energy-powered Rankine cycle for combined power and heat generation using supercritical carbon dioxide. *Renewable Energy*, 31, 1839–1854.

Zhang, X.R., Yamaguchi, H., Uneno, D. (2007). Thermodynamic analysis of the CO_2-based Rankine cycle powered by solar energy. *International Journal of Energy*, 31, 1414–1424.

9 Appendix

9.1 Appendix 1— Safety Group Classifications (from IIR)

This classification consists of two alphanumeric characters (e.g. A2); the capital letter corresponds to toxicity and the digit to flammability.

9.1.1 Toxicity classification

Refrigerants are divided into two groups according to toxicity:

- Class A signifies refrigerants for which toxicity has not been identified at concentrations less than or equal to 400 ppm;
- Class B signifies refrigerants for which there is evidence of toxicity at concentrations below 400 ppm.

9.1.2 Flammability classification

Refrigerants are divided into three groups according to flammability:

- Class 1 indicates refrigerants that do not show flame propagation when tested in air at 21°C and 101 kPa;
- Class 2 indicates refrigerants having a lower flammability limit of more than 0.10 kg/m3 at 21°C and 101 kPa and a heat of combustion of less than 19 kJ/kg;

- Class 3 indicates refrigerants that are highly flammable as defined by a lower flammability limit of less than or equal to 0.10 kg/m^3 at 21°C and 101 kPa or a heat of combustion greater than or equal to 19 kJ/kg.

9.2 Appendix 2— Heat Exchanger Proposed for Heat Recovery in Engine Exhaust Gases

9.2.1 Description of the heat exchanger

One of the proposed carbon dioxide power system applications in this study is to utilize the energy in the exhaust gases of automobile engines (i.e. truck engines) to produce power to reduce the fuel consumption. In such applications, the pressure drop in the engine's exhaust gas pipe is very important and will have crucial influence on the engine performance. To be able to utilize the energy in the engine's exhaust gas, a special heat exchanger with low pressure drop on its airside as proposed by one of the project partners (i.e. Ranotor AB) is designed and studied in this project.

The designed exchanger is characterized as a countercurrent heat exchanger with laminar flow at its gas side. The advantages of this type of heat exchanger are: high power density (kW/m^3), low pressure drop and flexible installation. The shape of this type of heat exchanger is sketched in the following figures (Figure 9-1 and Figure 9-2).

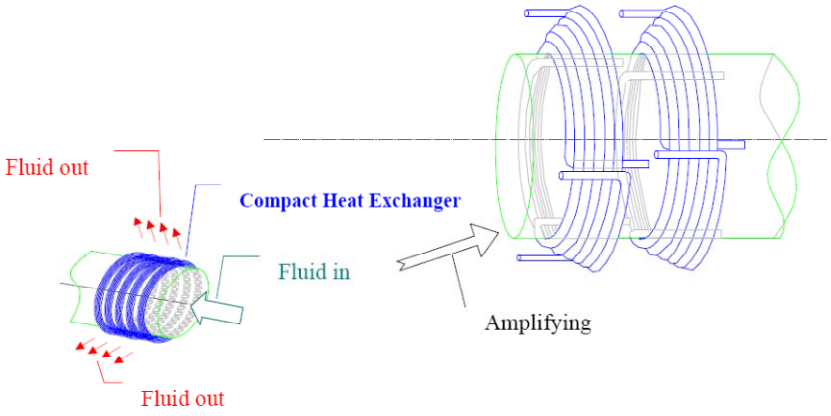

Figure 9-1 RANOTOR heat exchangers

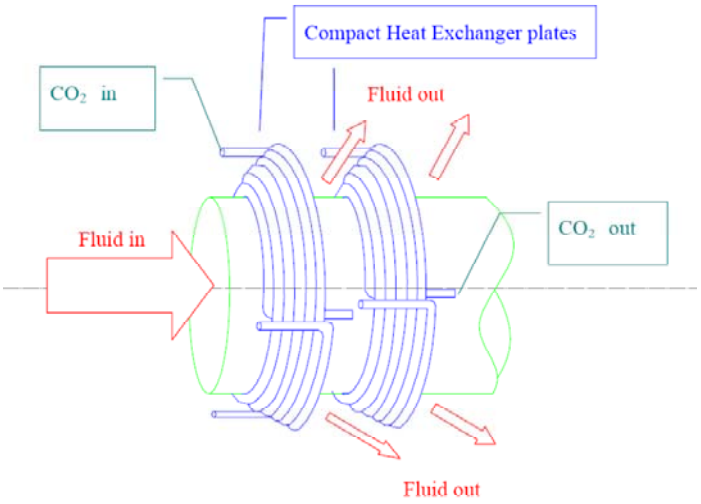

Figure 9-2 RANOTOR heat exchangers

As illustrated in Figure 9-1 and Figure 9-2, the heat exchanger is composed of a number of concentric conical plates, which are made up of several heat exchanger tubes, arranged in parallel. The distance between the heat exchanger plates is 1 mm. For each plate, there are three small diameter (1 mm) tubes placed one after another and bent to the concentric conical shape. Therefore, each heat exchanger plate has three inlets, which are placed on the front side. Carbon dioxide comes from a manifold and goes into the heat exchanger via the three inlets at the same time. After being heated up or cooled down, the exiting carbon dioxide will be collected at the back side of the heat exchanger by the other manifold. The heat source fluid (e.g. exhaust gas, steam, etc.) will flow through the center of the heat exchanger plate and spread out evenly through the aperture between each pair of heat exchanger plates.

9.2.2 Counter flow compact heat exchanger with laminar flow at the airside

According to the surface area density value, the heat exchangers can be divided mainly into three categories:

compact heat exchangers (surface area density above 700 m^2/m^3 on at least one fluid side, which usually has gas flow), laminar flow heat exchangers (surface area density above 3000 m^2/m^3) and micro heat exchangers (surface area density is above about 10000 m^2/m^3). The configurations of a compact heat exchanger are normally plate-fin, tube-fin and prime surface recuperators and compact regenerators. Basic flow arrangements of the two fluids are single-pass cross flow, counter flow and multipass cross-counter flow (R.K. Shah, 1991).

Based on the criteria described above, RANOTOR heat exchangers belong to the category of compact heat exchangers. The flow pattern in the heat exchanger may appear to be cross flow, but it is actually counterflow. This can be explained by the following drawings (Figure 9-3 and Figure 9-4). The left drawing in Figure 9-3 is the top view of one heat exchanger plate, and the one on the right is a schematic illustration to show the angels of the heat exchanger tubes on the heat exchanger plate. As shown in the figure, the heat exchanger plates are designed to have certain angles when bent. Therefore, the heat source fluid flow can be divided into two directions when crossing every small section of the heat exchanger tube (Figure 9-4). Along the X direction, there will be no heat transfer but only fluid flow, while along the Y direction heat transfer will take place. Thus, if one integrates along the tube to the total heat exchanger tube length, the heat exchanger will show the heat transfer characteristics of a perfect counterflow heat exchanger. Furthermore, the gas side fluid flow is designed to be laminar flow. Therefore, in general, the RANOTOR heat exchanger is characterized as a counterflow compact heat exchanger with laminar flow at the gas side.

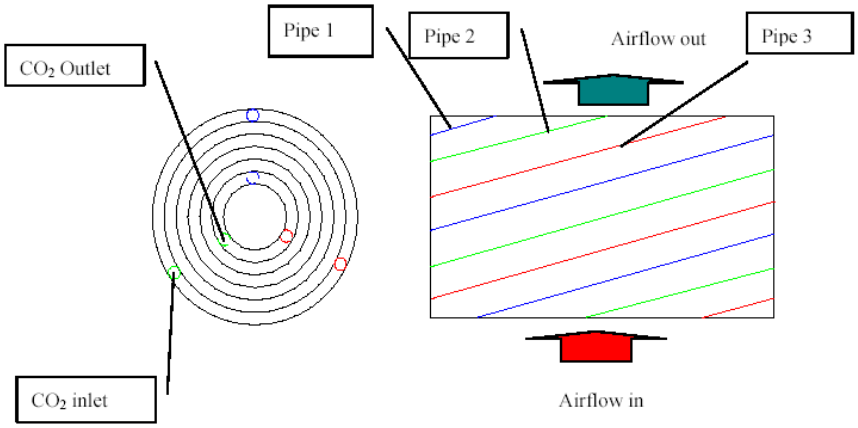

Figure 9-3 Schematic illustration of a RANOTOR compact heat exchanger

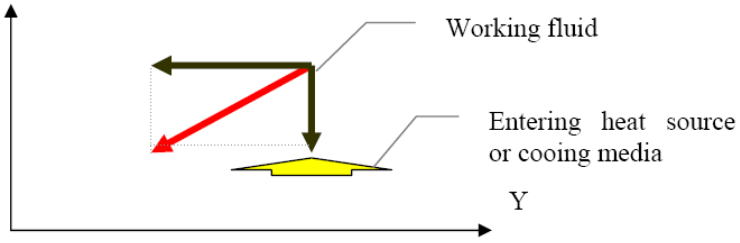

Figure 9-4 Schematic illustration of the flow scheme for a RANOTOR compact heat exchanger

9.2.3 Superiority of laminar flow

Traditionally, turbulent flow is desired in heat exchangers to achieve high heat transfer coefficients. However, for compact heat exchangers, a turbulent flow will require extremely high fan power and normally achieve lower heat transfer than laminar flow. Thus, laminar flow is more desirable for compact heat exchangers due to the fact that it achieves a higher heat transfer coefficient with a smaller heat exchanger volume and lower fan power compared with the turbulent flow. The reason

that laminar flow can achieve a higher heat transfer coefficient in compact heat exchangers can be explained as follows:

The heat transfer coefficient, h, can be expressed by Equation 9-1:

$$h = \frac{Nu \times k}{L_c} \qquad \text{Equation 9-1}$$

where

h — Heat transfer coefficient
Nu — Nusselt number
k — Thermal conductivity
L_c —Hydraulic diameter

For laminar flow, the Nusselt number will be constant for a certain geometry of a heat exchanger and k is constant for a certain fluid bulk mean temperature. Thus, the smaller the hydraulic diameter is, the higher the heat transfer coefficient will be. Therefore, when the hydraulic diameter is greatly reduced, an extremely high heat transfer coefficient can be expected although the flow is still in the laminar region.

The superiority of laminar flow is clearly illustrated in an example from the book Heat Exchanger Engineering (1991): For water at 310 K using k = 0.628 W/m·k and Pr = 4.62, h is shown as a function of the tube diameter (Figure 9-5). It can be seen that the heat transfer coefficient for a 20 mm diameter tube at $\mathrm{Re} = 10^4$ is the same as a 1 mm diameter tube in laminar flow. h is also the same for a 20 mm diameter tube at $\mathrm{Re} = 5 \times 10^4$ and a 0.3 mm diameter tube in laminar flow.

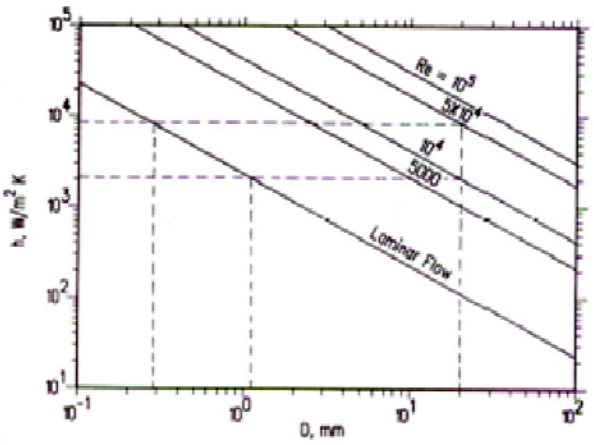

Figure 9-5 Superiority of laminar flow heat transfer coefficient vs. tube diameter (Shah, 1991)

9.2.4 Description of the heat exchanger calculation model

The concentric conical shape of the heat exchanger introduces more complexities for the inside (CO_2 side) heat transfer calculation. Due to the specific geometry of the heat exchanger, existing heat transfer correlations are not suitable to calculate the tube inside heat transfer for the current heat exchanger, except by employing very complicated numerical solutions. However, the overall objective of the current thesis is system design and validation instead of a detailed heat exchanger design; building up a complicated numerical model is, therefore, beyond the scope of the current work. Furthermore, considering the fact that compared with the CO_2 side heat transfer, the heat exchanger outside heat transfer is the dominating factor for the heat exchanger's heat transfer performance, only the dominant side (outside) heat transfer is calculated as a guideline for the preliminary heat exchanger design at the current stage.

According to the design, each heat exchanger plate is composed of three tubes. The flow of the outside fluid crosses the first

section of all three tubes at the same time, when reaching the first round of heat exchanger tubes. After passing the first round of tubes, the working fluid will flow further and pass the continued section of the three tubes in the same way. Consequently, the working fluid flow will pass all the sections of the three tubes until it passes the last round of heat exchanger tubes. For the outside heat transfer calculation, the module can be simplified by spreading the conically shaped heat exchanger plate into a trapezoid shape as shown in Figure 9-6. The airflow is indicated in the figure as an example of heat exchanger outside fluid flow and different colors symbolize different heat exchanger tubes. As shown in the figure, the incoming air will pass the first section of the three tubes at the same time, when it flows over the first round of heat exchanger tubes. After that, the air flow will then pass the second section of three tubes in the same way, when it crosses the second round of heat exchanger tubes. The air will keep flowing and cross the different loops of heat exchanger tubes continually, until it reaches the last section of tubes. For every loop, the CO_2 in each section of heat exchanger tubes is assumed to have the same conditions (i.e. the same temperature, the same heat transfer characteristics and pressure drop, etc.).

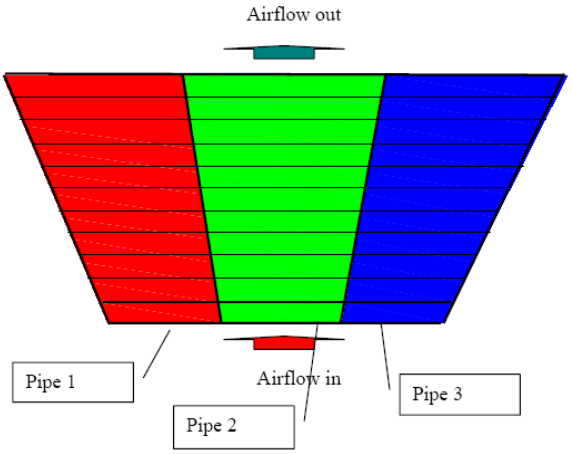

Figure 9-6 Heat exchanger calculation module, schematic 1

When calculating the heat transfer on the outside, due to the characteristics of the heat exchanger geometry, the fluid flow in the rectangular channel, with the channel width being much bigger than the channel height (b>>s), has been assumed as a simplified model for the heat exchanger preliminary design stage. The scheme is illustrated in the following figure (Figure 9-7):

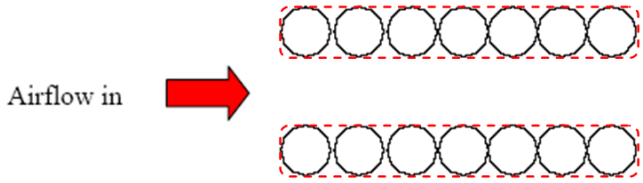

Figure 9-7 Illustration of heat exchanger outside gas flow (side view)

9.2.5 Basic correlations

The air mass flow can be calculated by the energy balance as shown below:

$$Q_{power} = \dot{m}_o \times Cp_o \times \Delta t_o \qquad \textit{Equation 9-2}$$

$$Q_{power} = \dot{m}_{CO_2} \times \Delta h \qquad \textit{Equation 9-3}$$

where Q_{power} denotes the heat input/output of the heat exchangers (gas cooler, condenser and gas heater), Δt_o is the heat exchanger outside fluid temperature change after passing the heat exchanger. Cp_o is the specific heat of the heat exchanger outside fluid at the mean temperature between the preset inlet and outlet temperature. Δh is the enthalpy difference between the outlet and the inlet refrigerant enthalpies.

As mentioned before, the RANOTOR heat exchanger is designed to work in the laminar flow regime for the heat exchanger outside working fluids. Therefore, the Reynolds number should be calculated and checked to make sure that the flow is well within the laminar region (Re<2300). To calculate the Reynolds number, the velocity of the heat exchanger

outside fluid flow is needed and it is obtained by the following equations:

$$\dot{m}_o = \rho_o \dot{V}_o \qquad \textit{Equation 9-4}$$

$$\dot{V}_o = u_o \times A_{cross} \qquad \textit{Equation 9-5}$$

where $\dot{V}_o$ is the volume flow of the heat exchanger outside working fluid, $\dot{m}_o$ denotes the mass flow of the outside working fluid and ρ_o denotes density of the outside working fluid. Furthermore, A_{cross} denotes the cross sectional area of the outside working fluid's flow channel (the cross section area between every two plates).

With knowledge of the velocity of the outside fluid flow, the Reynolds number can be calculated accordingly:

$$\mathrm{Re} = \frac{u_o \times d_h}{\nu} \qquad \textit{Equation 9-6}$$

where u_o denotes the velocity of the heat exchanger outside fluid flow, d_h is the hydraulic diameter of the heat exchanger channel, and ν is the kinematics viscosity of the working fluid at the mean temperature.

By checking the Reynolds number, one can verify that the heat exchanger outside flow is laminar. Furthermore, judging by Equation 9-7 and Equation 9-8, it is found that the flow is both in the hydrodynamic entry region and in the thermal entry region (i.e. so-called combined entry length) due to the geometry of the heat exchanger.

$$\frac{x}{d_h} = \frac{\mathrm{Re}}{20} \qquad \textit{Equation 9-7}$$

$$Gz^{-1} \equiv \frac{x/d_h}{\mathrm{Re} \times \mathrm{Pr}} = \frac{1}{20} \qquad \textit{Equation 9-8}$$

In the above equations, G_z is the Graetz number, x denotes the length of the working fluid flow and d_h denotes the hydraulic diameter.

Due to the flow conditions, the correlation for calculating the combined entry length heat transfer problem (Equation 9-9), which was developed by Sieder and Tate, can be used for a good approximation of the heat exchanger outside Nusselt number.

$$Nu_o = 1.86 \times \left(\frac{\mathrm{Re} \times \mathrm{Pr}}{L/d_h} \right)^{1/3} \times \left(\frac{\mu}{\mu_s} \right)^{0.14} \qquad \textit{Equation 9-9}$$

in which

$$\mathrm{Pr} = \frac{\mu \times Cp}{k} \qquad \textit{Equation 9-10}$$

$$d_h = \frac{4 \times A_{cross}}{P_{cross}} \qquad \textit{Equation 9-11}$$

In the above equations, L is the heat exchanger outside working fluid flow length, d_h denotes the hydraulic diameter of the outside fluid's flow channel and Pr is the Prandtl number. A_{cross} denotes the area of the flow channel's cross section and P_{cross} denotes the wet parameter of the cross section. The dynamic viscosity (μ) of the heat exchanger outside working fluid is taken at its mean temperature and μ_s is the dynamic viscosity of the outside working fluid at the heat exchanger's surface temperature.

With knowledge of the Nusselt number, the local heat transfer coefficient for each divided calculation section can be calculated by the relationship of the heat transfer coefficient and Nusselt number.

$$h_o = \frac{Nu \times k}{d_h} \qquad \textit{Equation 9-12}$$

Finally, the temperature of the working fluid after passing one loop of the heat exchanger tubes can be obtained by the energy balance as shown below:

$$h_o \times (t_{\text{infinite}} - t_s) \times A_o = \dot{m}_o \times Cp_o \times \Delta t_o \qquad \textit{Equation 9-13}$$

where, A_o is the heat exchanger outside surface area, T_s is the heat exchanger surface temperature and $T_{infinite}$ is a variable in the program. $\dot{m}_o$ denotes the mass flow of the heat exchanger outside working fluid and h_o denotes the local heat transfer coefficient for each specific section of the heat exchanger outside working fluid.

The heat exchanger outside fluid pressure drop will decide the fan power, which is also very important for heat exchanger design. The pressure drop is calculated by Equation 9-14.

$$\Delta P = f \times \frac{L}{d_h} \times \frac{\rho}{2} \times u^2 \qquad \textit{Equation 9-14}$$

where f is the friction coefficient, L is the pipe length, d_h is the pipe hydraulic diameter and u is the flow velocity. The density ρ is calculated at the fluid mean temperature.

Several friction coefficients have been suggested by different researchers for different geometries and for different flow conditions. For laminar flow in slots with small distance in

between (b>>s), $\frac{96}{\mathrm{Re}}$ (V.H. Hahnemann and L. Ehret, 1941) can be used for calculating the friction coefficient, which is based on Hagen-Poiseuilles solution for laminar flow between parallel plates (
Equation *9-15*).

$$f = \frac{96}{\mathrm{Re}}\left(1 - 1.3553\alpha + 1.9467\alpha^2 - 1.7012\alpha^3 + 0.9564\alpha^4 - 0.2537\alpha^5\right)$$

Equation 9-15

where *Re* is Reynolds number and α is the aspect ratio, which is defined as the ratio of the channel height to the channel width.

By replacing the friction coefficient with their suggestion, Equation 9-14 can be reformulated in the form of Equation 9-16, which is adopted for the pressure drop calculations in the present work.

$$\Delta P = \frac{12 \times \mu \times L \times \dot{m}}{s^3 \times b \times \rho} \qquad \textit{Equation 9-16}$$

In the above equation, *s* denotes the distance between every two heat exchanger plates, *m* is the mass flow of the working fluid, *b* is the width of the flow channels and *L* is the length of the flow channel. The density and the dynamic viscosity are calculated at the fluid mean temperature.

Due to the relatively high system working pressure, the heat exchanger wall thickness is also checked by Barlow's Formula, which is used for calculating the hoop stress of a certain material of a pressurized circular pipe (Equation 9-17).

$$\sigma_1 = \frac{R \times p}{t} \qquad \textit{Equation 9-17}$$

where *t* denotes the thickness of the heat exchanger tube, *p* denotes the tube's inside pressure, σ_1 is the hoop stress for the heat exchanger material and *R* is the heat exchange tube radius.

9.2.6 Program description

9.2.6.1 Evaporator

In the evaporator calculation, the input to design the heat exchanger geometry seeks the design effectiveness of the heat exchanger (i.e. the preset working fluid temperature after passing the heat exchanger), namely: fluid inlet temperature ($t_{fluid\ in}$); preset fluid outlet temperature ($t_{fluid\ out}$), heat exchanger tube's inner diameter, the tube's wall thickness, the tube's first loop diameter, the amount of heat exchanger plates and the distance between every two plates, etc.

The variable $t_{infinite}$ in the calculation loop is first set equal to fluid inlet temperature ($t_{fluid\ in}$), and then the fluid temperature after passing the first loop of heat exchanger tubes can be calculated by Equation 9-13. Furthermore, this temperature will be compared with the preset fluid outlet temperature, which was set as an input to the program, in the if-clause. If this temperature is higher than the preset fluid outlet temperature, $t_{infinite}$ will be set equal to this temperature and thus input into Equation 9-13 again to calculate a new heat source outlet temperature (The temperature after passing two rounds of heat exchanger tubes). The value of t_{wall} is a constant for the evaporator, since the temperature of evaporation is constant (for pure refrigerant regardless of the pressure drop) until the refrigerant totally vaporizes. Following the same procedure, the heat source outlet temperature is calculated until it reaches the preset heat source outlet temperature. Then the calculation loop will stop and the program will export the outputs as: minimum number of plates required to keep laminar flow at the outside of the heat exchanger, the heat source outlet temperature, the number of required tube loops in each heat exchanger plate, approximate heat exchanger size, etc. In addition, the Reynolds number is always checked before the program runs. If the heat exchanger outside fluid flow is out of the laminar region, a warning will be given by the program to ask the user to reset the heat exchange geometry in order to keep the heat exchanger

outside flow in the laminar region. The program flow chart is shown in Figure 9-8.

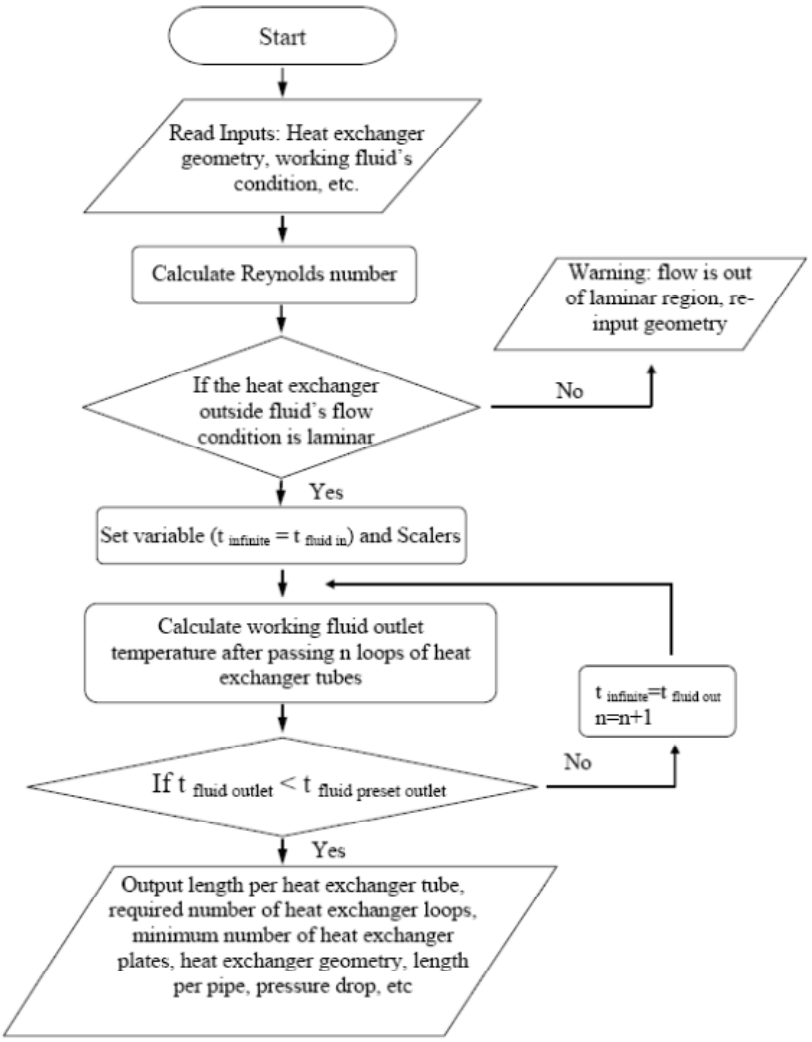

Figure 9-8 Program flow chart— evaporator

9.2.6.2 Gas cooler

In the gas cooler calculation, an iterative loop is needed. The inputs are fluid inlet temperature, preset fluid outlet temperature, heat exchanger tube inner diameter, the tube's wall thickness, the tube's first loop diameter, the amount of

heat exchanger plates and the distance between every two plates. The Reynolds's number is first checked before the program runs. If the heat exchanger outside flow is out of the laminar region, a warning will be given by the program to ask the user to reset the heat exchange geometry in order to keep the outside flow in the laminar region. Then several variables are set in this calculation, namely: $t_{infinite}$, which equals the fluid inlet temperature; the number of loops at each heat exchanger plate ($n_{loop\ preset}$), which equals 2 as an initial value; Scalars b and n_{loop} are both equal to 1 as initial values, etc. In the inner calculation loop, the fluid temperature after passing one loop of heat exchanger tubes is first calculated and then the number of tube loops on each heat exchanger plate (n_{loop}) is compared with the pre-set value ($n_{loop\ preset}$) in the if-clause. If n_{loop} is smaller than $n_{loop\ preset}$, the scalars start to be calculated as $n_{round} = n_{round}+1$, b=b+1, and the value of $t_{infinite}$ is reset as the fluid outlet temperature after passing n loops of heat exchanger tubes, then the calculation loop goes back to Equation 9-13 to calculate a new fluid outlet temperature after passing one more loop of heat exchanger tubes. The calculation loop is kept running until the scalar n_{loop} is bigger than $n_{loop\ preset}$. Then the temperature of the working fluid at this time will be compared with the pre-set preferred fluid outlet temperature, in the outer calculation loop. If this temperature is smaller than the preferred fluid outlet temperature, all the variables will be set back to the original values; the scalars are reset as $n_{loop\ preset} = n_{loop\ preset} + 1$, b=1 and the inner calculation loop will run again to calculate the new fluid outlet temperature.

Following the same procedure, the fluid outlet temperature is iterated until it reaches the preferred fluid outlet temperature that was set as a program' input before. Then the calculation will stop and the program will export the outputs as: minimum number of plates required to keep laminar flow at the heat exchanger outside, the heat source outlet temperature, the number of tube loops in each heat exchanger plate,

approximate heat exchanger size, etc. The program flow chart is shown in Figure 9-9.

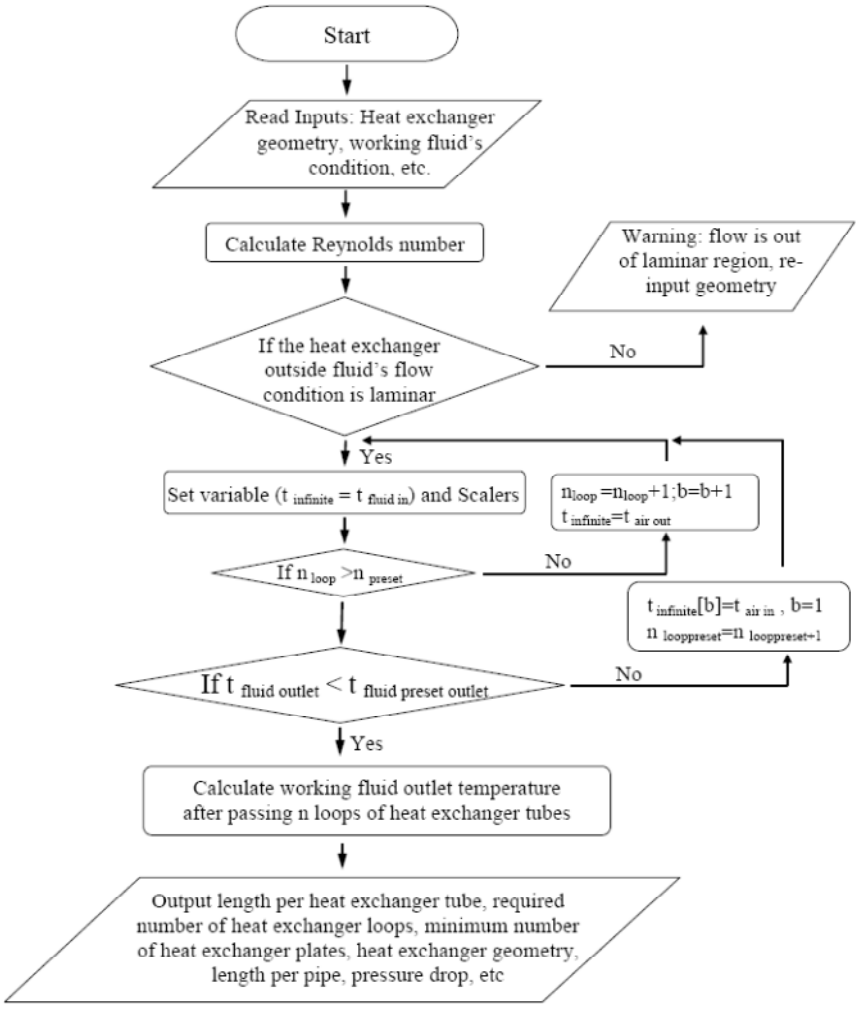

Figure 9-9 Program flow chart— gas cooler

9.2.6.3 Gas heater

In the gas heater calculation, the inputs are still fluid inlet temperature, preset fluid outlet temperature, heat exchanger tube inner diameter, the tube's wall thickness, the tube's first loop diameter, number of heat exchanger plates, and the distance between every two plates. First the Reynolds's number

is checked before the program runs. If the heat exchanger outside flow is out of the laminar region, a warning sign will be given by the program to reset the heat exchange geometry in order to keep the heat exchanger outside flow in the laminar region. Then several variables are set in this calculation, namely: $t_{infinite}$, which equals the fluid inlet temperature; the number of loops at each heat exchanger plate ($n_{loop\ preset}$), which equals 2 as an initial value; Scalars b and n_{loop} that both equal 1 as initial values, etc. In the inner calculation loop, the fluid temperature after passing one loop of heat exchanger tubes is first calculated and then the number of tube rounds on each heat exchanger plate (n_{round}) is compared with the pre-set value ($n_{loop\ preset}$) in the if-clause. If n_{loop} is smaller than $n_{loop\ preset}$, the scalars are then calculated as $n_{loop} = n_{loop}+1$, $b=b+1$, and the value of $t_{infinite}$ is set as the fluid outlet temperature after passing n loops of heat exchanger tubes. Then the calculation loop goes back to Equation 9-13 to calculate a new fluid outlet temperature after passing one more loop of heat exchanger tubes. The calculation loop is kept running until the scalar n_{loop} is bigger than $n_{loop\ preset}$. Then the temperature of the working fluid at this time will be compared with the preset preferred fluid outlet temperature, which was set as an input, in the outer calculation loop. If this temperature is bigger than the preferred fluid outlet temperature, all the variables will be set back to the original values; the scalars are reset as $n_{loop\ preset} = n_{loop\ preset} +1$, $b=1$ and the inner calculation loop will run again to calculate the new fluid outlet temperature. Following the same procedure, the fluid outlet temperature is iterated until it reaches the preferred fluid outlet temperature that was set as an input. Then the calculation will stop and the program will export the outputs as: minimum number of plates required to keep laminar flow at the outside of the heat exchanger, the heat source outlet temperature, the number of tube loops in each heat exchanger plate, approximate heat exchanger size, etc. The program flow chart is shown in Figure 9-10.

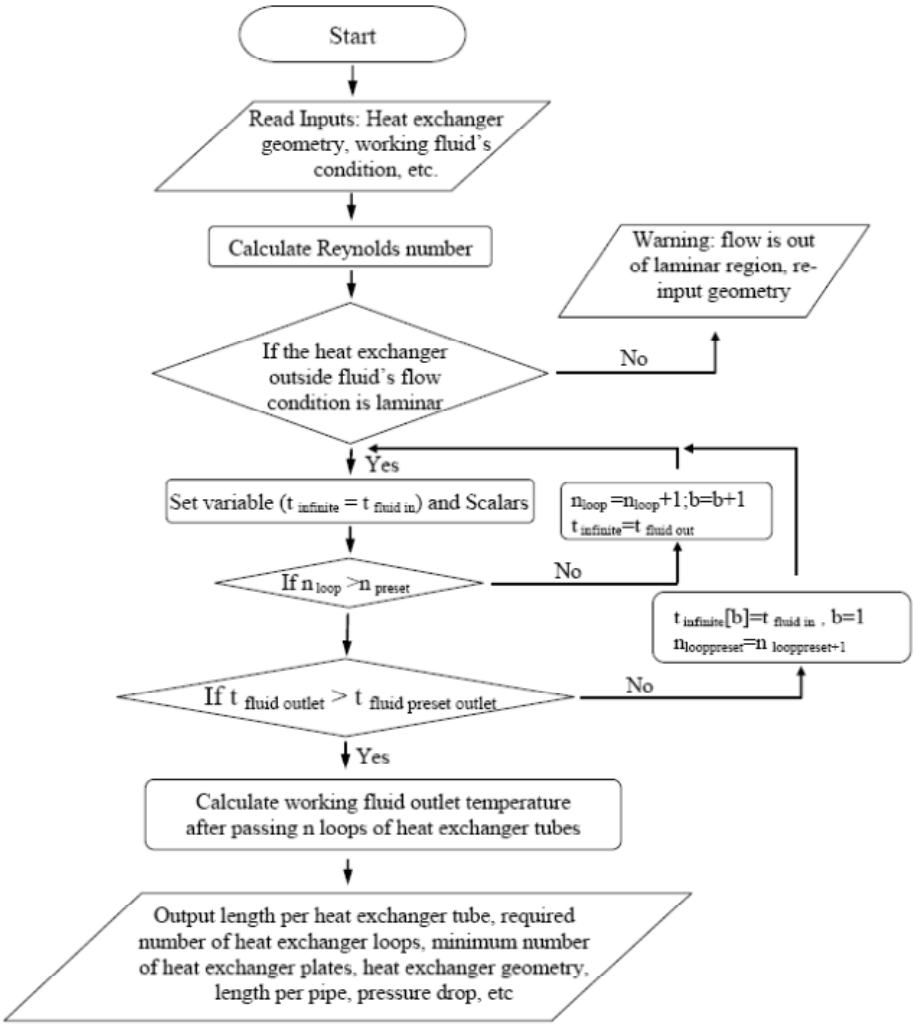

Figure 9-10 Program flow chart— gas heater

9.2.7 Example of program operation window

The program operation windows are shown in the following figures for different cycles and different heat exchanger design calculations:

Carbon dioxide transcritical power cycle

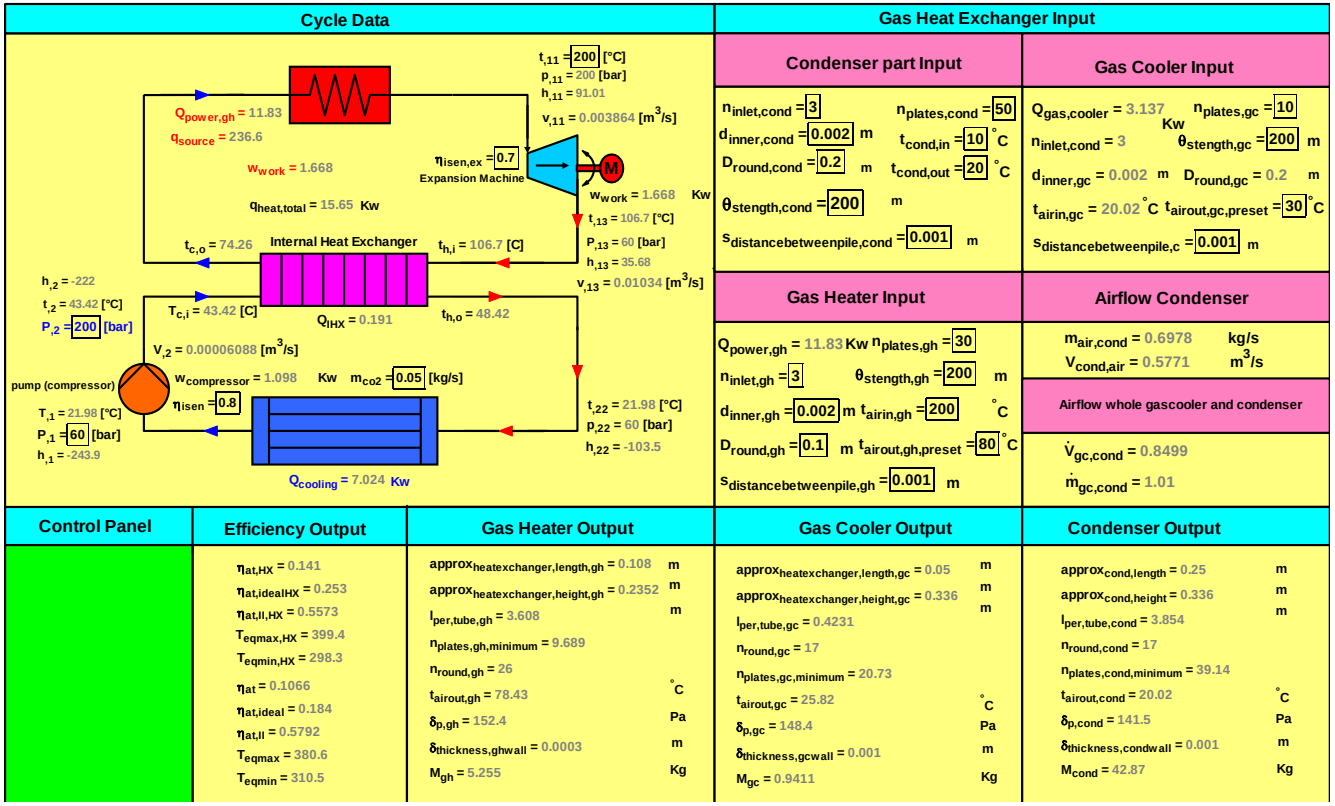

Figure 9-11 Program operation window—CO_2 transcritical power cycle

Carbon dioxide cooling and power combined cycle

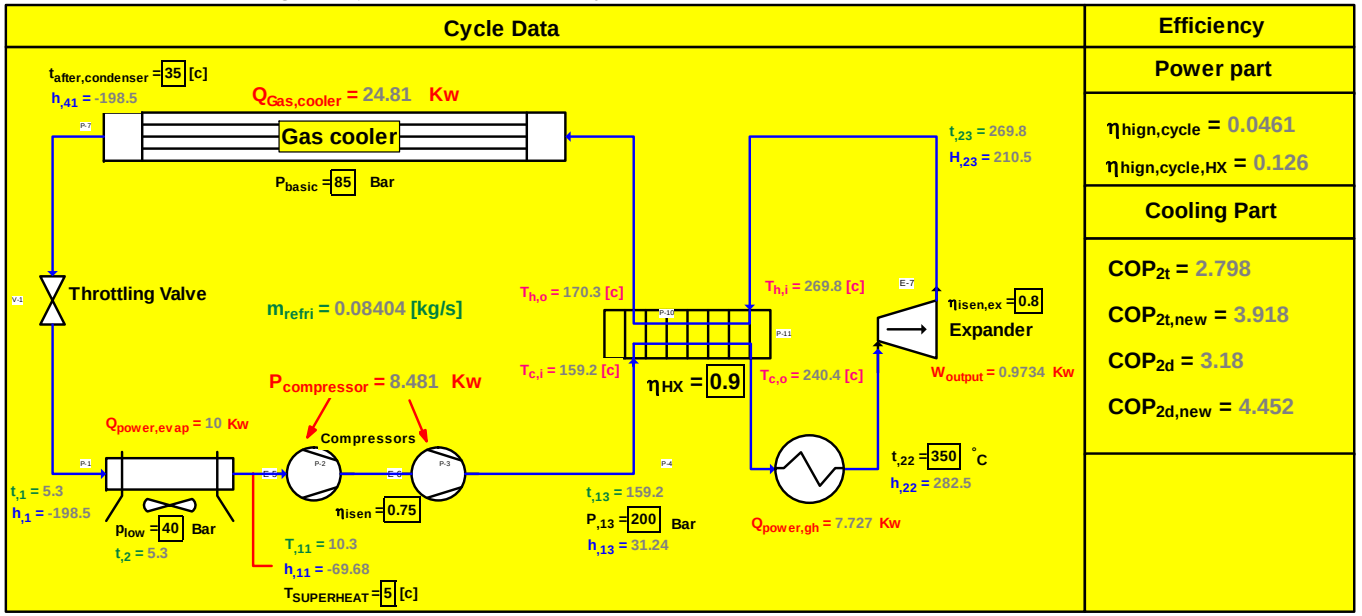

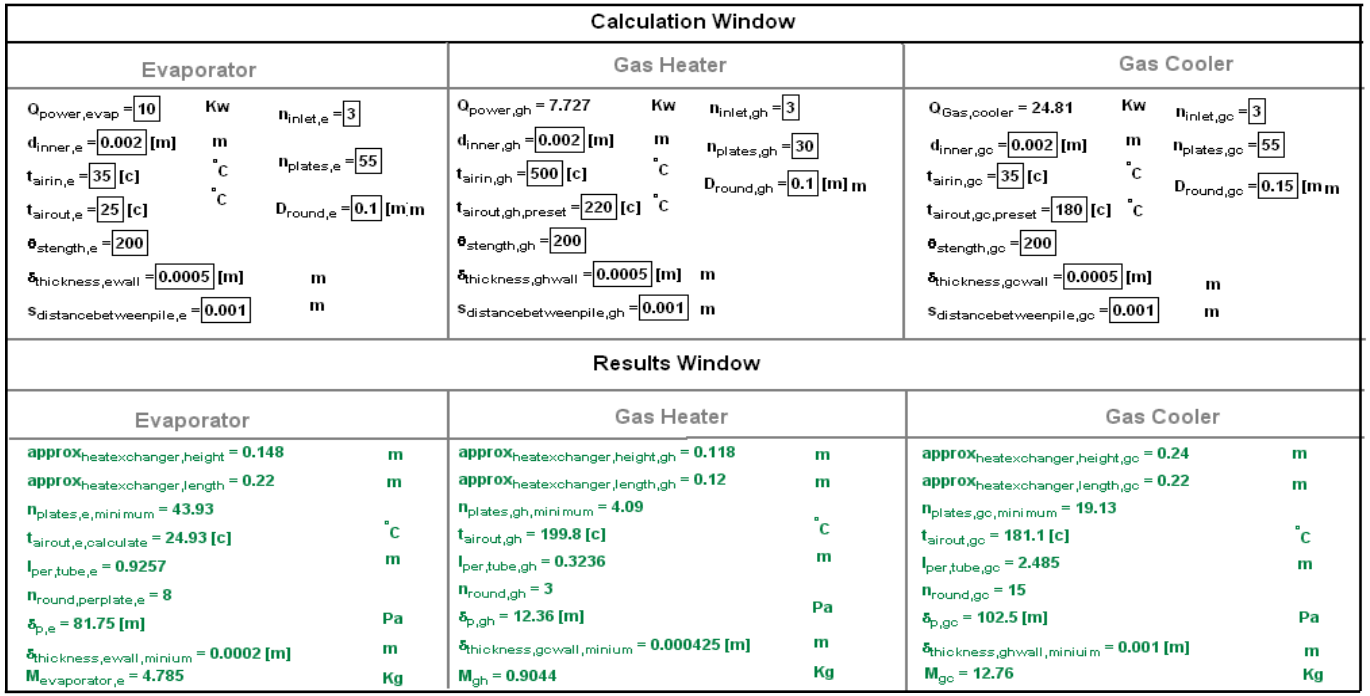

Figure 9-12 Program operation window—CO_2 cooling and power combined cycle

9.2.8 Results

The results will vary according to different designs and different application purposes; thus it is hard to give a general result here.

Some sketches according to several design calculations are also shown below to give a general idea of the heat exchanger geometry.

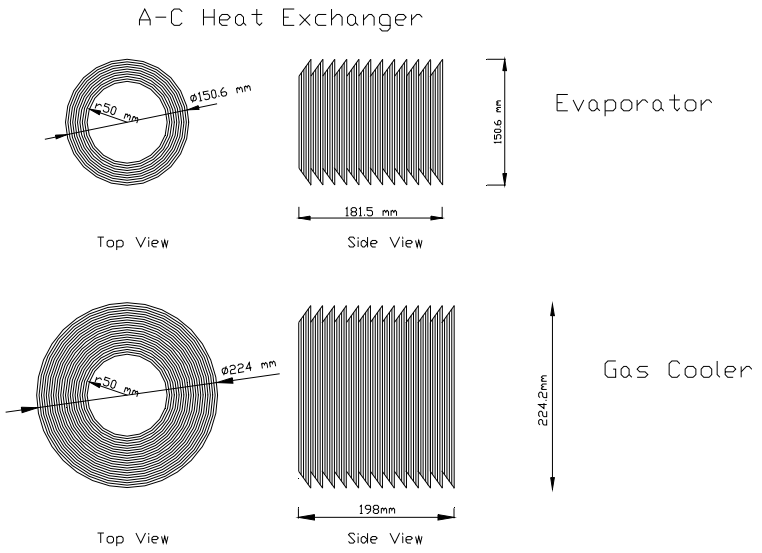

Figure 9-13 Carbon dioxide transcritical refrigeration cycle heat exchanger

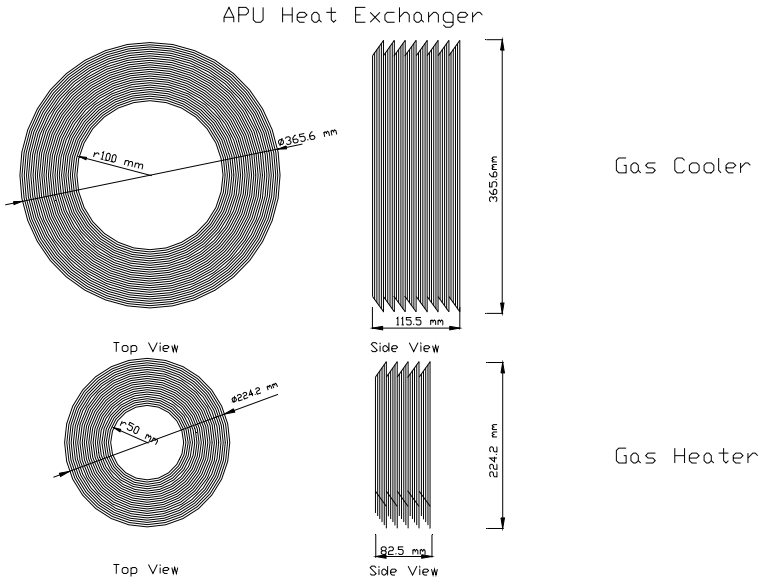

Figure 9-14 Carbon dioxide transcritical power cycle heat exchangers

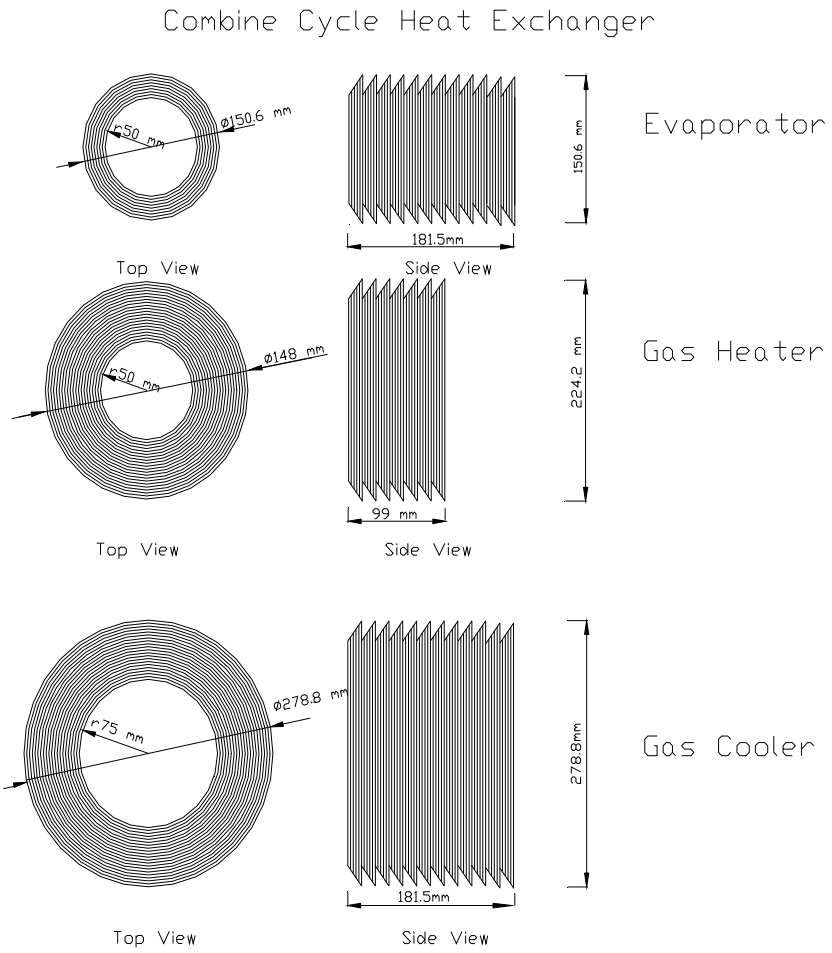

Figure 9-15 Carbon dioxide refrigeration and power combined cycle heat exchanger

9.3 Appendix 3— Summary of Attached Papers

Y. Chen, P. Lundqvist, P. Platell, "Theoretical Research of Carbon Dioxide Power Cycle Application in Automobile Industry to Reduce Vehicle's Fuel Consumption", ***Applied Thermal Engineering 25 (2005), pp 2041–2053***

This work discusses means to utilize low-grade energy in vehicle exhaust gases, to reduce the vehicle's fuel consumption and to make it run in a more environmentally friendly way. To utilize the energy in the exhaust gas, a CO_2 bottoming system in the vehicle's engine is proposed. Several basic cycles—according to the different design concepts—are presented, and the efficiencies are calculated using Engineering Equation Solver (EES).

Several thermodynamic models in EES show that after system optimization, in a CO_2 transcritical power cycle with a gas heater pressure of 130 bar and 200°C expansion inlet temperature, about 20% of the energy in the exhaust gas can be converted into useful work. Increasing the pressure in the gas heater to 300 bar and with the same expansion inlet temperature, about 12% of the exhaust gas energy can be converted. When the pressure is raised both in the gas cooler and in the gas heater, the cycle runs completely above the critical point, and the efficiency is about 19%. In addition, in the CO_2 combined cycle, the system COP is 2.32 and about 5% of the exhaust gas energy can be converted.

Y. Chen, P. Lundqvist, A. Johansson, P. Platell, "A comparative study of the Carbon Dioxide Transcritical Power Cycle compared with an Organic Rankine Cycle with R123 as working fluid in Waste Heat Recovery", ***Applied Thermal Engineering 26 (2006), pp 2142–2147***

The Organic Rankine Cycle (ORC) as a bottoming cycle to convert low-grade waste heat into useful work has been widely

investigated for many years. The CO_2 transcritical power cycle, on the other hand, is scarcely treated in the available literature. A CO_2 transcritical power cycle (CO_2 TPC) shows a higher potential than an ORC when taking into account the behavior of the heat source and the heat transfer between heat source and working fluid in the main heat exchanger. This is mainly due to a better temperature glide match between heat source and working fluid. The CO_2 cycle also shows no pinch limitation in the exchanger. This study looks at the performance of the CO_2 transcritical power cycle in utilizing energy from low-grade waste heat to produce useful work in comparison to an ORC using R123 as working fluid.

Due to the temperature gradients for the heat source and heat sink, the thermodynamic mean temperature has been used as a reference temperature when comparing both cycles. The thermodynamic models have been developed in EES. The relative efficiencies have been calculated for both cycles. The results obtained show that when utilizing the low-grade waste heat with the same thermodynamic mean heat rejection temperature, a transcritical carbon dioxide power system gives a slightly higher power output than the organic Rankine cycle.

Y. Chen, W. Pridasawas, P. Lundqvist, "Dynamic Simulation of a Solar-Driven Carbon Dioxide Transcritical Power System for Small Scale Combined Heat and Power Production", ***Solar Energy 84 (2010), pp 1103–1110***

This paper discusses the possibility of using carbon dioxide as a working medium for a solar-driven power system. In this study, the dynamic performance of a small scale solar-driven carbon dioxide power system is analyzed by dynamic simulation tool TRNSYS 16 and Engineering Equation Solver (EES) using co-solving technique.

Both daily performance and yearly performance of the proposed system have been simulated. Different system operating parameters which will influence the system

performance have been discussed. Under Swedish climatic conditions, the maximum daily power production is about 12 kWh and the maximum monthly power production is about 215 kW h with the working conditions of the proposed system.

Besides the power being produced, the system can also produce about 10 times as much thermal energy, which can be used for space heating, domestic hot water supply or driving absorption chillers. The simulation results show that the proposed system is a promising and environmentally benign alternative for conventional low-grade heat source utilization system.

Y. Chen, A. B. Workie, P. Lundqvist, "Second Law Analysis of a Carbon Dioxide Transcritical Power System in Low-grade Heat Source Recovery", ***submitted to Applied Thermal Engineering***

In this work, the performance of a CO_2 power cycle in utilizing the low-grade heat sources is simulated and the results are analyzed with a focus on second law thermodynamics (i.e. exergy and entropy). Different system parameters influencing the system exergy and entropy change are discussed.

Engineering Equation Solver (EES) is used for simulation. The simulation results show that the matching of the temperature profiles in the system heat exchangers has crucial influence on their exergy destruction and entropy generation. It is also an essential factor that influences the system thermodynamic efficiencies.

Y. Chen, P. Lundqvist, "Carbon Dioxide Cooling and Power Combined Cycle for Mobile Applications", ***7th IIR Gustav Lorentzen Conference on Natural Working Fluids, Trondheim, Norway, May 28-31, 2006***

A carbon dioxide cooling and power combined system, which can provide A/C and produce power at the same time, is proposed in this paper. The power part of the system can utilize

the energy in automobile exhaust gases to produce electricity for the A/C compressor, and thus both increases the cooling COP and decreases the vehicle's fuel consumption by reducing the compressor's energy demand. Moreover, different factors that influence the cycle's optimum working conditions are also discussed.

The software Engineering Equations Solver (EES) is used to model and to analyze the system performance. Results show that the proposed combined system can achieve a COP of 3.18 for the cooling part and 12.6% efficiency for the power part under typical working conditions. After transferring the energy gained from the cycle to its compressor, the new COP will be 4.45 and the improvement of the COP will be around 40% accordingly.

Y. Chen, P. Lundqvist, "Analysis of Supercritical Carbon Dioxide Heat Exchangers in Cooling Process", ***International Refrigeration and Air Conditioning Conference, Purdue, USA, July 17-20, 2006***

In this paper, the Cp variation of supercritical CO_2 and its influence on the temperature profile in heat exchangers used for supercritical carbon dioxide refrigeration process including a suction gas heat exchanger are simulated and analyzed.

A basic carbon dioxide transcritical refrigeration cycle has been adopted for the study. The results calculated in EES and Refprop 7 show that due to the sharp variation in the specific heat of supercritical carbon dioxide, the temperature profile in the gas cooler will show a concave shape. Due to the shape of the temperature profile, the temperature difference, which is the "driving force" for heat transfer to take place, will be much smaller inside the gas cooler than at its ends. Therefore,

- To remove a certain amount of heat from the gas cooler, the required heat exchanger surface will be much bigger than in one without such a shape of temperature profile.

- The logarithmic mean temperature difference, which is calculated by the measured temperature difference at the heat exchanger ends, will over-predict the real temperature difference for the heat exchanger (gas cooler).
- The UA value, which is calculated by the measured logarithmic mean temperature difference, will be under-estimated.

It is also found that the gas cooler outlet temperature has a crucial influence on the value of optimum gas cooler pressure and consequently the shape of the temperature profile in the gas cooler, i.e. the higher the gas cooler outlet temperature is, the less concave shape the temperature profile inside the gas cooler will be. However, the decrement of system COP with increasing gas cooler should also be considered in system design.

Y. Chen, P. Lundqvist, "Low-Grade Heat Source Utilization by Carbon Dioxide Transcritical Power Cycle", ***ASME conference, Vancouver, Canada, July 9-13, 2007***

In this paper, a transcritical carbon dioxide power cycle is analyzed for its potential in utilizing the low-grade heat sources. Solar thermal is selected as a representative of low-grade heat sources. TRNSYS 16 and Engineering Equation Solver (EES) are employed using co-solving technique to analyze the dynamic performance of the proposed system.

Both daily performance and annual performance of the proposed system under Swedish climate conditions are simulated. The simulation results show that the proposed system can achieve 8% average thermal efficiency and consequently 2.43 kW average power production during the system working period on a randomly selected summer day with a 30 m^2 solar collector. Over the whole year, the maximum daily power production is about 17 kWh and the maximum monthly power production is about 185 kWh.

Y. Chen, P. Lundqvist, "Theoretical Study of Carbon Dioxide Double Loop System" ***IIR Internal Refrigeration Congress, Beijing, China, August 21-26, 2007***

In this paper, a carbon dioxide double loop system is proposed. The system consists of two subsystems: a CO_2 power subsystem and a CO_2 refrigeration subsystem. The power subsystem is able to utilize the energy from the low-grade heat source to produce power. The power is then transferred to the refrigeration subsystem, partly or totally covering the power consumption of the compressor. Furthermore, it is possible to take advantage of the temperature glides of the heat rejection processes of both subsystems to produce hot water.

The influences of different cycle working parameters on the system performance are simulated and analyzed. The results show that the proposed system is a very promising way to provide cooling, heating and hot water more efficiently than traditional systems.

Y. Chen, P. Lundqvist, B. Palm, "A Novel Gas-Water Heat Exchanger with Minichannels", ***ASME Summer Heat Transfer Conference, Jacksonville, Florida USA, August 10-14, 2008***

In this study, a novel gas water heat exchanger with minichannels is designed, built and tested. The heat exchanger is mainly composed of a number of concentric ring shaped plates, which are made up of several heat exchanger tubes. The ring-shaped plates are arranged in parallel and placed in a shell. The heat exchanger is designed as a countercurrent heat exchanger with laminar flow on the heat exchanger's shell-side (gas side) and therefore has a very low pressure drop on the shell side.

The heat exchanger was tested with water and hot air on its tube-side and shell-side respectively. All the necessary parameters like inlet and outlet temperatures on tube-side and shell-side as well as the pressure drop, flow rate of fluids, etc.

were measured. Different existing correlations were used to calculate the overall heat transfer coefficient and the results were compared with the measured value. The measured results show that the new designed heat exchanger can achieve a good heat transfer performance and also maintain a low pressure drop on the shell-side (gas side).

Y. Chen, P. Lundqvist, "The CO_2 Transcritical Power Cycle for Low-Grade Heat Recovery—Discussion on Temperature Profiles in System Heat Exchangers", ***ASME Power and ICOPE Conference, Denver, USA, July 12-14, 2011***

This study discusses the advantage of a carbon dioxide power system in low-grade heat source recovery with a focus on the temperature profiles in the system heat exchangers.

The sharp Cp variation of supercritical CO_2 in the region close to its critical point is examined. The influence of this variation on the performance of the heat exchangers that are used in low-grade heat source utilization is studied and discussed. Moreover, the effect of inserting an internal heat exchange on the cycle performance is also investigated

The simulation results show that due to the dramatic change the Cp of supercritical CO_2 in the region close to its critical point, the temperature profiles in the system gas heater will show a concaved shape. This enables the system's gas heater to achieve a small temperature difference on both ends and at the same time maintain a small heat exchanger size. Furthermore, the Cp variation also enables supercritical CO_2 to recover the energy both in expansion outlet carbon dioxide and in low-grade heat sources sufficiently. For the influence of internal heat exchanger, up to about 50% of cycle thermal efficiency improvement was found.